SEISMIC DESIGN GUIDE FOR MASONRY BUILDINGS

Second Edition

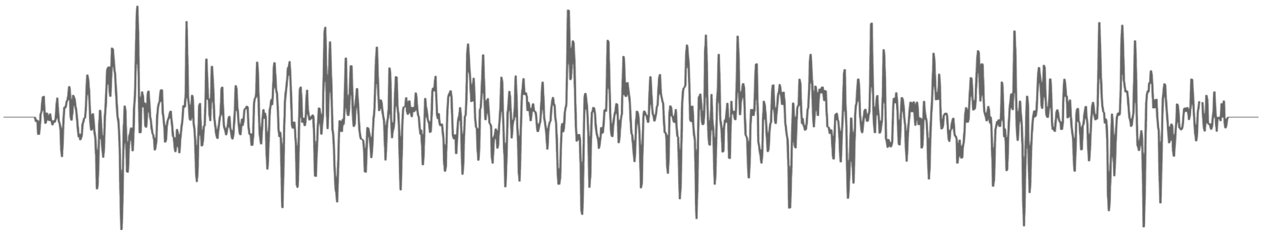

Svetlana Brzev Donald Anderson

Canadian Concrete Masonry Producers Association

2018

TABLE OF CONTENTS – APPENDIX A

A. RESPONSE OF STRUCTURES TO EARTHQUAKES A-2

A.1. Elastic Response A-2

A.2. Inelastic Response A-6

A.3. Ductility A-7

A.4. A Primer on Modal Dynamic Analysis Procedure A-8
A.4.1. Multi-degree-of-freedom systems A-8
A.4.2. Seismic analysis methods A-9
A.4.3. Modal analysis procedure: an example A-10
A.4.4. Comparison of static and modal analysis results A-14

A. Response of Structures to Earthquakes

This appendix contains background related to fundamentals of seismic response of structures to earthquakes. A discussion on elastic and inelastic response is included, and a primer on modal dynamic analysis.

A.1. Elastic Response

When an earthquake strikes, the base of a building is subject to lateral motion while the upper part of the structure initially is at rest. The forces created in the structure from the relative displacement between the base and upper portion cause the upper portion to accelerate and displace. At each floor the lateral force required to accelerate the floor mass is provided by the forces in the vertical members. The floor forces are inertial forces, not externally applied forces such as wind loads, and exist only as long as there is movement in the structure.

Earthquakes cause the ground to shake for a relatively short time, 15 to 30 seconds of strong ground shaking, although large subduction earthquakes may last for a few minutes. The motion is cyclic and the response of the structure can only be determined by considering the dynamics of the problem. A few important dynamic concepts are discussed below.

Consider a simple single-storey building with masonry walls and a flat roof. The building can be represented by a Single Degree of Freedom (SDOF) model (also known as a stick model) as shown in Figure A-1a). The mass, M , lumped at the top, represents the mass of the roof and a fraction of the total wall mass, while the column represents the combined wall stiffness, K , in the direction of earthquake ground motion. If an earthquake causes a lateral deflection, Δ, at the top of the building, Figure A-1b), and if the building response is elastic with stiffness, K , then the lateral inertial force, F , acting on the mass M will be

$$F = K \cdot \Delta$$

When the mass of a SDOF un-damped structure is allowed to oscillate freely, the time for a structure to complete one full cycle of oscillation is called the period, T , which for the SDOF system shown is given by

$$T = 2\pi\sqrt{\frac{M}{K}} \quad \text{(seconds)}$$

Instead of period, the term *natural frequency*, ω , is often used in seismic design. It is related to the period as follows

$$\omega = \frac{2\pi}{T} = \sqrt{\frac{K}{M}} \quad \text{(radians/sec)}$$

Frequency is sometimes also expressed in Hertz, or cycles per second, instead of radians/sec, denoted by the symbol ω_{cps} , where

$$\omega_{cps} = \frac{1}{T} = \frac{\omega}{2\pi}$$

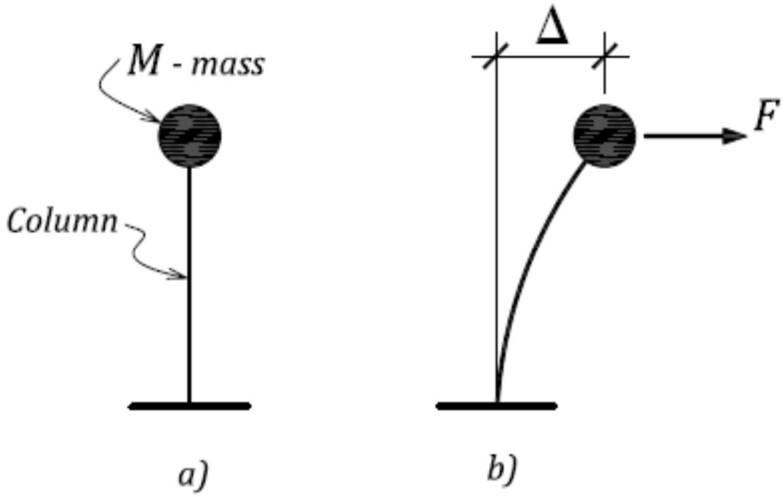

Figure A-1. SDOF system: a) stick model; b) displaced position.

As the structure vibrates, there is always some energy loss which will cause a decrease in the amplitude of the motion over time - this phenomenon is called *damping*. The extent of damping in a building depends on the materials of construction, its structural system and detailing, and the presence of architectural components such as partitions, ceilings and exterior walls. Damping is usually modelled as viscous damping in elastic structures, and hysteretic damping in structures that demonstrate inelastic response. In seismic design of buildings, damping is usually expressed in terms of a *damping ratio,* β, which is described in terms of a percentage of critical viscous damping. Critical viscous damping is defined as the level of damping which brings a displaced system to rest in a minimum time without oscillation. Damping less than critical, an under-damped system, allows the system to oscillate; while an over-damped system will not oscillate but take longer than the critically damped system to come to rest. Damping has an influence on the period of vibration, *T*, however this influence is minimal for lightly damped systems, and in most cases, is ignored for structural systems. For building applications, the damping ratio can be as low as 2%, although 5% is used in most seismic calculations where some nonlinear response is present. Damping in a structure increases with displacement amplitude since with increasing displacement more elements may crack or become slightly nonlinear. For linear seismic analysis viscous damping is usually taken as 5% of critical as the structural response to earthquakes is usually close to or greater than the yield displacement. A smaller value of viscous damping is usually used in non-linear analyses as hysteretic damping is also considered.

One of the most useful seismic design concepts is that of the *response spectrum*. When a structure, say the SDOF model shown in Figure A-1, is subjected to an earthquake ground motion, it cycles back and forth. At some point in time the displacement relative to the ground and the absolute acceleration of the mass reach a maximum, $\Delta_{\max}$ and $a_{\max}$, respectively. Figure A-2a) shows the maximum displacement plotted against the period, T. Denote the period of this structure as T_1. If the dynamic properties, i.e. either the mass or stiffness change, the period will change, say to T_2. As a result, the maximum displacement will change when the structure is subjected to the same earthquake ground motion, as indicated in Figure A-2b). Repeating the above process for many different period values and then connecting the points produces a plot like that shown in Figure A-2c), which is termed the *displacement response spectrum.* The spectrum so determined corresponds to a specific input earthquake motion and a specific damping ratio, β. The same type of plot could be constructed for the maximum acceleration, $a_{\max}$, rather than the displacement, and would be termed the *acceleration response spectrum.*

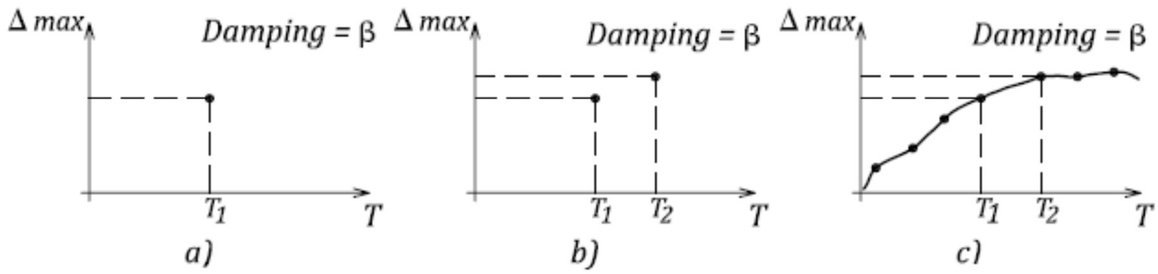

Figure A-2. Development of a displacement response spectrum - maximum displacement response for different periods T : a) $T = T_1$; b) $T = T_2$; c) many values of T .

Figure A-3a) shows the displacement response spectrum for the 1940 El Centro earthquake at different damping levels. Note that the displacements decrease with an increase in the damping ratio, β , from 2% to 10%. Figure A-3b) shows the acceleration response spectrum for the same earthquake. For the small amount of damping present in the structures, the maximum acceleration, $a_{\max}$, occurs at about the same time as the maximum displacement, $\Delta_{\max}$, and these two parameters can be related as follows

$$a_{\max} = \left(\frac{2\pi}{T}\right)^2 \Delta_{\max}$$

Thus, by knowing the spectral acceleration, it is possible to calculate the displacement spectral values and vice versa. It is also possible to generate a response spectrum for maximum velocity. Except for very short and very long periods, the velocity, $v_{\max}$, is closely approximated by

$$v_{\max} = \left(\frac{2\pi}{T}\right) \Delta_{\max}$$

This is generally called the pseudo velocity response spectrum as it is not the true velocity response spectrum.

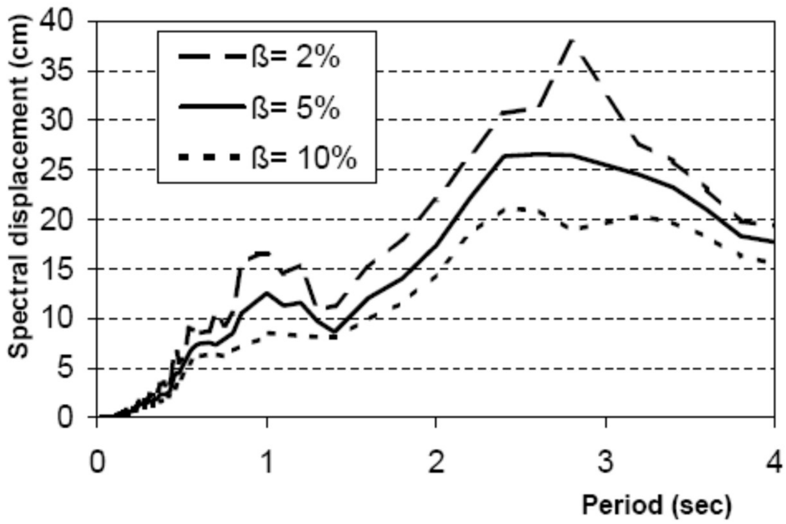

a)

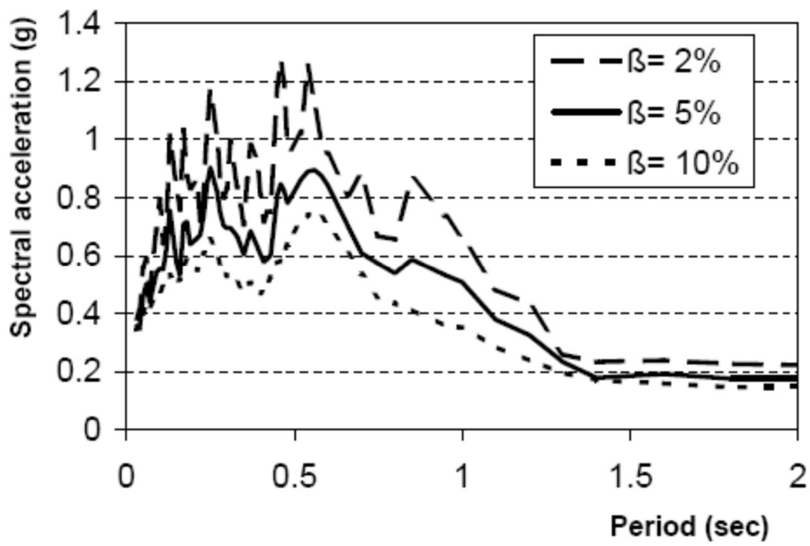

b)

Figure A-3. Response spectra for the 1940 El Centro NS earthquake at different damping levels: a) displacement response spectrum; b) acceleration response spectrum.

The response spectrum can be used to determine the maximum response of a SDOF structure, given its fundamental period and damping, to a specific earthquake acceleration record. Different earthquakes produce widely different spectra and so it has been the practice to choose several earthquakes (usually scaled) and use the resulting average response spectrum as the *design spectrum*. For years, the NBC seismic provisions have used this procedure where the design spectrum for a site was described by one or two parameters, either peak ground acceleration and/or peak ground velocity, that were determined using probabilistic means.

More recently, probabilistic methods have been used to determine the spectral values at a site for different structural periods. Figure A-4 shows the 5% damped acceleration response spectrum for Vancouver used in developing the NBC 2005. This is a uniform hazard response spectrum, i.e., spectral accelerations corresponding to different periods are based on the same probability of being exceeded, that is, 2% in 50 years. This is discussed further in Section 1.3. The NBC 2015 code uses the same method but has been updated by using many more records to determine the hazard and has extended the period range out to 10 seconds.

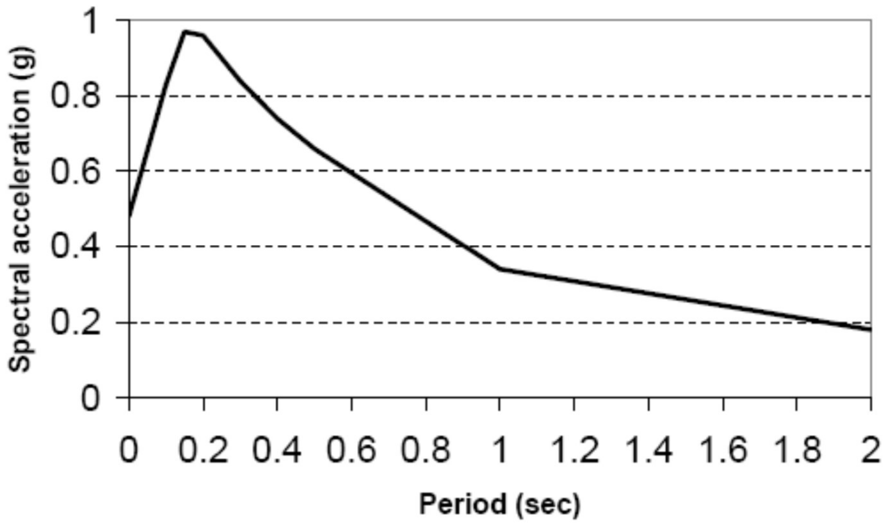

Figure A-4. Uniform hazard acceleration response spectrum for Vancouver, 2% in 50 year probability, 5% damping.

A.2. Inelastic Response

For any given earthquake ground motion and SDOF elastic system it is possible to determine the maximum acceleration and the related inertia force, F_{el} , and the maximum displacement, Δ_{el} . Figure A-5a) shows a force-displacement relationship with the maximum elastic force and displacement indicated. If the structure does not have sufficient strength to resist the elastic force, F_{el} , then it will yield at some lower level of inertia force, say at lateral force level, F_y . It has been observed in many studies that a structure with a nonlinear cyclic force-displacement response similar to that shown in Figure A-5b) will have a maximum displacement that is not much different from the maximum elastic displacement. This is indicated in Figure A-5c) where the inelastic (plastic) displacement, Δ_u , is shown just slightly greater than the elastic displacement, Δ_{el} . This observation has led to the *equal displacement rule*, an empirical rule which states that the maximum displacement that the structure reaches in an earthquake is independent of its yield strength, i.e. irrespective of whether it demonstrates elastic or inelastic response. The equal displacement rule is thought to hold because the nonlinear response softens the structure and so the period increases, thereby giving rise to increased displacements. However, at the same time, the yielding material dissipates energy that effectively increases the damping (the energy dissipation is proportional to the area enclosed by the force-displacement loops, termed hysteresis loops). Increased damping tends to decrease the displacements; therefore, it is possible that the two effects balance one another with the result that the elastic and inelastic displacements are not significantly different.

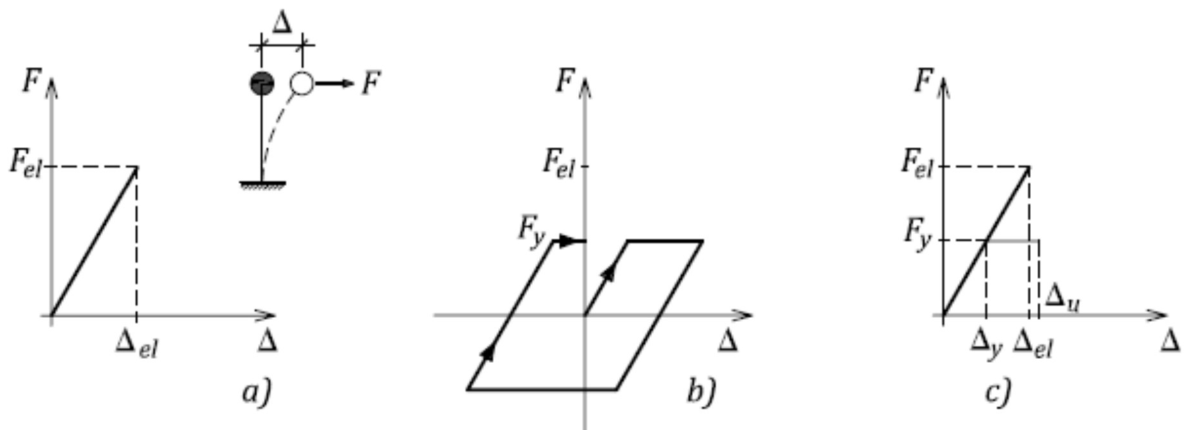

Figure A-5. Force-displacement relationship: a) elastic response; b) nonlinear (inelastic) response; c) equal displacement rule.

There are limits beyond which the equal displacement rule does not hold. In short period structures, the nonlinear displacements are greater than the elastic displacements, and for very long period structures, the maximum displacement is equal to the ground displacement. However, the equal displacement rule is, in many ways, the basis for the seismic provisions in many building codes which allow the structure to be designed for forces less than the elastic forces. But there is always a trade-off, and the lower the yield strength, the larger the nonlinear or inelastic deformations. This can be inferred from Figure A-5c) where it is noted that the difference between the nonlinear displacement, Δ_u, and yield displacement, Δ_y, which represents the inelastic deformation, would increase as the yield strength decreases. Inelastic deformations generally relate to increased damage, and the designer needs to ensure that the strength does not deteriorate too rapidly with subsequent loading cycles, and that a brittle failure is prevented. This can be achieved by additional "seismic" detailing of the structural members, which is usually prescribed by the material standards. For example, in reinforced concrete structures, seismic detailing consists of additional confinement reinforcement that ensures ductile performance at critical locations in beams, columns, and shear walls. In reinforced masonry structures, it is difficult to provide similar confinement detailing, and so restrictions are placed on limiting the reinforcement spacing, on levels of grouting, and on certain strain limits in the masonry structural components (e.g. shear walls) which provide resistance to seismic loads (see Chapter 2 for more details on seismic design of masonry shear walls).

A.3. Ductility

Ductility relates to the capacity of the structure to undergo inelastic displacements. For the SDOF structure, whose force-displacement relation is shown in Figure A-5c) the displacement ductility ratio, μ_Δ, is a measure of damage that the structure might undergo and can be expressed as

$$\mu_\Delta = \frac{\Delta_u}{\Delta_y}$$

The ratio between the maximum elastic force, F_{el}, and the yield force, F_y, is given by the force reduction factor, R, defined as

$$R = \frac{F_{el}}{F_y}$$

If the material is elastic-perfectly plastic, i.e. there is no strain hardening as it yields (see Figure A-5b), and if Δ_u is equal to Δ_{el}, then it can be shown that μ_Δ is equal to R.

For different types of structures and detailing requirements, most building codes tend to prescribe the R value while not making reference to the displacement ductility ratio, μ_Δ, thus implying that the μ_Δ and R values would be similar.

A.4. A Primer on Modal Dynamic Analysis Procedure

The main objective of this section is to explain how more complex multi-degree-of-freedom structures respond to earthquake ground motions and how such response can be quantified in a form useful for structural design. This background should be helpful in understanding the NBC seismic provisions.

A.4.1. Multi-degree-of-freedom systems

The idea of modelling the building as a SDOF structure was introduced in Section A.1, and the dynamic response to earthquake ground motions was developed in terms of a response spectrum. Such a simple model might well represent the lateral response of a single storey warehouse building with flexible walls or bracing system, and with a rigid roof system where the roof comprises most of the weight (mass) of the structure. However, this is not a good model for a masonry warehouse with a metal deck roof, where the walls are quite stiff and the deck is flexible and light relative to the walls. Such a system requires a more complex model using a multi-degree-of-freedom (MDOF) system. A shear wall in a multi-storey building is another example of a MDOF system.

Figure A-6 shows two examples of MDOF structures. A simple four-storey structure is shown in Figure A-6a), and a simple MDOF model for this building consists of a column representing the stiffness of vertical members (shear walls or frames), with the masses lumped at the floor levels. If the floors are rigid, it can be assumed that the lateral displacements at every point in a floor are equal, and the structure can be modelled with one degree of freedom (DOF) at each floor level (a DOF can be defined as lateral displacement in the direction in which the structure is being analyzed). This will result in as many degrees of freedom as the number of floors, so this building can be modelled as a 4-DOF system. It must also be assumed that there are no torsional effects, that is, there is no rotation of the floors about a vertical axis (torsional effects are discussed in Section 1.11). The analysis will be the same irrespective of the lateral force resisting system (a shear wall or a frame), aside from details in finding the lateral stiffness matrix for the floor displacements.

The warehouse building shown in Figure A-6b) is another example of a MDOF structure. The walls are treated as a single column with some portion of the wall and roof mass, M_1, located at the top. The roof can be treated as a spring (or several springs) with the remaining roof mass, M_2, attached to the spring(s). How much mass to attach to each degree of freedom, and how to determine the stiffness of the roof, are major challenges in this case.

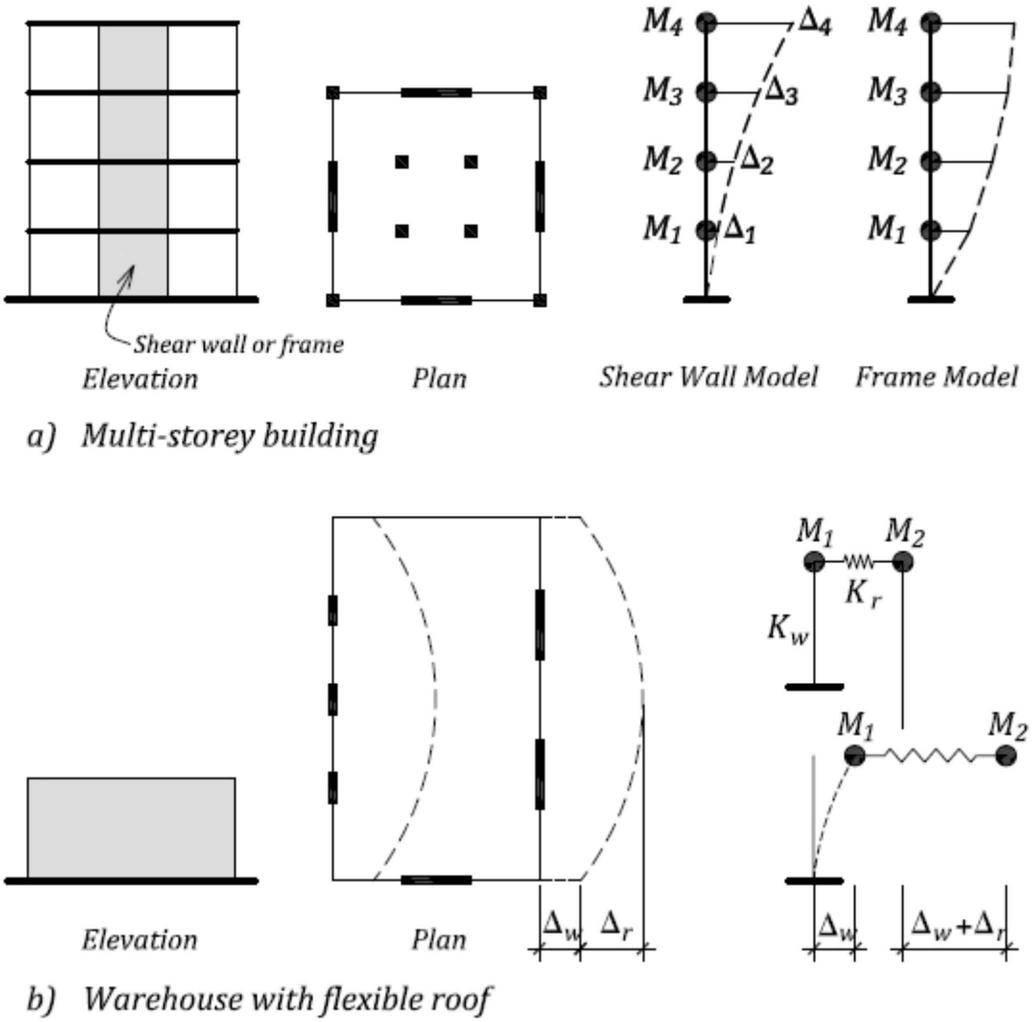

Figure A-6. MDOF systems: a) multi-storey shear wall building; b) warehouse with flexible roof.

A.4.2. Seismic analysis methods

The question of interest to structural engineers is how to determine a realistic seismic response for MDOF systems? The possible approaches are:

- static analysis, and
- dynamic analysis (modal analysis or time history method).

The simplest method is the *equivalent static analysis procedure* (also known as the quasi-static method) in which a set of static horizontal forces is applied to the structure (similar to a wind load). These forces are meant to emulate the maximum effects in a structure that a dynamic analysis would predict. This procedure works well when applied to small, simple structures, and also to larger structures if they are regular in their layout.

NBC 2015 specifies a dynamic analysis as the default method. The simplest type of dynamic analysis is the *modal analysis method*. This method is restricted to linear systems, and consists of a dynamic analysis to determine the mode shapes and periods of the structure, and then uses a response spectrum to determine the response in each mode. The response of each mode is independent of the other modes, and the modal responses can then be combined to determine the total structural response. In the next section, the modal analysis procedure will be explained with an example.

The second type of dynamic analysis is the *time history method.* This consists of a dynamic analysis model subjected to a time-history record of an earthquake ground motion. Time history analysis is a powerful tool for analyzing complex structures and can take into account nonlinear structural response. This procedure is complex and time-consuming to perform, and as such, not warranted for low-rise and regular structures. It requires an advanced level of knowledge of the dynamics of structures and it is beyond the scope of this document. For detailed background on dynamic analysis methods the reader is referred to Chopra (2007).

A.4.3. Modal analysis procedure: an example

Consider a four-storey shear wall building example such as that shown in Figure A-6a). The building can be modelled as a stick model, with a weight, W, of 2,000 kN lumped at each floor level, and a uniform floor height of 3 m (see Figure A-7). For simplicity, the wall stiffness and the masses are assumed uniform over the height. This model is a MDOF system with four degrees of freedom consisting of a lateral displacement at each storey level. A MDOF system has as many modes of vibration as degrees of freedom. Each mode has its own characteristic shape and period of vibration. The periods are given in Table A-1, the four mode shapes are given in Table A-2 and shown in Figure A-7. In this example, the stiffness has been adjusted to give a first mode period of 0.4 seconds, which is representative of a four-storey structure based on a simple rule-of-thumb that the fundamental period is on the order of 0.1 sec per floor. Note that the first mode, also known as the *fundamental mode*, has the longest period. The first mode is by far the most important for determining lateral displacements and interstorey drifts, but higher modes can substantially contribute to the forces in structures with longer periods. In this example the mode shapes have been normalized so that the largest modal amplitude is unity.

For linear elastic structures, the equations governing the response of each mode are independent of the others provided that the damping is prescribed in a particular manner. Thus, the response in each mode can be treated in a manner similar to a SDOF system, and this allows the maximum displacement, moment and shear to be calculated for each mode. In the final picture, the modal responses have to somehow be combined to find the design forces (this will be discussed later in this section). Modal analysis can be performed by hand calculation for a simple structure, however, in most cases, the use of a dynamic analysis computer program would be required.

Knowing the mode shapes and the mass at each level, it is possible to calculate the *modal mass* for each mode, which is given in Table A-1 as a fraction of the total mass of the structure. The modal masses are representative of how the mass is distributed to each mode, and the sum of the modal masses must add up to the total mass. When doing modal analysis, a sufficient number of modes should be considered so that the sum of the modal masses adds up to at least 90% of the total mass. In the example here this would indicate that only the first two modes would need to be considered (0.696 + 0.210 = 0.906).

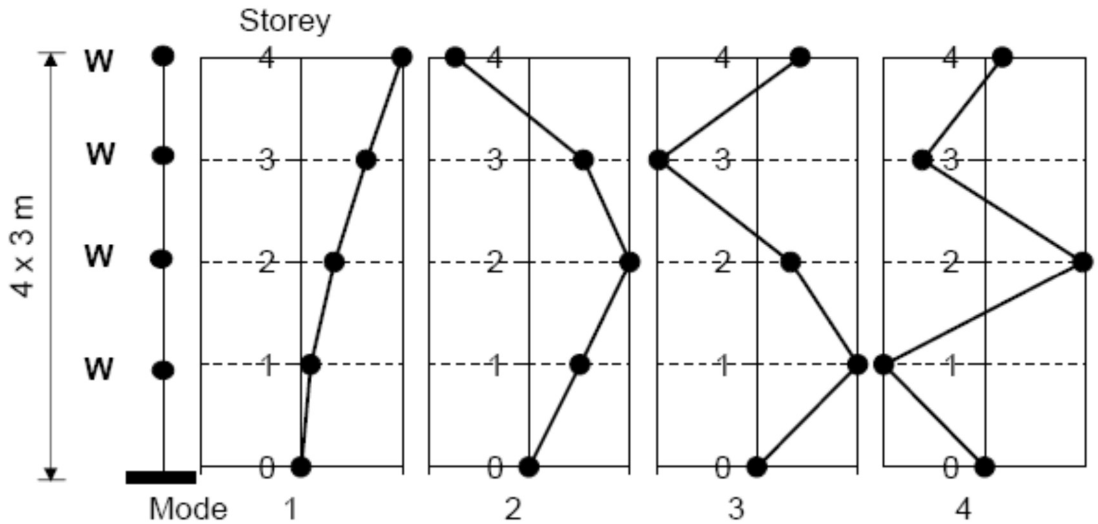

Figure A-7. Four-storey shear wall building model and modal shapes.

As an example of how the different modes can be used to determine the structural response, Figure A-8 shows a typical design acceleration response spectrum which will be used to determine the modal displacements and accelerations. The four modal periods are indicated on the spectrum (note that only the first two periods are identified on the diagram; T_1=0.40 and T_2=0.062 sec) and the spectral acceleration S_a at each of the periods is given in Table A-3.

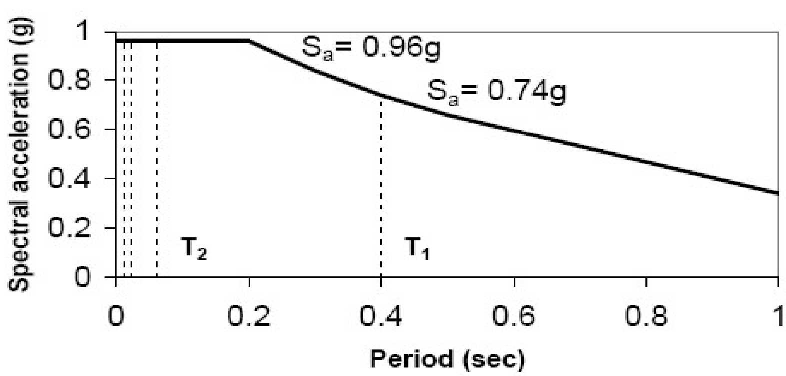

Figure A-8. Design acceleration response spectrum.

A very useful feature of the modal analysis procedure is that it gives the base shear in each mode as a product of the modal mass and the spectral acceleration S_a for that mode, as shown in Table A-3. For example, the base shear for the first mode is equal to (8000kN x 0.696) x 0.74 = 4127 kN). Note that the spectral acceleration is higher for the higher modes, but because the modal mass for these modes is smaller, the base shear is smaller. The inertia forces from each floor mass act in the same directions as the mode shape, that is, some forces are positive while others are negative for the higher modes (refer to mode shapes shown in Figure A-7). It can be seen from the figure that the forces from the first mode all act in the same direction at the same time, while the higher modes will have both positive and negative forces. Thus, the base shear from the first mode is usually larger than that from the other modes.

The modal base shears shown in Table A-3 are the maximum base shears for each mode. It is very unlikely that these forces will occur at the same time during the ground shaking, and they could have either positive or negative signs. Summing the contribution of each mode where all values are taken as positive, known as the absolute sum (ABS) method, produces a very high upper bound estimate of the total base shear. Statistical analyses have shown that the square-root-of-the-sum-of-the squares (RSS) procedure, where the contribution of each mode is squared, and the square root is then taken of the sum of the squares, gives a reasonably good estimate of the modal sum, especially if the modal periods are widely separated.

Table A-3 shows the base shear values estimated by the two methods and gives an indication of the conservatism of the ABS method for this case (total base shear of 6,462 kN), where the modal periods are widely separated, and use of the RSS method is appropriate since it gives a lower total base shear value of 4,468 kN. Note that there is a third method that is incorporated in many modal analysis programs called the complete-quadratic-combination (CQC) method. This method should be used if the periods of some of the modes being combined are close together, as would be the case in many three-dimensional structural analyses, but for most structures with well-separated periods and low damping, the result of the RSS and CQC methods will be nearly identical (this is true for most two-dimensional structural analyses).

The amplitude of displacement in each mode is dependent upon the spectral acceleration for that mode and its *modal participation factor*, which is a measure of the degree to which a certain mode participates in the response. The value of the modal participation factor depends on how the mode shapes are normalized, and so will not be given here, however the values are smaller for the higher modes with the result that the displacements for the higher modes are generally smaller than those of the first mode. The modal displacements are presented in Table A-4 (to three decimal places, which is why some values are shown as zero) and plotted in Figure A-9 for the first two modes as well as the RSS value. In this example, the influence of the two highest modes is very small and has been omitted from the diagram. It is difficult to distinguish between the first mode displacements and the RSS displacements in Figure A-9; this is characteristic of structures with periods less than about 1 second, such as would be the case for most masonry structures.

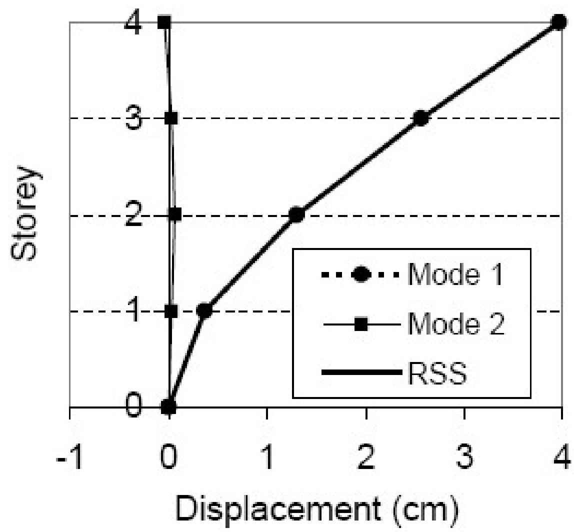

Figure A-9. Modal displacements.

Modal analysis gives the modal shears and bending moments in each member and these values can be used to generate the shear and moment diagrams. These are summarized in Tables A-5 and A-6 and are graphically presented in Figure A-10. Only the results from the first two modes are shown as the higher modes contribute very little to the response. Except for some contribution to the shears, the second mode is insignificant in contributing to the total values calculated using the RSS method.

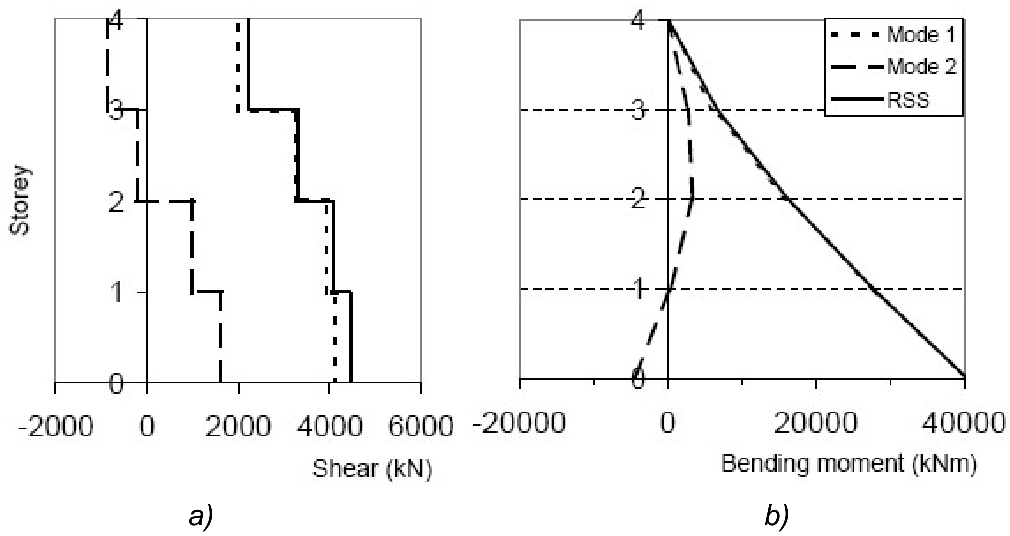

Figure A-10. Modal analysis results: a) shear forces; b) bending moments.

The inertia force at each floor for each mode can be determined by taking the difference between the shear force above and below the floor in question. Modal inertia forces along with the RSS values are summarized in Table A-7, and show that the higher modes at some levels contribute more than the first mode. Note that the sum of the inertia forces for each mode is equal to the base shear for that mode. However, the sum of the RSS values of the floor forces at each level is 6284 kN (obtained by adding values for storeys 1 to 4 in the last column of the table); this is not equal to the total base shear of 4468 kN found by taking the RSS of the base shears in each mode (see Table A-3). This demonstrates the key rule in combining modal responses: **only primary quantities from each mode should be combined**. For example, if the designer is interested in the shear force diagram for the structure, it is necessary to find the shear forces in each mode and then combine these modal quantities using the RSS method. It is incorrect to find the total floor forces at each level from the RSS of individual modal values, and then use these total forces to draw the shear diagram. Even interstorey drift ratios, defined as the difference in the displacement from one floor to the next divided by the storey height, should be calculated for each mode and then combined using the RSS procedure. It would be incorrect to divide the total floor displacements by the storey height; although in this example since the deflection is almost entirely given by the first mode, this approach would be very close to that found using the RSS method.

One of the disadvantages of modal analysis is that the signs of the forces are lost in the RSS procedure and so equilibrium of the final force system is not satisfied. Equilibrium is satisfied in each mode, but this is lost in the procedure to combine modal quantities since each quantity is squared. That is why it is important to determine quantities of interest by combining only the original modal values.

A.4.4. Comparison of static and modal analysis results

The equivalent static force analysis procedure, which will be presented in more detail in Section 1.6, has been applied to the four-storey structure described above for the spectrum shown in Figure A-8. Table A-8 compares the results of the two types of analyses. It can be seen that both the base shear and moment given by the modal analysis method is about 75% of that given by the static method. This occurs with short period MDOF structures that respond in essentially the first mode because the modal mass of the first mode for walls is about 70 to 80% of the total mass. The top displacement from the modal analysis is 78% of the static displacement, nearly the same as the ratio of the base moments; this would be expected given that the deflection is mostly tied to the moment.

If the structure is a single-storey, SDOF system, the two analyses methods will give the same result. But for MDOF systems, such as two-storey or higher buildings, dynamic analysis will generally result in smaller forces and displacements than the static procedure.

The floor forces from the two analyses are quite different. The floor forces in the upper storeys obtained by modal analysis are less than the static forces, but in the lower storeys, a reverse trend can be observed. The reason for this is the contribution of the higher modes to the floor forces. It can be seen in Table A-7, that at the 2nd storey, the second mode contribution is the largest of all the modes. To ensure the required safety level when seismic design is performed using the equivalent static analysis procedure, NBC 2015 seismic provisions (e.g. Clause 4.1.8.15) provides additional guidance on the level of floor forces to be used in connecting the floors to the lateral load resisting elements.

Table A-1. Modal Periods and Masses

Mode	Period (sec)	Modal mass/ Total mass
1	0.400	0.696
2	0.062	0.210
3	0.022	0.070
4	0.012	0.024
Sum		1.000

Table A-2. Mode Shapes

Storey	Mode Shapes			
	1st mode	2nd mode	3rd mode	4th mode
0	0.000	0.000	0.000	0.000
1	0.093	0.505	1.000	-1.000
2	0.328	1.000	0.334	0.969
3	0.647	0.544	-0.972	-0.619
4	1.000	-0.727	0.427	0.175

Note: mode shapes are normalized to a maximum of 1

Table A-3. Spectral Accelerations, S_a, and Base Shears

Mode	Period (sec)	Spectral Acceleration S_a (g)	Modal mass / Total mass	Base Shear (kN)
1	0.400	0.74	0.696	4127
2	0.062	0.96	0.210	1617
3	0.022	0.96	0.070	534
4	0.012	0.96	0.024	184
Total base shear ABS				6462
Total base shear RSS				4468

Note: total weight = 8000 kN

Table A-4. Modal Displacements

Storey	Modal Displacements (cm)				RSS
	1st mode	2nd mode	3rd mode	4th mode	
Base	0.000	0.000	0.000	0.000	0.00
1	0.367	0.021	0.002	0.000	0.37
2	1.300	0.042	0.001	0.000	1.30
3	2.564	0.023	-0.002	0.000	2.56
4	3.963	-0.031	0.001	0.000	3.96

Table A-5. Modal Shear Forces

Storey	Shear Forces (kN)				RSS
	1st mode	2nd mode	3rd mode	4th mode	
0-1	4127	1617	534	-184	4468
1-2	3942	999	-143	204	4074
2-3	3287	-224	-369	-172	3320
3-4	1996	-888	289	68	2205

Table A-6. Modal Bending Moments

Storey	Bending Moments (kNm)				RSS
	1st mode	2nd mode	3rd mode	4th mode	
Base	40053	-4511	-931	255	40320
1	27675	339	670	-298	27686
2	15849	3335	240	313	16201
3	5988	2665	-867	-204	6614
4	0	0	0	0	0

Table A-7. Modal Inertia Forces (Floor Forces)

Storey	Floor Forces (kN)				RSS
	1st mode	2nd mode	3rd mode	4th mode	
1	185	618	677	-388	1012
2	655	1223	226	376	1455
3	1291	665	-658	-240	1612
4	1996	-888	289	68	2205
Sum	4127	1617	534	-184	4468

Table A-8. Comparison of Static and Dynamic Analyses Results

Storey	Shear Forces (kN)		Floor Forces (kN)		Moments (kNm)		Deflections (cm)	
	Static	Modal(1)	Static	Modal(2)	Static	Modal(3)	Static	Modal(4)
Base			0	0	53280	40320	0	0
	5920	4468						
1			592	1012	35520	27686	0.48	0.37
	5328	4074						
2			1184	1455	19536	16201	1.70	1.30
	4144	3320						
3			1776	1612	7104	6614	3.32	2.56
	2368	2205						
4			2368	2205	0	0	5.11	3.96

Notes: (1) see Table A-5, last column
(2) see Table A-7, last column;
(3) see Table A-6, last column;
(4) see Table A-4, last column.

TABLE OF CONTENTS – APPENDIX B

B	**RELEVANT RESEARCH STUDIES AND CODE BACKGROUND**	**B-2**
B.1	**Shear/Diagonal Tension Resistance**	**B-2**
B.2	**Sliding Shear Resistance**	**B-8**
B.3	**Ductile Seismic Response of Reinforced Masonry Shear Walls**	**B-12**
B.4	**Wall Height-to-Thickness Ratio Restrictions**	**B-16**

B Relevant Research Studies and Code Background

This appendix contains additional background material relevant to the aspects of masonry design discussed in Chapter 2. Findings of some relevant research studies, as well as the discussion on provisions of masonry design codes from other countries, are included. This information may be useful to readers interested in gaining a more detailed insight into the subject. However, it should be noted that designers may use alternative design provisions in situations where CSA S304 is silent on a specific issue. The design provisions contained in design standards from other countries cannot supersede the provisions of pertinent Canadian standards.

B.1 Shear/Diagonal Tension Resistance

The CSA S304 shear strength design equation for RM shear walls was first included in the 1994 version of the standard (CSA S304.1-94) and it is largely based on the research performed in 1970s and 1980s, e.g. research program by the US-Japan Joint Technical Coordinating Committee for Masonry Research (TCCMAR). Numerous experimental studies on RM shear walls subjected to reversed cyclic loading conducted since the 1990's provide additional data for developing new or revised shear strength design equations.

The CSA S304 shear strength equation was evaluated by several researchers, including Seif ElDin and Galal (2015a); El-Dakhakhni et al. (2013); Davis et al. (2010); Voon and Ingham (2007). Davis et al. (2010) compared the estimated shear strength predictions based on 8 different code expressions (including the CSA S304.1-04) with the results from 56 tests of fully grouted RM shear walls with shear dominated response. The average ratio of the test strength to the estimated strength for the CSA S304 expression was 1.50 with a Coefficient of Variation (COV) of 0.15; this is considered a rather conservative prediction.

El-Dakhakhni et al. (2013) tested 8 fully grouted cantilever RM shear wall specimens with shear dominated behaviour subjected to reversed cyclic loading. The specimens were squat walls with aspect ratio ranging from 0.6 to 1.5, were characterized by horizontal reinforcement ratios of 0.07 to 0.13%, and the level of applied axial stress varied from 0 to approximately $0.08xf'_m$. The study examined the effectiveness of design shear strength expressions included in the Canadian (CSA S304.1-04), US (TMS 402/ACI 530/ASCE 5-11), New Zealand (NZS 4230:2004) and European (Eurocode 6) masonry design codes. The results demonstrated that the CSA S304.1-04 produced the most conservative predictions of all the codes (mean experimental/calculated ratio = 1.51 and COV= 18.1%). Shear strength predictions based on international masonry codes, especially the US TMS 402/602 code (mean= 1.14 COV= 12.7%) and New Zealand code NZS 4230:2004 (mean= 1.13 COV= 16.9%) gave a better fit of the experimental results.

El-Dakhakhni et al. (2013) also observed that the shear strength expression of the Canadian concrete design standard CSA A23.3-04, based on the Simplified Modified Compression Field Theory (SMCFT) approach (Bentz et al. 2006), gave the most accurate prediction of shear strength for squat walls (mean= 1.06 COV= 10.8%). The underlying theory is the Modified Compression Field Theory developed in the 1980s (Vecchio and Collins,1986), which has been referred to as the General Method for Shear Design of RC flexural members in Canada (CSA A23.3-04). The same approach was adopted for the design of RM beams in Canada in CSA S304-14 (Cl.11.3.4). The design equations are similar to CSA A23.3-04, but the input parameter values were calibrated for masonry design purposes. Also, a new parameter K_b has been introduced to take into account the level of grouting and type of masonry units. This is based on the research by Sarhat and Sherwood (2010; 2013), which included the results of their own experimental studies and a survey of the experimental data by other researchers.

The New Zealand Masonry Standard NZS 4230:2004 (SANZ, 2004) states that the axial load contribution to masonry shear resistance in squat shear walls is equal to $0.9N\tan\alpha$. This contribution results from a diagonal strut mechanism, which is based on an assumption that axial compression load N forms a compression strut at an angle α to the vertical axis (see Figure B-1). The axial load must be transmitted through the flexural compression zone, while the horizontal component of the strut force resists the applied shear force (Priestley et al., 1994). This model implies that the shear strength of squat walls under axial loads should be greater than that of more slender walls, and higher than that prescribed in CSA S304-14. According to this model, the axial load contribution is limited to $N \leq 0.1f'_m A_g$.

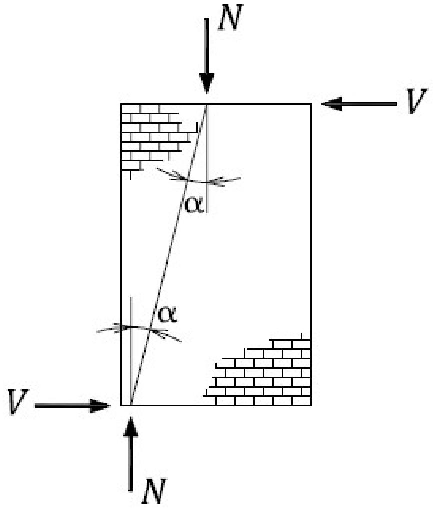

Figure B-1. Contribution of axial load to wall shear strength (reproduced from NZS 4230:2004 with the permission of Standards New Zealand under License 000725).

The shear strength equation in the US masonry design code TMS 402/602-16 (previous versions were labelled as TMS 402/ACI 530/ASCE 5) was derived from research dating back to the 1980s (Shing et al. 1990a; 1990 b). The equation has been evaluated by several researchers, including Alogla et al. (2014); Davis et al. (2010); and Voon and Ingham (2007). Davis et al. (2010) compared the estimated shear strength predictions based on the TMS 402/602 expression with the results from 56 tests of fully grouted RM shear walls with a shear dominated response. The average ratio of the test strength to the estimated strength was 1.17 with a COV of 0.15, indicating that the expression is somewhat conservative. Alogla et al. (2014) also examined the TMS 402/602 shear strength expression predictions for more than 60 walls from literature. It was observed that the shear strength calculated using the TMS 402/602 design expression overestimated the shear strength of the examined walls by about 10%.

Several design factors influence the shear/diagonal tension resistance of RM walls. A brief overview of the available experimental research evidence on RM shear walls subjected to reversed cyclic loading related to these factors is discussed below. El-Dakhakhni and Ashour (2017) performed a detailed review of past experimental studies on the subject.

Axial compression:

An experimental study on 16 fully grouted RM wall specimens examined the effect of axial stress on the wall's shear resistance (Shing et al., 1989). The axial stress ranged from 0 to approximately 0.1xf'_m. The results indicated that the load at the first diagonal crack increased with the applied axial load. The study also demonstrated that an increasing axial load could result in a change in the failure mechanism from a flexural/shear mode to a brittle shear mode.

An experimental study on RM wall specimens by Voon and Ingham (2006) showed that a relatively moderate increase in axial compression stress level from 0 to 0.025xf'_m resulted in an increase in the maximum wall shear resistance of more than 20%. However, RM walls subjected to higher axial compression had a reduced post-cracking deformation capacity, resulting in a more brittle response. Ibrahim and Suter (1999) tested 5 squat RM shear walls under reversed cyclic loading (aspect ratio ranged from 0.47 to 1.0) and observed that the level of applied axial stress has a significant effect on the shear capacity.

Wall aspect ratio (squat shear walls):

The findings of several experimental studies, e.g. Matsumura (1987), Okamoto et al. (1987), and Voon (2007), confirmed that RM walls with lower aspect ratios exhibited shear strengths that were larger than more slender masonry walls. The researchers concluded that the shear strength enhancement was due to the more prominent role of arching action in RM walls with low aspect ratios, in which shear was mainly resisted by compression struts (see Figure 2-16a). Voon and Ingham (2006) reported that the shear resistance decreased by 15% when the wall aspect ratio increased from 1.0 to 2.0. A squat wall specimen with an aspect ratio of approximately 0.6 showed a significant increase in shear resistance (by over 100%) compared to an otherwise similar specimen with an aspect ratio of 1.0. The findings of an experimental study by Okamoto et al. (1987) confirmed that the wall shear strength increased by 20 % when the aspect ratio decreased from 2.3 to 1.6, and by 30 % when aspect ratio decreased from 2.3 to 0.9. A study on partially grouted RM walls by Schultz (1996) showed that a decrease in the wall aspect ratio was reported to have a beneficial effect on the shear resistance, that is, squat walls are expected to have larger shear resistance than flexural walls of the same height. However, squat wall specimens also showed a reduced deformation capacity and increased strength deterioration.

A few studies on RM squat shear walls subjected to reversed cyclic loading were performed in Canada (Seif ElDin and Galal, 2015b; 2016a; 2016b; 2017; El-Dakhakhni et al., 2013). The results confirmed the findings of other studies with regard to the shear strength of squat RM shear walls.

Horizontal reinforcement:

Shing et al. (1989) concluded that horizontal reinforcement influences the post-cracking response of RM walls. The study included 8 walls that failed in a shear dominated mode. and had horizontal reinforcement ratios ranging from 0.12 to 0.22 %. The onset of cracking (occurrence of the first major diagonal crack) depends primarily on the tensile strength of the masonry and the applied axial load. However, increasing the amount of horizontal reinforcement caused a change in the failure mechanism from a brittle shear mode to a ductile flexural mode.

Sveinsson et al. (1985) tested 10 RM piers (a double curvature loading condition) and varied the amount of horizontal reinforcement from 0.075 to 0.394%. They concluded that the horizontal reinforcement was effective in increasing shear strength, but higher amounts of reinforcement did not correspond to a proportional gain in strength. For example, a 16% increase in the shear strength was observed in a specimen which had twice the amount of horizontal reinforcing bars compared to an otherwise similar specimen.

Shear reinforcement in RM shear walls does not seem to be as effective as in RC shear walls. A possible explanation is that the reinforcing bars located where the inclined crack crosses near the end of the bar are unable to develop their full yield strength in the masonry walls. To account for this phenomenon, the New Zealand Masonry Standard NZS 4230:2004 (SANZ, 2004) prescribes a coefficient of 0.8 in the V_s equation, while CSA S304-14 uses a 0.6 factor. This phenomenon is particularly pronounced in short walls, where it is likely that the length of the shear reinforcement is insufficient to fully develop its yield strength.

Seif ElDin and Galal (2015b) tested 9 squat RM walls under quasi-static cyclic loading. Contrary to the previous experimental studies, they observed that the horizontal reinforcement contributes to the wall shear resistance with its full yield capacity (there is no reduction coefficient as discussed above). This can be explained by the redistribution in the shear resistance between the reinforcement and the masonry, especially at high ductility demands. Most previous researchers quantified shear contribution of reinforcement based on the difference between the shear capacities of specimens with different transverse reinforcement ratios.

It appears that horizontal reinforcement in RM shear walls does not have as good anchorage as the corresponding reinforcement in RC shear walls. Anderson and Priestley (1992) have noted that straight bars or 90° hooks were used in some experimental studies (see Figure B-2a), whereas the horizontal reinforcement in RC shear walls is usually anchored in a more effective way, such as by 180° hooks. The type and extent of anchorage are expected to influence the effectiveness of shear reinforcement. Sveinsson et al. (1985) tested 10 fully grouted RM piers and studied (among other factors) the effect of anchorage conditions in horizontal reinforcement (90° versus 180° hooks). They recommended the use of 180° hooked end anchorage for horizontal reinforcement because it produced better energy dissipation, and enabled the bars to develop their full tensile strength This is particularly true for shorter walls/piers.

Seif ElDin and Galal (2016a) tested 3 squat RM wall specimens with shear dominant behaviour under reversed cyclic loading. The specimens were identical, except for the end anchorage of the horizontal reinforcing bars: the first specimen had 180° hooks, the second one 90° hooks, and the third one had straight bars (no hooks). The results showed that the specimen with 180° hooks provided the most effective anchorage and attained the largest shear capacity and displacement ductility, while the specimen with straight bars attained the smallest shear capacity and displacement ductility. However, the difference in the strength values was not significant (it was within 10%). The most significant difference was in the post-peak behaviour. The specimen with straight bars showed the most rapid post-peak degradation of the lateral load resistance. The 180° hooks proved to be effective in providing confinement for the vertical end bars in the wall, while the 90° hooks were less effective. For that reason, displacement ductility of the specimen with 180° hooks (4.2) was higher than the specimen with 90° hooks (3.9) and the one with straight bars (3.6). This difference again indicates the superior ductility potential of the 180° end hooks, but the other anchorage conditions may be acceptable in some cases. The researchers recommended the use of horizontal reinforcing bars with 90° hooks for masonry structures located in regions of low to moderate seismic hazard, and/or outside the plastic hinge regions in ductile shear walls.

Vertical reinforcement:

Anderson and Priestley (1992) found that shear strength didn't show any correlation with the vertical reinforcement ratio, hence the CSA S304 shear design equation ignore the effect of vertical reinforcement. However, according to some researchers (Shing et al., 1990; Tomazevic, 1999; Voon, 2007), a fraction of the wall shear resistance can be attributed to the presence of vertical reinforcement. Dowel action in vertical reinforcing bars enables shear transfer across a diagonal crack by the localized kinking in reinforcing bars due to their relative displacement (see Figure B-2b) (note that compression kinks cancel out some of the tension kinks). However, once the vertical reinforcement yields, as it would in the plastic hinge zone of ductile walls, its contribution to the shear resistance drops significantly and could be ignored.

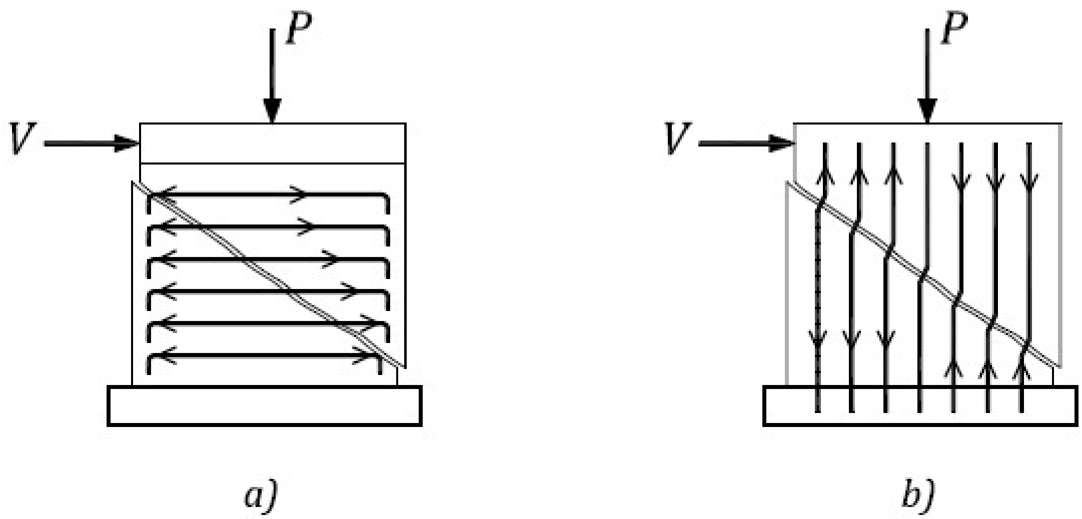

Figure B-2. Wall reinforcement contributing to shear resistance: a) horizontal reinforcement acting in tension; b) dowel action in vertical reinforcement (Tomazevic, 1999, reproduced by permission of the Imperial College Press).

Ductility:

Experimental studies on RM shear walls with shear dominant behaviour (aspect ratio less than 2.0) have demonstrated that significant levels of ductility and energy dissipation capacity are possible in these walls (Sveinsson et al. 1985; Shing et al. 1989; Voon and Ingham 2006; El-Dakhakhni et al. 2013). Shing et al. (1989) observed that the displacement ductility ratio tends to increase with an increase of axial load for the shear dominated specimens. They attributed the increased ductility level to the aggregate interlock forces which are enhanced by the increase of axial load.

It has been recognized that shear degradation at higher ductility demands occurs in shear-dominated RM walls. In their empirical equation which estimates the shear strength of RM shear walls, Anderson and Priestley (1992) proposed factor *k* to account for the degradation of the shear resistance provided by masonry for the inelastic response when the displacement ductility ratio increases from 2.0 to 4.0. The value decreases linearly from 1.0 to 0 as the displacement ductility ratio increases from 2.0 to 4.0.

Grouting:

Experimental studies have reported a significant reduction in the shear resistance of partially grouted walls compared to otherwise identical fully grouted walls. Brzev (2011) performed a review of available experimental data related to the subject. The review included 29 partially grouted RM wall specimens tested in the period from 1978 to 2010, including Nolph (2010); Nolph and ElGawady (2012); Elmapruk (2010); Minae et al. (2010); Maleki (2008); Maleki et al. (2009); Voon (2007a); Schultz (1996); and Chen et al. (1978). Most specimens (24 out of 29) were squat RM walls and had a horizontal reinforcement ratio of 0.07% or higher and 180° hooks. All specimens had a vertical reinforcement ratio of 0.07% or higher, while 15 out of 29 specimens had a vertical reinforcement ratio of 0.3% or higher.

Lateral load resisting mechanisms for lightly reinforced partially grouted RM shear walls are significantly different than for fully grouted walls. Research evidence related to the seismic response of partially grouted walls consists primarily of experimental studies where individual wall specimens were subjected to quasi-static cyclic loading, although there are also a few shake-table studies.

Most research studies on specimens subjected to quasi-static cyclic loading report shear dominated mechanism of seismic response characterized by stair-stepped and/or diagonal tension cracks in the masonry panels enclosed by grouted bond beams and vertical cells. These cracks are indicative of the formation of compression struts within the panel. The failure is often accompanied by spalling of face shells in the block units (Nolph, 2010).

In general, the response of tested specimens to the cyclic loads was reasonably stable. None of the specimens displayed a sudden failure, and the resistance gradually deteriorated with progressively increasing cyclic loading.

Most specimens achieved a displacement ductility ratio of 2.0 or higher, except for the specimens tested by Nolph (2010) and Elmapruk (2010), which were characterized by relatively high vertical reinforcement ratios (0.46% for the Nolph specimens and 0.33% for the Elmapruk specimens). It was observed that the displacement ductility ratio decreased with an increase in the vertical reinforcement ratio. The specimens tested by Voon (2007a) also showed a ductility ratio of less than 2.0, but these specimens had no horizontal reinforcement.

Schultz (1996) tested a series of 6 partially grouted RM wall specimens under in-plane cyclic loads. Only the outermost vertical cores and a single course bond beam at midheight were grouted. The mechanism of shear resistance in the tested walls was characterized by the development of vertical cracks between the ungrouted and grouted masonry due to stress concentrations or planes of weakness (this mechanism is different from the one expected to develop in solidly grouted RM walls). It was also reported that an increase in horizontal reinforcement ratio did not have a significant effect on the overall shear resistance.

An experimental study by Voon and Ingham (2006) showed that the shear strength of a solidly grouted wall specimen was approximately 110% higher than an otherwise identical specimen with 30% grouted cores. Also, the specimen with 55% grouted cores had a shear strength more than 50% higher than the specimen with 30% grouted cores. However, the difference decreases when the shear stress is compared using the net wall area.

Ingham et al. (2001) reported the results of an experimental study on 12 full-scale RM squat wall specimens subjected to in-plane cyclic lateral loading (aspect ratios ranged from 0.57 to 1.33). Of the twelve specimens, nine were partially grouted, and three were fully grouted. The walls were designed to fail in the diagonal tension shear mode. The test results showed that the fully grouted RM wall specimens demonstrated significantly higher displacement ductility (on the order of 6.0) than the displacement ductility of otherwise identical partially grouted specimens (about 4.0) It should be noted that all partially grouted specimens achieved a displacement ductility of 2.0 or higher. A possible reason for the higher ductility in the fully grouted RM wall specimens is that they ultimately failed in a sliding shear mode, which is characterized by large deformations at the base of the wall. The partially grouted specimens failed in the diagonal tension mode. Force-displacement responses for a partially grouted Wall 2 and a fully grouted Wall 3 specimen are shown in Figure B-3 (the specimens were otherwise similar, except for the grouting pattern).

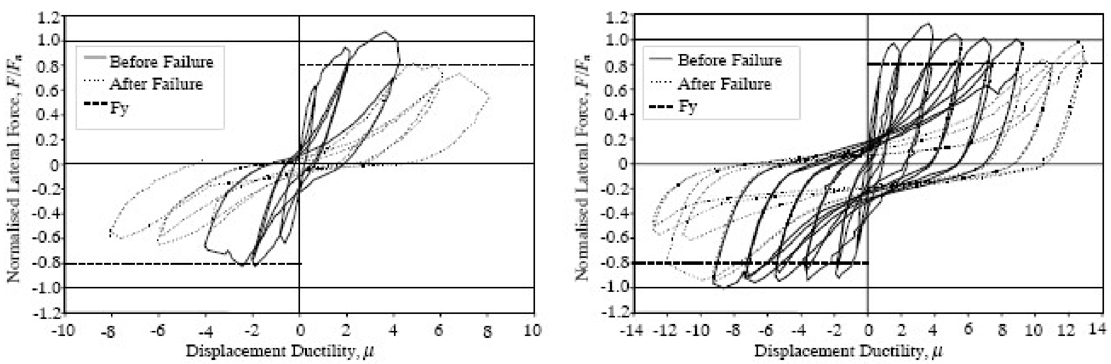

(a) Wall 2, 2600 x 2400 x 100, Partial Grout-filled

(b) Wall 3, 2600 x 2400 x 100, Solid Grout-filled

Figure B-3. Force-displacement responses for partially grouted (left) and fully grouted (right) wall specimens (Ingham et al., 2001, reproduced by permission of the Masonry Society).

B.2 Sliding Shear Resistance

Sliding shear resistance according to the CSA S304-14 standard has been determined based on friction resistance from Coulomb's Law, as discussed in Section 2.3.3. However, a sliding shear mechanism is also characterized by sliding displacements along the sliding interface (usually base of the wall). In long walls with openings consisting of several interconnected piers, sliding movements at the base of one pier might cause damage in the adjacent piers. However, current international masonry design codes, including CSA S304-14, do not contain provisions for estimating sliding displacements in the walls or corresponding displacement limits. Centeno (2015) studied sliding failure mechanisms in RM shear walls and estimated sliding displacements due to lateral loading. He proposed a Sliding Shear Behavior (SSB) method for estimating the base sliding displacements in RM shear walls (Centeno, 2015; Centeno et al., 2015). This section summarizes the method, which can be applied through a step-by-step process. The objective of the process is to determine: 1) the wall's yield mechanism, and 2) the magnitude of sliding displacements that occur in that mechanism. There are two principal yield mechanisms associated with sliding shear (Figure B-4): a) a sliding shear mechanism and b) a combined flexural-sliding shear mechanism. The sliding shear mechanism occurs when the lateral force, V, is equal to or greater than the sliding shear resistance of the RM wall, where the sliding displacements develop at the base of the wall. The combined flexural-sliding shear mechanism occurs when the RM wall yields in flexure and forms an open flexural crack along the wall length. Inelastic displacements in the wall are equal to the sum of flexural and shear displacements.

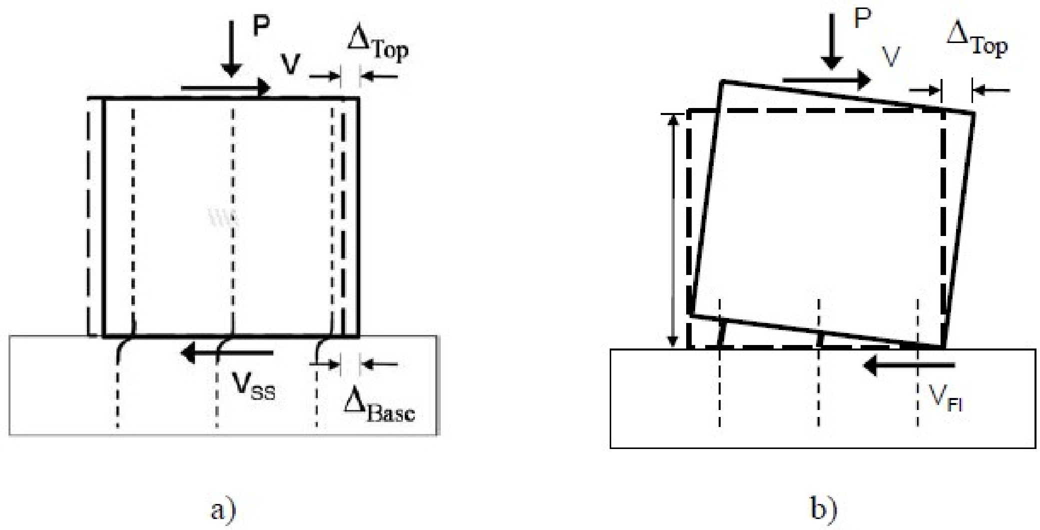

Figure B-4. Yield mechanisms in RM shear walls subjected to monotonic lateral loading: a) sliding shear mechanism and b) flexural yield mechanism (Centeno, 2015).

For displacement estimation purposes, Centeno (2015) identified three yield mechanisms that lead to sliding displacements: i) Sliding Shear (SS) mechanism, ii) Combined Flexural-Sliding Shear (CFSS) mechanism, and iii) Sliding Failure (SF) mechanism. These mechanisms are based on the two mechanisms illustrated in Figure B-4. The SS mechanism is illustrated in Figure B-4a), while the remaining two mechanisms (CFSS and SF) are variants of mechanism shown in Figure B-4b). In RM walls that experience a SS mechanism, sliding displacements occur when an applied lateral force exceeds the wall's sliding shear resistance. In the walls that experience a CFSS or a SF mechanism, sliding displacements are the result of dowel deformations that occur in order for dowel action to transfer shear across an open flexural crack during cyclic loading. In a CFSS mechanism, displacements are elastic but influenced by degradation in dowel action shear stiffness, while in a SF mechanism, the displacements are inelastic and occur when the applied shear force exceeds the dowel action yield resistance.

The procedure for estimating sliding displacements according to the SSB method is presented below.

Part 1: Determine the Wall's Yield Mechanism

Step 1: Determine the plastic moment resistance, M_p, and its corresponding lateral force resistance, V_{Fl}.

Step 2: Establish the Upper Bound Sliding Shear Resistance, V_{SS_U}:

$$V_{SS_U} = Fr_A + Fr_{Fl_U} + DA_y \tag{B.1}$$

$$Fr_A = \mu_{Fr} P, \text{ where } \mu_{Fr} \leq 0.6 \tag{B.2}$$

$$Fr_{Fl_U} = \mu_{Fr}\left[0.9\left(\frac{1-\frac{c}{L}-\frac{d'}{L}}{1+\frac{s}{L}-2\frac{d'}{L}}\right)\right]A_s f_y \tag{B.3}$$

$$DA_y = \left(C_{DA}\sqrt{f'_g f_y}\right) A_s \quad \text{(B.4)}$$

$$C_{DA} = \begin{cases} 2.2, & H/L \leq 0.5 \\ \left[2.2 - 2\left(\frac{H}{L} - 0.5\right)\right], & 0.5 < H/L < 1.0 \\ 1.2, & H/L \geq 1.0 \end{cases} \quad \text{(B.5)}$$

where:

d':	masonry cover	s:	rebar spacing
f'_g:	masonry grout compression strength (MPa)	f_y:	reinforcing steel yield stress
A_s:	total area of reinforcing steel	P:	axial compression force
μ_{Fr}:	friction coefficient, (μ_{Fr} = 0.6)	c:	depth of compression zone
H:	wall height	L:	wall length
H/L:	height to length aspect ratio		
Fr_A:	friction force due axial compression	$Fr_{Fl_{II}}$:	friction force due to flexural compression (upper bound)
DA_y:	dowel action yield resistance	C_{DA}:	dowel action strength coefficient

Step 3: Determine if the yield mechanism is a Sliding Shear (SS) Mechanism:
If $V_{SS_U} < V_{Fl}$, then yield mechanism is Sliding Shear Mechanism. Continue to Part II, Step A1.
If $V_{SS_U} \geq V_{Fl}$, then yield mechanism is not Sliding Shear Mechanism. Continue to Step 4.

Step 4: Calculate the overturning moment, M_o, and corresponding lateral force, Vo, required to close flexural crack during cyclic loading:
4.1: Determine the overturning moment, M_o:

$$M_o = C_M A_s f_y L \quad \text{(B.6)}$$

$$C_M = 0.21\left(1 + \frac{S}{L}\right)\left(1 - \frac{P}{A_s f_y}\right)$$

$$V_o = M_o / H \quad \text{(B.7)}$$

where:

M_o: overturning moment to close flexural crack
C_M: overturning moment coefficient
V_o: lateral force to close flexural crack

Step 5: Determine if yield mechanism is Sliding Failure Mechanism
If $DA_y < V_o$, then yield mechanism is Sliding Failure Mechanism. Must increase the wall's dowel resistance, DA_y, and return to step 1.
If $DA_y > V_o$, then yield mechanism is not Sliding Failure Mechanism. Continue to Step 6.

Step 6: Determine if yield mechanism is a Combined Flexural Sliding Shear (CFSS) Mechanism.
6.1: Calculate the upper limit aspect ratio, TAR2, for which a wall develops a CFSS mechanism.

$$TAR2 = 0.8\left[1 + C_M\sqrt{\frac{f_y}{f'_g}}\right] \quad \text{(B.8)}$$

If H/L < TAR2 then yield mechanism is CFSS Mechanism. Continue to Part II, Step B1.

If H/L ≥ TAR2 then yield mechanism is a Flexural Mechanism. Sliding displacements in the wall design will be small. If necessary, the sliding displacements can be measured by continuing to Part II, Step B1.

Part II: Estimate the Sliding Displacements

Step A: Estimate sliding displacements for a SS mechanism

A1: Calculate the upper limit aspect ratio, TAR1, for which a wall develops a SS mechanism.
TAR1 = H/L (when $V_{Fl} = V_{SS_U}$) (B.9)
(Note: Calculating TAR1 requires trying multiple values of H/L until finding the aspect ratio that meets the condition in equation B.9)
A2: Calculate the friction from flexural compression, Fr_{Fl},
This is a correction of the friction force component that corresponds to flexural yielding, because in a wall that develops a sliding shear mechanism not all of the tension reinforcement will reach its yielding stress due to flexure. Therefore, the friction force, Fr_{Fl}, is only a fraction of the upper bound friction force, Fr_{Fl_U}, determined in step 2.

$$Fr_{Fl} = \left(\frac{H/L}{TAR1}\right)^2 Fr_{Fl_U} \tag{B.10}$$

A3: Determine sliding shear resistance, V_{SS}, due to a SS mechanism:

$$V_{SS} = Fr_A + Fr_{Fl} + DA_y \tag{B.11}$$

A4: Calculate wall lateral stiffness, K_{shear},
Following the recommended empirical equation by Shing et al. (1990) for the lateral stiffness of a wall with a shear-dominant response:

$$K_{shear} = \left(0.2 + 0.1073\frac{P}{Lt}\right)K_e \tag{B.12}$$

$$K_e = \frac{E_m Lt}{2.4H(1+\upsilon)} \tag{B.13}$$

where:

K_e:	elastic shear stiffness	E_m:	Elastic Modulus of Masonry
K_{shear}:	post-cracking shear stiffness	υ:	Poisson ratio, (for Masonry, υ = 0.2)
t:	wall thickness		

A5: Sliding Displacement Equation for SS Mechanism,

$$\Delta_{base} = (\mu - 1)\frac{V_{SS}}{K_{shear}}, \text{ when } \mu > 1 \tag{B.14}$$

where:
Δ_{base}: wall base sliding displacement
μ: displacement ductility ratio

Step B: Estimate sliding displacements for a CFSS mechanism

B1: Determine Triggering aspect ratios: TAR1, TAR2 and TAR3.
TAR1 = H/L when $V_{Fl} = V_{SS_U}$ (B.9)

$$TAR2 = 0.8\left[1 + C_M\sqrt{\frac{f_y}{f'_g}}\right] \tag{B.8}$$

TAR3 = H/L when $V_o = DA_y$ (B.15)

Note that calculation of TAR1 and TAR3 requires trying multiple values of H/L until finding the aspect ratio that meets the condition in equations B.9 and B.15, respectively)

B2: Calculate dowel action secant stiffness coefficient, C_k.

$$C_k = \left[\frac{0.40}{\mu} + \left(1 - \frac{0.40}{\mu}\right)\left(\frac{H/L - TAR1}{TAR2 - TAR1}\right)\right], \quad \text{if } TAR3 < TAR1 \qquad (B.16a)$$

$$C_k = \left[\frac{0.12}{\mu} + \left(1 - \frac{0.12}{\mu}\right)\left(\frac{H/L - TAR3}{TAR2 - TAR3}\right)\right], \quad \text{if } TAR3 \geq TAR1 \qquad (B.17b)$$

where:

μ: displacement ductility ratio

B3: Determine dowel action yield stiffness, k_{DA}.

$$k_{DA} = n_{db} E_s I_s \left(\frac{k_g d_b}{4 E_s I_s}\right)^{3/4} \qquad (B.18)$$

$$k_g = \frac{127\sqrt{f'_g}}{d_b^{2/3}}, \quad \text{Note: } f'_g \text{ (MPa)}, d_b \text{ (mm)} \qquad (B.19)$$

B4: Calculate base sliding displacement, Δ_{Base}.

$$\Delta_{Base} = 1.25\frac{V_o}{C_k k_{DA}} \qquad (B.20)$$

B.3 Ductile Seismic Response of Reinforced Masonry Shear Walls

A prime consideration in seismic design is the need to have a structure that is capable of deforming in a ductile manner when subjected to several cycles of lateral loading well into the inelastic range. This section explains a few key terms related to ductile seismic response, including ductility ratio, curvature, plastic hinge, etc. It is important for a structural designer to have a good understanding of these concepts before proceeding with the seismic design and detailing of ductile masonry walls according to CSA S304-14. In particular, the content of this section is related to the ductility check for RM shear walls discussed in Section 2.6.3.

Ductility is a measure of the capacity of a structure or a member to undergo deformation beyond yield level, while maintaining most of its load-carrying capacity. Ductile structural members are able to absorb and dissipate earthquake energy by inelastic (plastic) deformations that are usually associated with permanent structural damage. These inelastic deformations are concentrated mainly in regions called *plastic hinges*. In general, plastic hinges develop in shear walls responding in the flexural mode and are typically formed at their base. An example of a plastic hinge formed in a RM wall subjected to seismic loading is shown in Figure 2-8a. The concept of ductility and ductile seismic response was introduced in Section 1.4.3.

A common way to quantify ductility in a structure is through the *displacement ductility ratio* μ_Δ. This is the ratio of the maximum lateral displacement experienced by the structure at the ultimate (Δ_u), to the displacement at the onset of inelastic response (Δ_y) (see Figure 1-5c).

$$\mu_\Delta = \frac{\Delta_u}{\Delta_y}$$

Next, the concept of curvature will be explained by an example of a RM shear wall subjected to bending due to a shear force applied at the top, as shown in Figure B-5a. Consider a wall segment ABCD of unit height. This segment deforms due to bending moments, so sections AB and CD rotate by a certain angle relative to their original horizontal position (these deformed sections are denoted as A'B' and C'D'). Rotation between the ends of the segment defines the curvature φ, as shown in Figure B-5b. Curvature represents relative section rotations per unit length. It should be noted that curvature is directly proportional to the bending moment at the wall section under consideration, if the section remains elastic.

Consider any section CD that undergoes curvature φ, as shown in Figure B-5c. Strain distribution along the wall section is defined by the product of curvature and the distance from the neutral axis, located by the depth c. The maximum compressive strain in masonry ε_m is given by

$$\varepsilon_m = \varphi \cdot c$$

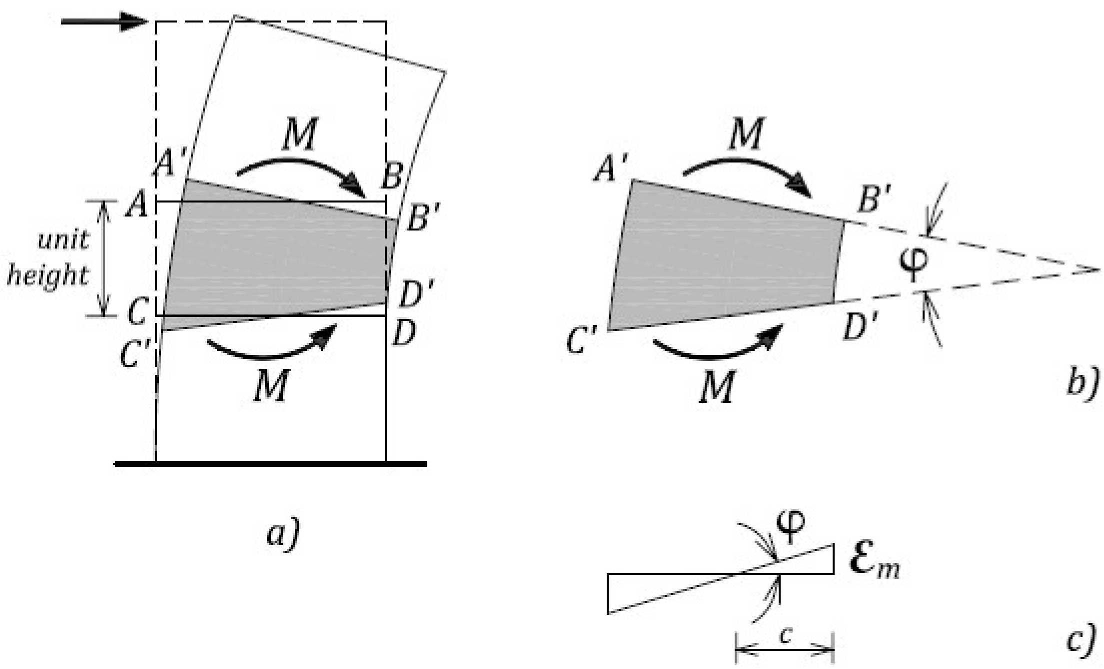

Figure B-5. Curvature in a shear wall subjected to flexure: a) wall elevation; b) deformed wall segment ABCD; c) strain distribution along the section CD.

For the seismic design of RM walls, it is of interest to determine curvatures at the following two stages: the onset of steel yielding and at the ultimate stage. Consider a RM wall section subjected to axial load and bending shown in Figure B-6a.
Yield curvature φ_y corresponds to the onset of yielding characterized by tensile yield strain ε_y developed in the end rebars, as shown in Figure B-6b, where

$$\varphi_y = \frac{\varepsilon_y}{l_w - d' - c}$$

Ultimate curvature φ_u corresponds to the ultimate stage, when the maximum masonry compressive strain ε_m has been reached. The maximum ε_m value has been limited to 0.0025 by CSA S304-14 (see Figure B-6c) to prevent damage to the outer blocks in the plastic hinge region. Note that the neutral axis depth c is going to decrease as more of the reinforcement has yielded (see Figure B-6c).

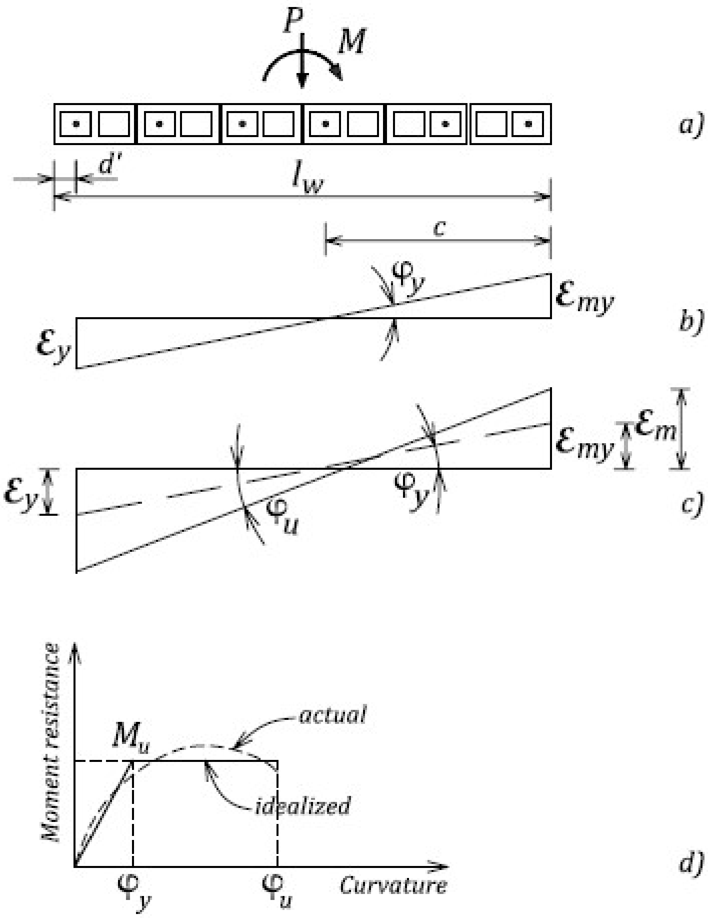

Figure B-6. Curvature in a RM wall section: a) wall cross section; b) yield curvature; c) ultimate curvature; d) moment-curvature relationship.

The curvature value depends on the load level, the section geometry, the amount and distribution of reinforcement, and the mechanical properties of steel and masonry. An actual moment-curvature relationship for ductile sections is nonlinear, however it is usually idealized by elastic-plastic (bilinear) relationship, as shown in Figure B-6d.

Once the curvatures at the critical stages have been determined, the *curvature ductility ratio* μ_φ can be found as follows

$$\mu_\varphi = \frac{\varphi_u}{\varphi_y}$$

When the curvature distribution along a structural member (e.g. shear wall) is defined, rotations and deflections can be calculated by integrating the curvatures along the member. This can be accomplished in several ways, including the moment area method.

Rotations and deflections in a masonry shear wall at the ultimate state can be determined following the approach outlined above. Consider a cantilevered shear wall of length l_w and height h_w, and the plastic hinge length l_p (see Figure B-7a). The wall is subjected to a seismic shear force at the top, which results in a corresponding bending moment diagram as shown in Figure B-7b. The curvature diagram shown in Figure B-7c has two distinct portions: an elastic portion, with the maximum curvature equal to the yield curvature φ_y, and the plastic portion with the maximum curvature equal to the ultimate curvature φ_u. Note that the elastic portion of the curvature diagram has the same shape as the bending moment diagram (since the curvatures and bending moments are directly proportional). The actual curvature distribution in the plastic region varies in a nonlinear manner, as shown in Figure B-7c. For design purposes, the curvature can be taken as constant over the plastic hinge length l_p (note that the areas under the actual and the equivalent plastic curvature are set to be equal). The elastic rotation θ_e and the plastic rotation θ_p are presented in Figure B-7d. The plastic rotation can be determined as the area of the equivalent rectangle of width $\varphi_u - \varphi_y$ and height l_p, as shown in Figure B-7c. These rotations can be calculated from the curvature diagram as follows:

$$\theta_u = \theta_e + \theta_p$$

where

$$\theta_e = \frac{\varphi_y \cdot h_w}{2}$$

$$\theta_p = (\varphi_u - \varphi_y) \cdot l_p$$

The maximum deflection Δ_u at the top of the wall is shown in Figure B-7d. This deflection has two components: elastic deflection Δ_y corresponding to the yield curvature φ_y, and the plastic deflection Δ_p due to a rigid body rotation, since bending moments do not increase once the yielding has taken place. Deflection values can be found by taking the moment of the curvature area around point A, as follows:

$$\Delta_y = \frac{\varphi_y h_w}{2} \cdot \frac{2h_w}{3} = \frac{\varphi_y h_w^{\,2}}{3}$$

$$\Delta_p = (\varphi_u - \varphi_y) \cdot l_p (h_w - 0.5 l_p)$$

$$\Delta_u = \Delta_y + \Delta_p$$

The above equations can be used to determine the displacement ductility ratio μ_Δ, in terms of the curvature ductility μ_φ and other parameters, as follows:

$$\mu_\Delta = \frac{\Delta_u}{\Delta_y} = 1 + 3(\mu_\varphi - 1)\left(\frac{l_p}{h_w}\right)\left(1 - 0.5\frac{l_p}{h_w}\right)$$

Alternatively, the curvature ductility ratio μ_φ can be expressed in terms of the displacement ductility ratio, as follows:

$$\mu_\varphi = \frac{\varphi_u}{\varphi_y} = \frac{h_w^{\,2}(\mu_\Delta - 1)}{3 l_p (h_w - 0.5 l_p)} + 1$$

It should be noted that μ_Δ and μ_φ values are different for the same member. Once the yielding has taken place, the deformations concentrate at the plastic hinges, so the curvature ductility μ_φ

is expected to be larger than the displacement ductility μ_{Δ}. This difference is more pronounced in walls with larger displacement ductility ratios.

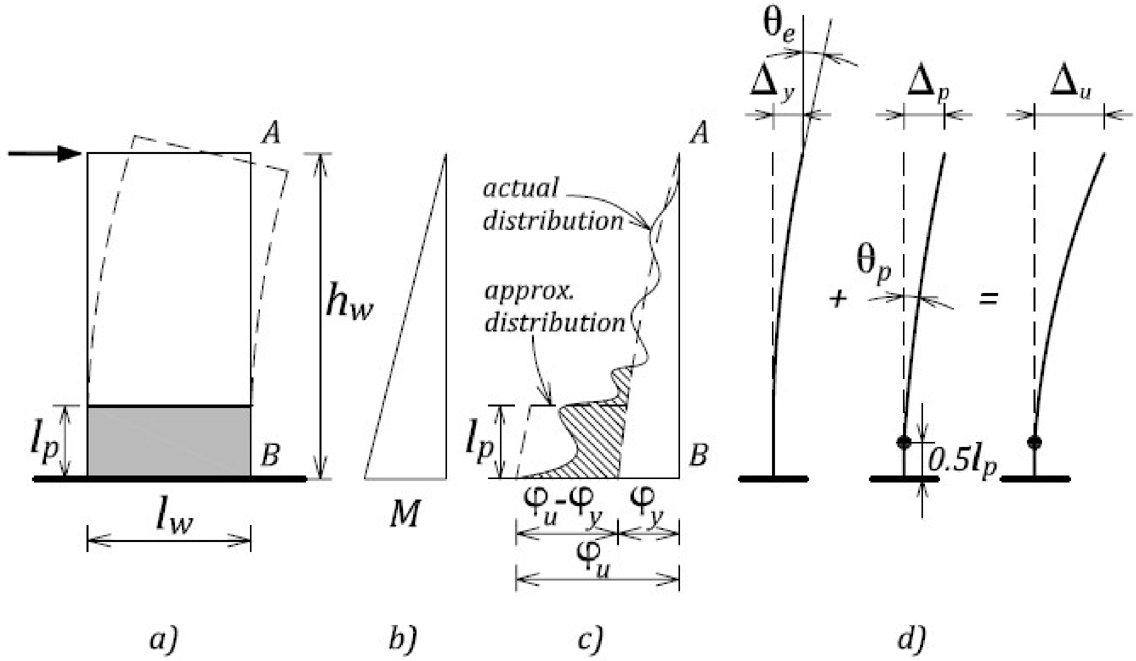

Figure B-7. Shear wall at the ultimate: a) wall elevation; b) bending moment diagram; c) curvature diagram; d) deflections.

B.4 Wall Height-to-Thickness Ratio Restrictions

The out-of-plane wall instability of RM and RC shear walls due to in-plane lateral reversed cyclic loading is a complex phenomenon, which has proven to be difficult to account for by means of a rational mechanics-based approach. The out-of-plane instability of RC shear walls in multi-storey buildings was observed in the 2010 Maule, Chile earthquake (M 8.8) (Westenenk et al. 2012) and the 2011 Christchurch, New Zealand earthquake (M 6.3) (Elwood 2013). However, there is no evidence of out-of-plane instability for RM shear walls in past earthquakes, and experimental research evidence is extremely limited. Azimikor et al. (2011) and Herrick (2014) performed a literature review of past experimental studies related to this subject.

A pioneering research study on this subject was undertaken by Paulay and Priestley (1992, 1993). They concluded that a RC or RM shear wall can experience lateral instability when the longitudinal reinforcement in its end zones is subjected to compression loads subsequent to cycles of tensile plastic strain. Horizontal cracks form along the height of the plastic hinge region in the wall end zone during tension load cycles, and may not fully close during subsequent compression load cycles. Due to the presence of open cracks and the residual plastic strains in the vertical reinforcement within the wall end zone, that zone becomes very flexible and susceptible to significant out-of-plane displacements at low compression stress levels. It is possible to determine the critical out-of-plane displacement beyond which instability will occur for a specific design case. This displacement is equal to the minimum distance between the centroid of steel and face of masonry block. For example, the critical displacement is equal to *b/2* for a wall with thickness *b* and one layer of longitudinal reinforcement (where a reinforcing bar is placed in the centre of a hollow core).

Paulay and Priestley (1993) developed an analytical model which offers a means to find the minimum wall thickness required to avoid out-of-plane instability. The minimum thickness value depends on several parameters, including the vertical reinforcement ratio, the desired curvature and displacement ductility ratios, the plastic hinge length, and the mechanical properties of the steel and masonry. Paulay and Priestley also performed an experimental study to confirm their analytical model. They tested a few reinforced concrete shear wall specimens and a concrete masonry wall specimen. The masonry wall specimen failed by out-of-plane buckling at a very large displacement ductility μ_Δ of around 14.

The application of this procedure will be illustrated on an example of a RM wall. The equation for the critical wall thickness b_c is as follows (Paulay and Priestley, 1992)

$$b_c = 0.022 l_w \sqrt{\mu_\varphi}$$

Curvature ductility, μ_φ, is related to displacement ductility, μ_Δ, as shown in Section B.3. The plastic hinge length l_p is taken equal to $h_w/6$, and so the equation can be simplified as follows

$$\mu_\varphi = 2.2(\mu_\Delta - 1)$$

The displacement ductility ratio μ_Δ can be considered equal to R_d prescribed by NBC 2015 for different SFRSs (note that μ_Δ values in the range from 2.0 to 3.0 are considered in this example). By following the above procedure, it is possible to obtain the b_c/l_w ratios corresponding to different μ_Δ values. The results are summarized in Table B-1.

For example, if the wall length l_w is equal to 5,000 mm, the corresponding critical thickness b_c is equal to 150 mm for μ_Δ = 2.0, or 230 mm for μ_Δ = 3.0. Paulay and Priestley suggest that the critical wall thickness should be expressed as a fraction of the wall length rather than its height.

Table B-1. Critical Wall Thickness b_c Versus the Displacement Ductility Ratio μ_Δ

μ_Δ	μ_φ	l_w/b_c
2.0	2.2	31
2.5	3.3	25
3.0	4.4	22

A recent Canadian experimental program (Azimikor 2012; Robazza 2013; Azimikor et al. 2012; 2017; Robazza et al. 2017a; 2017b; 2018) demonstrated that the out-of-plane wall instability is difficult to induce in RM shear walls at the ductility demand levels relevant for Canadian masonry design practice. Phase 1 of the program focused on simulating the behaviour of the wall end zones using uniaxial specimens. The purpose of the study was to understand the out-of-plane instability phenomenon and identify key factors influencing its development. Phase 2 consisted of testing several full-scale RMSW specimens under in-plane reversed cyclic loading. Masonry for the test specimens was laid in 50% running bond using Type S mortar for faceshell bedding and standard Canadian concrete hollow block units.

Phase 1 consisted of testing 5 prismatic specimens with a rectangular cross-section (600 mm length and 140 mm thickness), which were designed to simulate the end zone of a RM shear wall (Azimikor 2012; Azimikor et al. 2012; 2017). All specimens had the same height (3.8 m), resulting in a *h/t* ratio of 27. The vertical reinforcement ratio varied from 0.24% (the minimum permissible by CSA S304.1-04) to 1.07% (the maximum practical in the masonry industry). The loading protocol consisted of reversed-cyclic uniaxial tension and compression displacement cycles of incrementally increasing magnitude until failure. Four specimens experienced out-of-plane instability, while the fifth specimen was a reference specimen which was subjected to monotonic compression and experienced a compression/crushing failure. These tests had some limitations: the specimens were isolated and were not able to simulate actual boundary conditions along the wall height and the effect of strain gradient along the wall length. It was concluded that the level of applied tensile strain in a wall end-zone was one of the critical factors governing its out-of-plane stability. The maximum tensile strain that may be imposed on a ductile RM shear wall's end-zone could be determined, at least in part, by a kinematic relationship between the axial strain and the out-of-plane displacement. A preliminary mechanical model was proposed which provided a theoretical prediction of the maximum tensile strain before an instability would take place.

Phase 2 comprised of an experimental study of 8 full-size RMSW specimens of varying *h/t* and aspect (*h/L*) ratios, vertical and horizontal reinforcement amounts and detailing, applied axial pre-compression, and cross-section shape (6 specimens had regular rectangular cross-sections, while the other 2 specimens had T-shaped cross-sections) (Robazza 2013; Robazza et al. 2017a; 2017b; 2018). The specimens were subjected to either cyclic or reversed-cyclic loading until failure. All specimens were designed to exhibit flexure-controlled behavior characterized by the development of high tensile strains over a distinct region of plastic hinging, which is a theoretical prerequisite for the occurrence of out-of-plane instability. The specimens had aspect ratios varying from 1.5 to 3.0, which were required to maintain a relatively large plastic hinge height while still avoiding a shear failure. The specimens were designed with relatively high *h/t* ratios, ranging from 21.1 to 28.6, which exceeded the maximum CSA S304.1-04 limits for ductile RM shear walls. However, only one specimen experienced out-of-plane displacements large enough to precipitate instability, which occurred only after the wall had reached its ultimate shear capacity and experienced substantial degradation.

It was found that several factors may influence the out-of-plane response of RM shear wallsubjected to in-plane loading, including ductility and tensile strain demands, applied pre-compression levels and construction practices, as well as the effects of alternative failure mechanisms. This research also demonstrated that the strain gradient in a RM wall is a very important factor. This was not included in previous numerical models for out-of-plane stability in RM or RC shear walls, which were developed exclusively based on data from testing uniaxial specimens (e.g. Paulay and Priestley, 1993; Chai and Elayer, 1999). The estimates based on these models may lead to overly conservative h/t requirements.

Findings of the research by Paulay and Priestley (1992; 1993) were incorporated in the seismic design provisions for RM shear walls in New Zealand. The New Zealand masonry design standard NZS 4230:2004 prescribes the following minimum thicknesses for limited ductility walls (μ_Δ of 2.0) and ductile walls (μ_Δ of 4.0):

1. For *walls up to 3 storeys high* (Cl.7.4.4.1 and 7.3.3), minimum thickness t should not be less than $L_n/20$ (or $0.05L_n$), where L_n denotes clear vertical distance between lines of effective horizontal support or clear horizontal distance between lines of effective vertical support. Commentary to Cl.7.3.3 states that "for a given wall thickness, t, and the case when lines of horizontal support have a clear vertical spacing of $L_n > 20t$, then vertical lines of support having a clear horizontal spacing of $L_n < 20t$ shall be provided."
2. For *walls more than 3 storeys high* (Cl.7.4.4.1) minimum thickness t shall not be less than $L_n/13.3$ (or $0.075L_n$). However, a smaller wall thickness can be used provided that one of the following conditions is satisfied (maximum strain in masonry ε_u is equal to 0.003 according to NZS 4230:2004) (see Figure 2-28):
    a) $c \le 4t$ or

b) $c \le 0.3l_w$ or

c) $c \le 6t$ from the inside of a wall return of a flanged wall, which has a minimum length $0.2L_n$.

The relaxed thickness requirement applies to the cases where the neutral axis depth is small, and so the compressed area may be so small that the adjacent vertical strips of the wall will be able to stabilize it. This is likely the case with rectangular walls subjected to low axial compression.

Commentary to NZS 4230 Cl.7.4.4.1 states that it is considered unlikely that failure due to lateral instability of the wall will occur in structures less than 3 storeys high, because of the rapid reduction in flexural compression with height. This is also in line with the statement made by Paulay (1986), that out-of-plane stability is likely to take place in walls with large plastic hinge length (one storey or more).

Paulay and Priestley (1992) stated that "where the wall height is less than three storeys, a greater slenderness should be acceptable. In such cases, or where inelastic flexural deformations cannot develop, the wall thickness t need not be less than $0.05L_n$" (where L_n denotes clear wall length between the supports).

FEMA 306 (1999) also discusses the issue of wall instability. This document also refers to the procedure by Paulay and Priestley (1993) and provides the following recommendation for minimum wall thickness in ductile walls (μ_Δ of 4.0):

$t \le l_w/24$ or $t \le h/18$

Note that the above requirement, which applies to the walls with displacement ductility ratio (μ_Δ) equal to 4.0.

FEMA 306 (1999) also points out that "the lack of evidence for this type of failure in existing structures may be due to the large number of cycles at high ductility that must be achieved – most conventionally designed masonry walls are likely to experience other behaviour modes such as diagonal shear before instability becomes a problem."

TABLE OF CONTENTS – APPENDIX C

C RELEVANT DESIGN BACKGROUND C-2

C.1 Design for Combined Axial Load and Flexure C-2
C.1.1 Reinforced Masonry Walls Under In-Plane Seismic Loading C-2
C.1.2 Reinforced Masonry Walls Under Out-of-Plane Seismic Loading C-9

C.2 Wall Intersections and Flanged Shear Walls C-15
C.2.1 Effective Flange Width C-15
C.2.2 Types of Intersections C-16
C.2.3 Shear Resistance at the Intersections C-18

C.3 Wall Stiffness Calculations C-22
C.3.1 Lateral Load Distribution C-22
C.3.2 Wall Stiffness: Cantilever and Fixed-End Model C-23
C.3.3 Approximate Method for Force Distribution in Masonry Shear Walls C-24
C.3.4 Advanced Design Approaches for Reinforced Masonry Shear Walls with Openings C-27
C.3.5 The Effect of Cracking on Wall Stiffness C-32

C Relevant Design Background

This appendix contains additional information relevant for masonry design as discussed in Chapter 2, but it is not directly related to the seismic design provisions of CSA S304-14. Applications of the design methods and procedures presented in this appendix can be found in Chapter 3, which contains several design examples. This appendix addresses in detail several topics of interest to masonry designers, e.g., the calculation of in-plane wall stiffness, including the effect of cracking, and force distribution in perforated shear walls. However, modeling and analysis of multi-storey perforated shear walls are not covered in this document.

C.1 Design for Combined Axial Load and Flexure

C.1.1 Reinforced Masonry Walls Under In-Plane Seismic Loading

10.2

Seismic shear forces acting at floor and roof levels cause overturning bending moments in shear walls, which reach a maximum at the base level. In general, shear walls are subjected to the combined effects of flexure and axial gravity loads. The theory behind the design of masonry wall sections subjected to effects of flexure and axial load is well established, and is essentially the same as that of reinforced concrete walls. A typical reinforced masonry wall section is shown in Figure C-1a), along with the distribution of internal forces and strains arising from the axial load and moment. According to CSA S304-14, the strain distribution along the wall length is based on the assumptions that the wall section remains plane and that the maximum compressive masonry strain ε_m is equal to 0.003 (see Figure C-1b)). Figure C-1c) shows the distribution of internal forces on the base of the wall, as well as the axial load, P_f and the bending moment, M_f. In the compression zone, the equivalent rectangular stress block has a depth a, and a maximum stress intensity of $0.85\chi\phi_m f'_m$. Note that the χ factor assumes a value of 1.0 for members subjected to compression perpendicular to the bed joints, such as structural walls (S304-14 Cl.10.2.6). Each reinforcing bar develops an internal force (either tension or compression) equal to the product of the factored stress and the corresponding bar area. The internal vertical forces must be in equilibrium with P_f, and the factored moment capacity M_r can be determined by taking the sum of the moments of the internal forces around the centroid of the section.

The following three design scenarios and the related simplified design procedures will be discussed in this section:

1. Wall reinforcement (both concentrated and distributed) and axial load are given – find moment capacity
2. Wall is reinforced with distributed reinforcement only – find moment capacity
3. Wall reinforcement needs to be estimated (factored bending moment and axial force are given)

The first two are applicable for the common situations where a designer assumes the minimum seismic reinforcement amount and desires to find its moment capacity.

Approximate design approaches that can be used to assist designers in each of these scenarios are presented below. For detailed analysis and design procedures, the reader is referred to Drysdale and Hamid (2005) and Hatzinikolas, Korany and Brzev (2015).

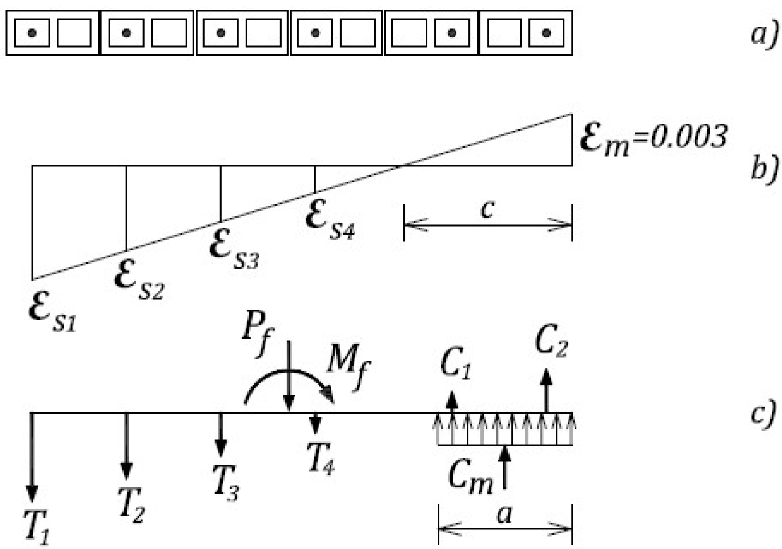

Figure C-1. A reinforced masonry shear wall under the combined effects of axial load and flexure: a) plan view cross section; b) strain distribution; c) internal force distribution.

C.1.1.1 Moment capacity for a wall section with concentrated and distributed reinforcement

<u>Rectangular section</u>

A simplified wall design model is shown in Figure C-2. The wall reinforcement can be divided into:

- Concentrated reinforcement at the ends (area A_c at each end), and
- Distributed reinforcement along the wall length (total area A_d).

It is assumed that the concentrated wall reinforcement yields either in tension or in compression at the wall ends. Also, it is assumed that the distributed reinforcement yields in tension.

A procedure to find the factored moment capacity M_r for a shear wall with a given vertical reinforcement (size and spacing) is outlined below.

From the equilibrium of vertical forces (see Figure C-2b)), it follows that

$$P_f + T_1 + T_2 - C_3 - C_m = 0 \qquad (1)$$

where

$$T_1 = C_3 = \phi_s f_y A_c$$

$$T_2 = \phi_s f_y A_d$$

$$C_m = (0.85\phi_m f'_m)(t \cdot a)$$

The compression zone depth, a , can be determined from equation 1 as follows

$$a = \frac{P_f + \phi_s f_y A_d}{0.85\phi_m f'_m t} \qquad (2)$$

$\beta_1 = 0.8$ when $f'_m < 20$ MPa (note that β_1 value decreases when $f'_m > 20$ MPa, as prescribed in S304-14 Cl.10.2.6)

The neutral axis depth, c, measured from the extreme compression fibre to the point of zero strain is given by

$$c = a/\beta_1$$

Next, the factored moment capacity, M_r, can be determined by summing up the moments around the centroid of the wall section (point **O**) as follows

$$M_r = C_m(l_w - a)/2 + 2\left[\phi_s f_y A_c \left(l_w/2 - d'\right)\right] \qquad (3)$$

where d' is the distance from the extreme compression fibre to the centroid of the concentrated compression reinforcement.

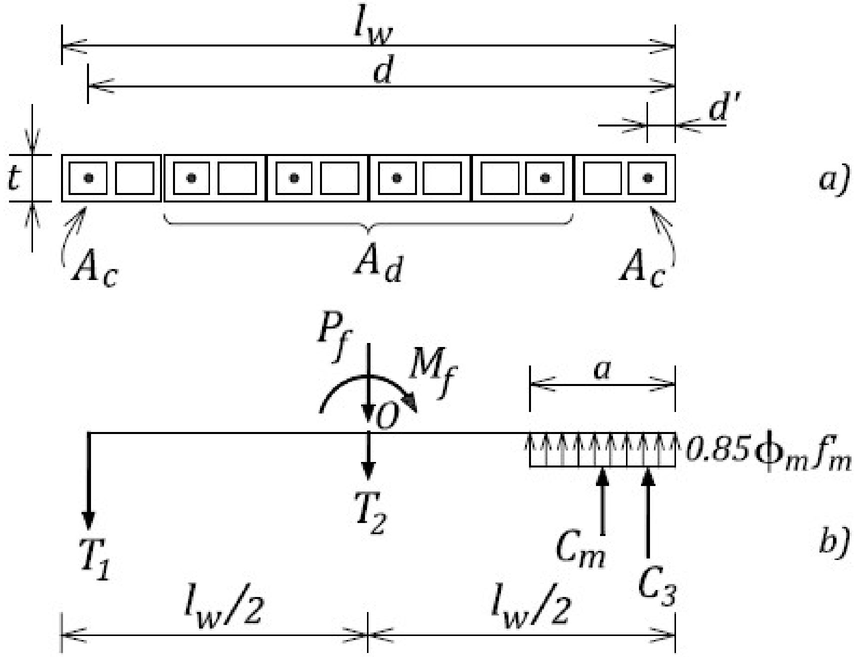

Figure C-2. A simplified design model for rectangular wall section: a) plan view cross-section showing reinforcement; b) internal force distribution.

10.2.8

For squat shear walls, CSA S304-14 prescribes the use of a reduced effective depth d for flexural design, i.e.

$$d = 0.67 l_w \le 0.7h$$

As a result, the moment capacity should be reduced by taking a smaller lever arm for the tensile steel, as follows:

$$M_r = C_m(l_w - a)/2 + \left[\phi_s f_y A_c \left(l_w/2 - d'\right)\right] + \left[\phi_s f_y A_c \left(d - l_w/2\right)\right] \qquad (4)$$

Note that the reinforcement area A_c in squat walls should be increased to provide more than one reinforcing bar, since the end zone constitutes a larger portion of the overall wall length in these cases.

The CSA S304-14 provision for the reduced effective depth in squat walls contained in Cl.10.2.8 is intended to account for the effect of the deep beam behaviour of squat walls. This provision makes more sense for non-seismic design, and it should not be used if the tension steel yields in seismic conditions.

Flanged section

In the case of the flanged wall section shown in Figure C- 3, the factored moment capacity M_r can be determined by summing up the moments around the centroid of the wall section (point **O**) as follows

$$M_r = C_m\left(l_w/2 - x\right) + 2\left(\phi_s f_y A_c\right)\left(l_w/2 - d'\right)$$

where

$$A_L = \frac{P_f + \phi_s f_y A_d}{0.85\phi_m f'_m}$$

is the area of compression zone, and its depth is

$$a = \frac{A_L - b_f * t + t^2}{t}$$

$$x = \frac{t*\left(a^2/2\right) + (b_f - t)\left(t^2/2\right)}{A_L}$$

and the resultant of masonry compression stress is

$$C_m = \left(0.85\phi_m f'_m\right)A_L$$

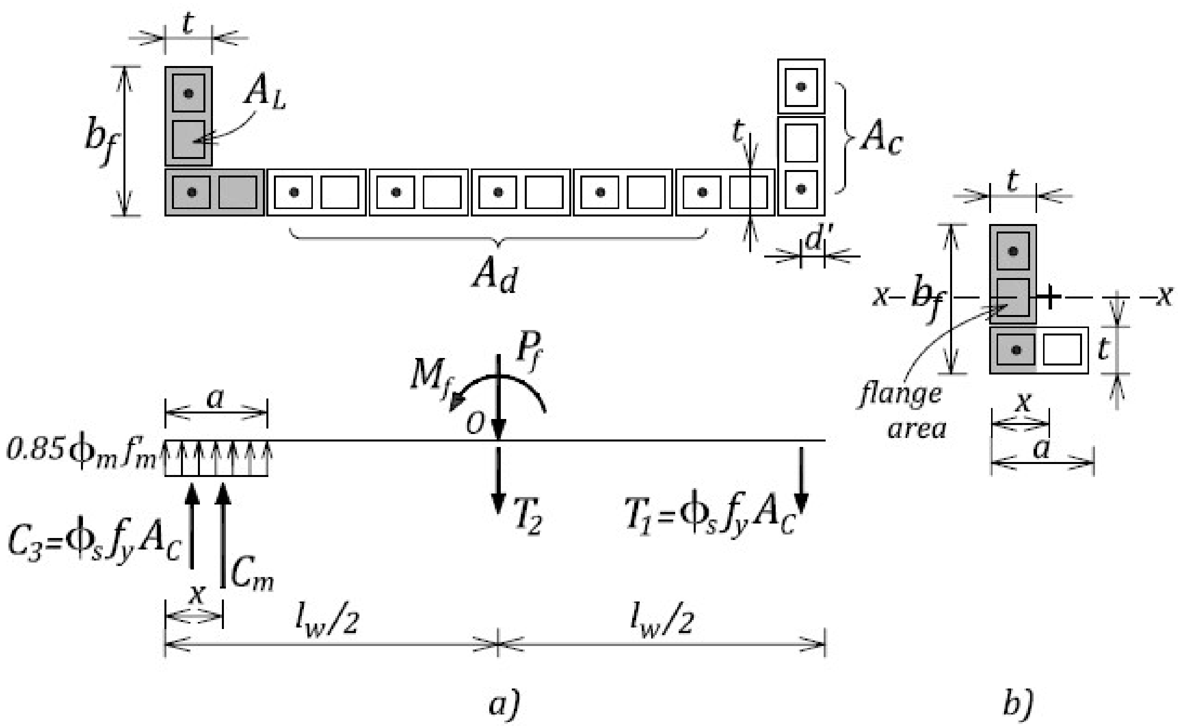

Figure C- 3. A simplified design model for a flanged wall section.

Section with boundary elements

In the case of the wall section with boundary elements shown in Figure C-4, the factored moment capacity M_r can be determined by summing up the moments around the centroid of the wall section (point **O**) as follows

$$M_r = C_m\left(l_w/2 - x\right) + 2\left(\phi_s f_y A_c\right)\left(l_w/2 - d'\right)$$

Where

$$A_L = \frac{P_f + \phi_s f_y A_d}{0.85\phi_m f'_m}$$

is the area of compression zone. When the neutral axis falls within the boundary element, the depth of compression block is

$$a = \frac{A_L}{b_f}$$

but if neutral axis falls in the wall web, the depth of the compression zone is

$$a = \frac{A_L - b_f \cdot l_f}{t} + l_f$$

The centroid of the masonry compression zone can be determined from the following equation:

$$x = \frac{b_f \cdot l_f\left(a - \frac{l_f}{2}\right) + \left(a - l_f\right)^2 \cdot t/2}{A_L}$$

and the resultant of masonry compression stress is

$$C_m = \left(0.85\phi_m f'_m\right)A_L$$

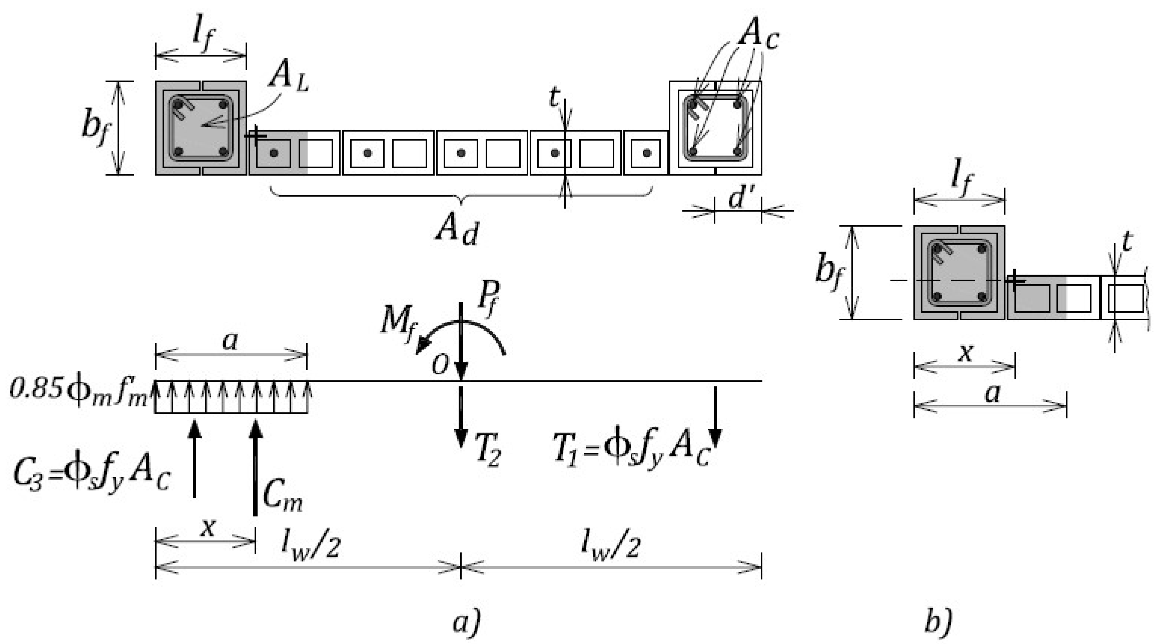

Figure C-4. A simplified design model for a wall section with boundary elements.

C.1.1.2 Moment capacity for rectangular wall sections with distributed vertical reinforcement

The previous section discussed a general case of a shear wall with both concentrated and distributed vertical reinforcement. In low to medium-rise concrete and masonry wall structures, the provision of distributed vertical reinforcement is often sufficient to resist the effects of combined flexure and axial loads (see Figure C-5a)). The factored moment capacity for walls with distributed vertical reinforcement can be determined based on the approximate equation proposed by Cardenas and Magura (1973), which was originally developed for reinforced concrete shear walls. The equation was derived based on the assumption that the distributed wall reinforcement shown in Figure C-5b) can be modeled like a thin plate of length l_w (equal to the wall length), and the thickness is such that the total area A_{vt} is the same as that provided by distributed reinforcement along the wall length. The factored moment capacity can be determined as follows:

$$M_r = 0.5\phi_s f_y A_{vt} l_w \left(1 + \frac{P_f}{\phi_s f_y A_{vt}}\right)\left(1 - \frac{c}{l_w}\right) \qquad (5)$$

where

A_{vt} - the total area of distributed vertical reinforcement

c - neutral axis depth

$$\omega = \frac{\phi_s f_y A_{vt}}{\phi_m f'_m l_w t}$$

$$\alpha = \frac{P_f}{\phi_m f'_m l_w t}$$

$$\frac{c}{l_w} = \frac{\omega + \alpha}{2\omega + \alpha_1 \beta_1}$$

$\alpha_1 = 0.85$ and $\beta_1 = 0.8$

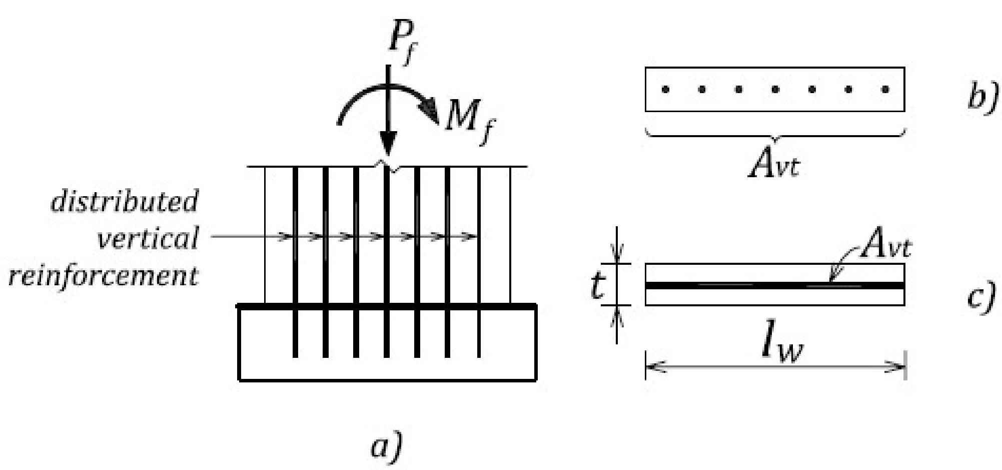

Figure C-5. Shear wall with distributed vertical reinforcement: a) vertical elevation; b) actual cross section; c) equivalent cross-section.

C.1.1.3 An approximate method to estimate the wall reinforcement

Consider the wall cross-section shown in Figure C-6a). In design practice, there is often a need to produce a quick estimate of wall reinforcement based on the given factored loads. In this case, the loads consist of the factored bending moment M_f and the axial force P_f acting at the centroid of the wall section (point **O**).

The goal of this procedure is to find the total area of wall reinforcement A_s. To simplify the calculations, an assumption is made that the reinforcement yields in tension and that the resultant force T_r acts at the centroid of the wall section, that is, (see Figure C-6b)).

$$T_r = \phi_s f_y A_s \qquad (6)$$

Initially, the compression zone depth a can be estimated in the range from $0.2l_w$ to $0.3l_w$. The moment resistance is usually not too sensitive to the a value as long it is relatively small. For example, the designer could use an estimate $a \cong 0.3l_w$.

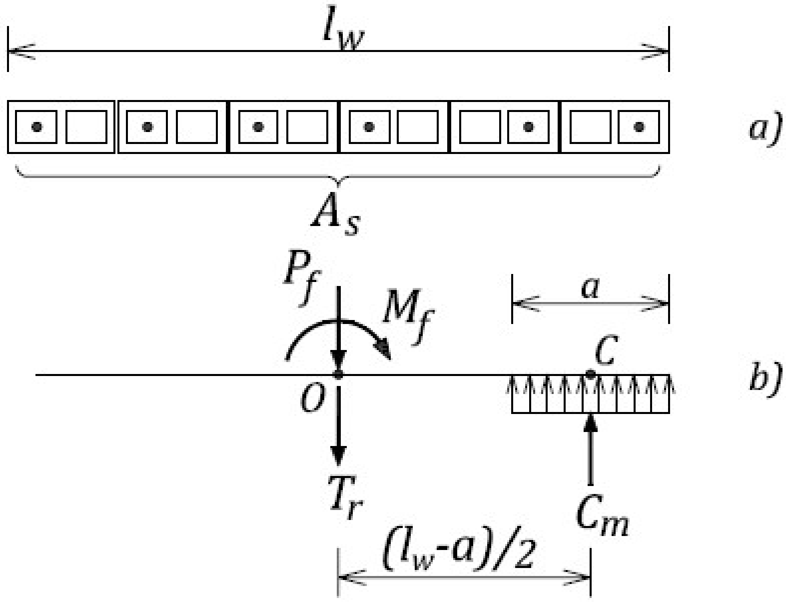

Figure C-6. Reinforcement estimate: a) plan view wall cross-section; b) distribution of internal forces.

Next, compute the sum of moments of all forces around the centroid of the compression zone (point **C**), as follows

$$M_f - P_f(l_w - a)/2 - T_r(l_w - a)/2 = 0$$

From the above equation it follows that

$$T_r = \frac{M_f - P_f(l_w - a)/2}{(l_w - a)/2} \qquad (7)$$

The area of reinforcement can then be determined from equation (7) as follows

$$A_s = T_r / \phi_s f_y$$

The area of reinforcement estimated by this procedure is usually close to the required value. A uniform reinforcement distribution over the wall length is recommended for seismic design, since research studies have shown that shear walls with a uniform reinforcement distribution show better seismic response in the post-cracking range. In addition, the seismic detailing requirements for vertical reinforcement need to be followed.

C.1.2 Reinforced Masonry Walls Under Out-of-Plane Seismic Loading

Masonry walls are subjected to the effects of seismic loads acting perpendicular to their surface – this is called *out-of-plane seismic loading*. For design purposes, wall strips of a predefined width are treated as beams spanning vertically or horizontally between lateral supports. When the walls span in the vertical direction, floor and/or roof diaphragms provide the lateral supports.

Walls can also span horizontally, in which case the lateral supports need to be provided by cross walls or pilasters, as shown in Figure C-7. Note that support on four edges is very efficient, since these walls behave as two-way slabs.

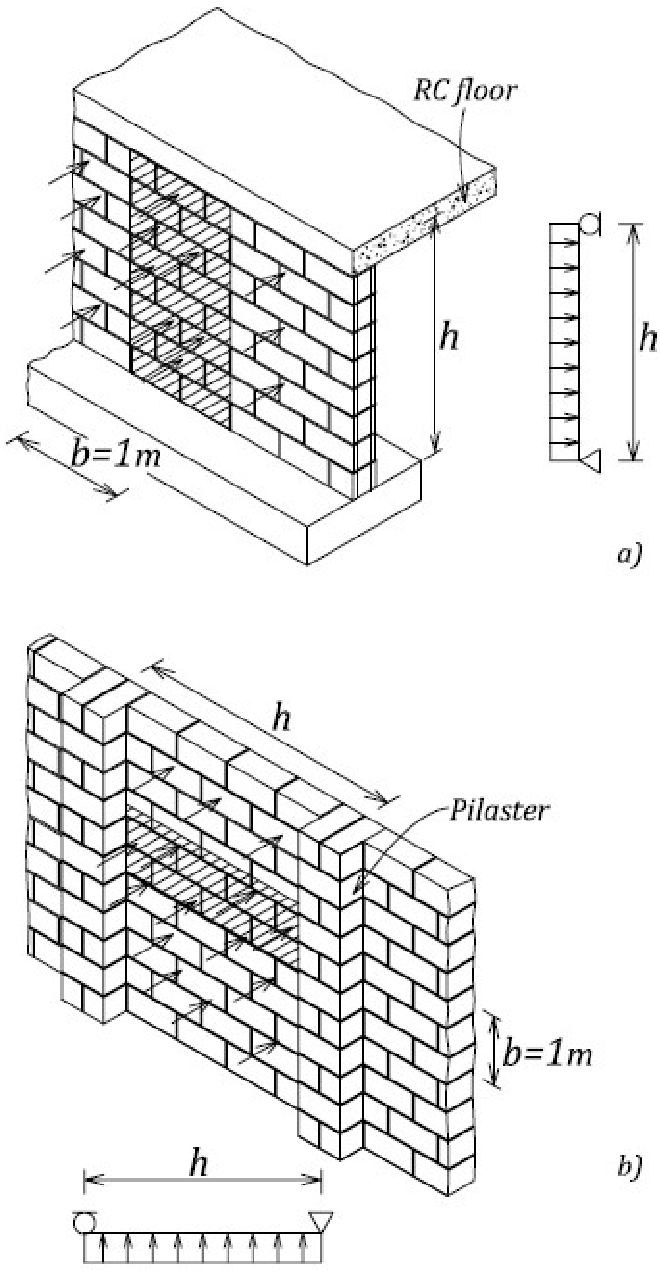

Figure C-7. Masonry walls under out-of-plane seismic loads: a) spanning vertically between floor/roof diaphragms; b) spanning horizontally between pilasters.

Consider a reinforced concrete masonry wall subjected to the effects of a factored axial load P_f and a bending moment M_f, as shown in Figure C-8a). The wall is reinforced vertically, with only the reinforced cores grouted. It is assumed that the size and distribution of vertical reinforcement are given. The notation used in Figure C-8b) is explained below:

t - overall wall thickness (taken as actual block width, e.g. 140 mm, 190 mm, etc.)

t_f - face shell thickness

b - effective width of the compression zone (see Section 2.4.2 and Figure 2-19)

d - effective depth, that is, distance from the extreme compression fibre to the centroid of the wall reinforcement; typically, the reinforcement is placed in the centre of the wall, so $d = t/2$

A_s - total area of steel reinforcement placed within the effective width b

It is assumed that the steel has yielded, that is, $\varepsilon_s \geq \varepsilon_y$, and the corresponding stress in the reinforcement is equal to the yield stress, f_y. This is a reasonable assumption for low-rise masonry buildings, since the axial load is low and the walls are expected to fail in the steel-controlled mode. The design procedure is outlined below.

- The resultant forces in steel T_r and masonry C_m can be determined as follows:

$$T_r = \phi_s f_y A_s$$

$$C_m = (0.85\phi_m f'_m)(b \cdot a)$$

- The equation of equilibrium of internal forces gives (see Figure C-8d))

$$C_m = P_f + T_r$$

- The depth of the compression stress block a is equal to

$$a = \frac{C_m}{0.85\phi_m f'_m b} \qquad (8)$$

- The moment resistance can be found from the following equation

$$M'_r = C_m (d - a/2) \qquad (9)$$

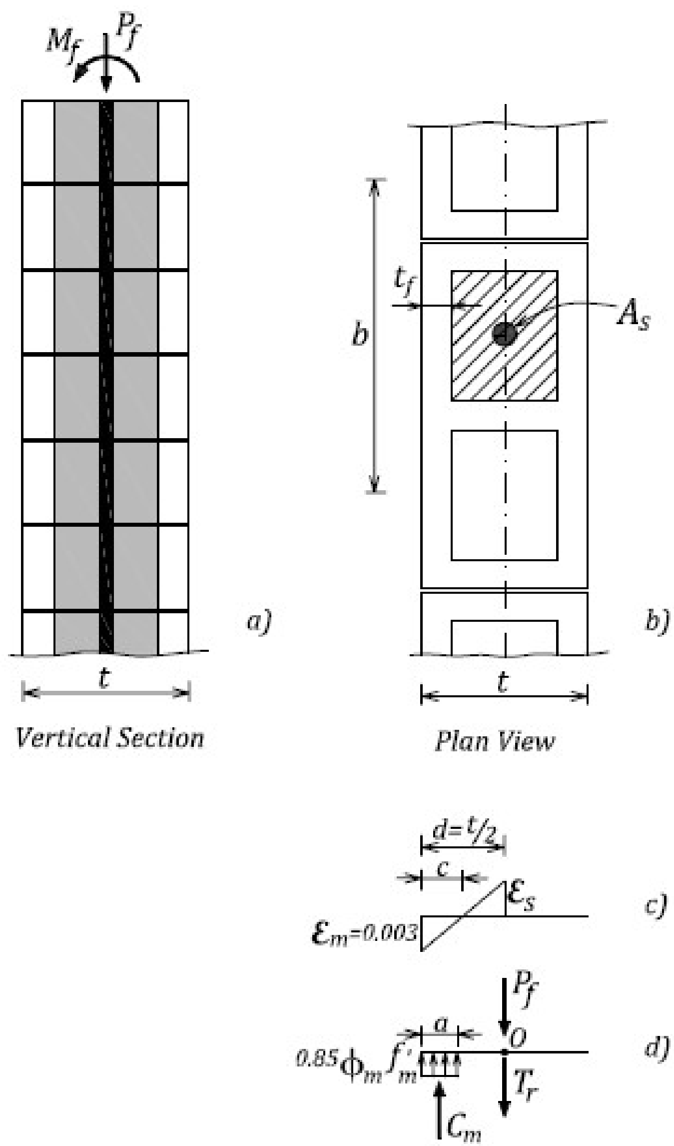

Figure C-8. A wall under axial load and out-of-plane bending: a) vertical section showing factored loads; b) plan view of a wall cross-section; c) strain distribution; d) internal force distribution.

For partially grouted wall sections (where only reinforced cores are grouted), the designer needs to confirm that

$$a \le t_f$$

When the above relation is correct, then the compression zone is rectangular, as shown in Figure C-9a). Note: in solidly grouted walls, the compression zone is always rectangular!

When $a \ge t_f$, the compression zone needs to be treated as a T-section and an additional calculation is required to determine the a value. The following equations can be used to determine the moment resistance in sections with a T-shaped compression zone:

- The resultant force in the steel T_r can be determined as follows:

$$T_r = \phi_s f_y A_s$$

- The resultant force in the masonry, C_m, acts at the centroid of the compression zone and can be determined from the equation of equilibrium of internal forces, that is,

$$C_m = P_f + T_r$$

Once the compression force in the masonry is found, the area of the masonry compression zone, A_m (see Figure C-9b)), is given by

$$C_m = (0.85\phi_m f'_m) \cdot A_m$$

- The depth of the compression stress block a can be found from the following equation

$$A_m = b \cdot t_f + (a - t_f) \cdot b_w$$

where

b_w = width of the grouted cell plus the adjacent webs

- The distance from the extreme compression fibre to the centroid of the compression zone $\bar{a}$ is equal to

$$\bar{a} = \frac{b \cdot (t_f^2/2) + (a - t_f) \cdot \left(t_f + \dfrac{a - t_f}{2}\right)}{A_m} \qquad (10)$$

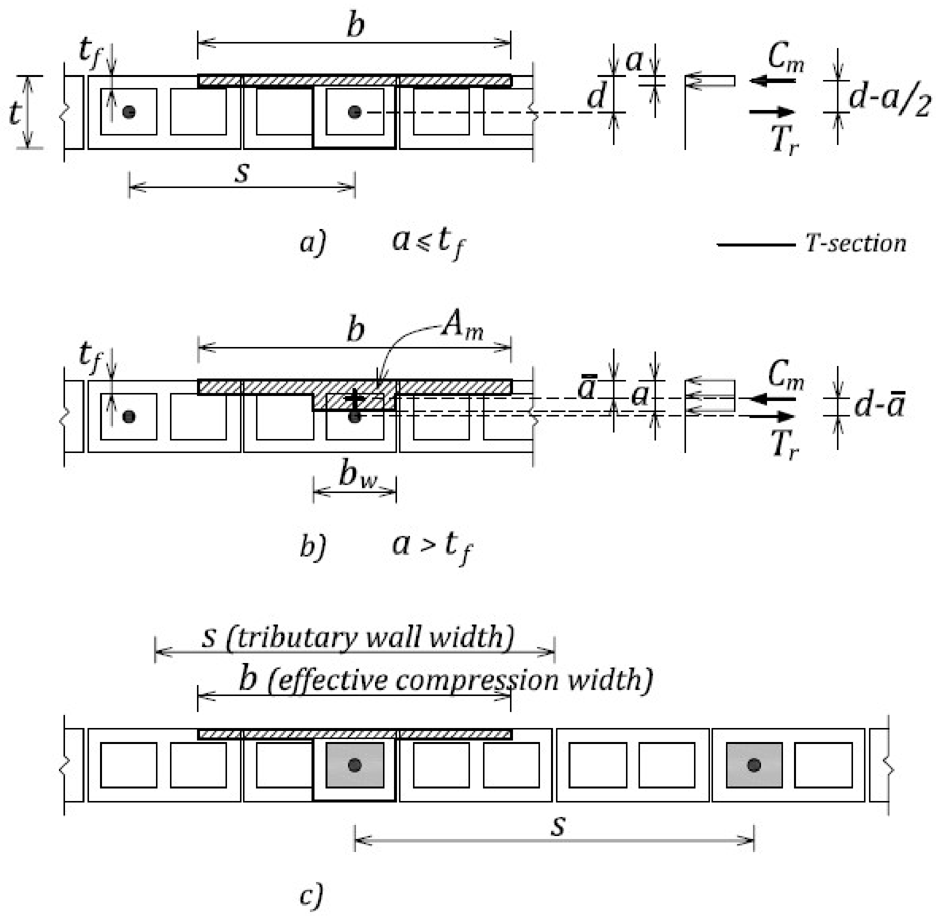

Figure C-9. Masonry compression zone: a) rectangular shape; b) T-shape; c) effective width and tributary width.

- The moment resistance can be found from the following equation

$$M'_r = C_m\left(d - \bar{a}\right) \quad (11)$$

Note that M'_r denotes the moment capacity for a wall section of width b. It is usually more practical to convert the M'_r value to a unit width equal to 1 metre (see Figure C-9c)), as follows

$$M_r = M'_r\left(1.0/s\right) \quad (12)$$

where
s - spacing of vertical reinforcement expressed in metres (where $b \le s$)
M_r - factored moment capacity in kNm/m.

The design of masonry walls subjected to the combined effects of axial load and bending is often performed using P-M interaction diagrams. The axial load capacity is shown on the vertical axis of the diagram, while the moment capacity is shown on the horizontal axis. The points on the diagram represent the combinations of axial forces and bending moments corresponding to the capacity of a wall cross-section. An interaction diagram is defined by the following four distinct points and/or regions: 1) balanced point, 2) points controlled by steel yielding, 3) points controlled by masonry compression, and 4) pure compression (zero eccentricity). A conceptual wall interaction diagram is presented in Figure C-10.

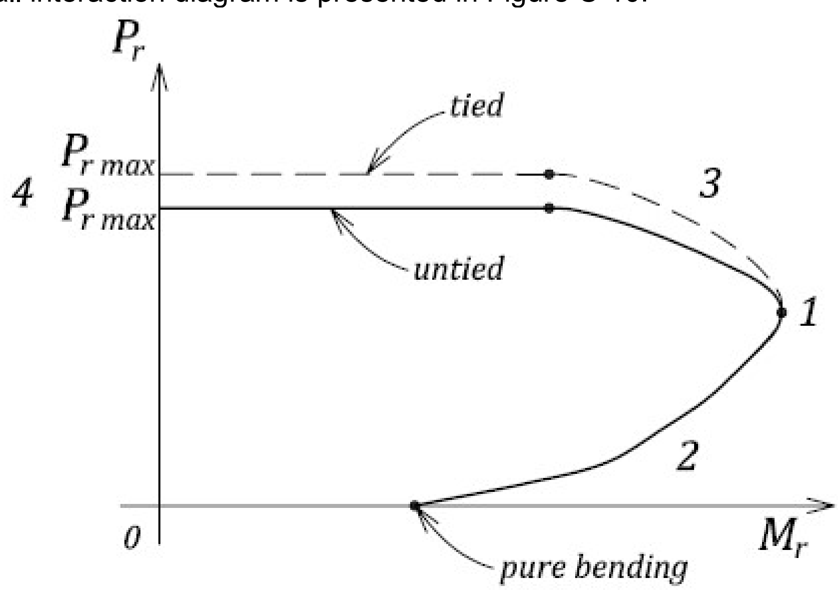

Figure C-10. P-M interaction diagram.

1. Balanced point

At the load corresponding to the balanced point, the steel has just yielded, that is, $\varepsilon_s = \varepsilon_y$. The position of the neutral axis c_b can be determined from the following proportion (refer to strain diagram in Figure C-8c)):

$$\frac{c_b}{d - c_b} = \frac{\varepsilon_m}{\varepsilon_y}$$

or

$$c_b = d\left(\frac{\varepsilon_m}{\varepsilon_m + \varepsilon_y}\right)$$

For $f_y = 400$ MPa and $\varepsilon_y = 0.002$ it follows that

$c_b = 0.6d$

2. Points controlled by steel yielding

For $c < c_b$, the steel will yield before the masonry reaches its maximum useful strain (0.003). Since the steel is yielding, it follows that $\varepsilon_s > \varepsilon_y$. The designer needs to assume the neutral axis depth (c) value so that $c < c_b$. The compression zone depth can then be calculated as $a = \beta_1 c = 0.8c$ (this is valid for $f'_m < 20MPa$ according to S304-14 Cl.10.2.6). Combinations of axial force and moment values corresponding to an assumed neutral axis depth can be found from the following equations of equilibrium (see Figure C-8d)).

$P_r = C_m - T_r$

where

$T_r = \phi_s f_y A_s$ (note that the stress in the steel is equal to f_y since the steel is yielding)

Moment resistance depends on the shape of the masonry compression zone, that is, on whether the section is partially or solidly grouted.

- For a solidly grouted section or a partially grouted section with the compression zone in the face shells only:

$M'_r = C_m(d - a/2)$

where

$C_m = (0.85\phi_m f'_m)(b \cdot a)$

- For a partially grouted section with the compression zone extending into the grouted cells:

$M'_r = C_m(d - \overline{a})$

where

$C_m = (0.85\phi_m f'_m) \cdot A_m$

3. Points controlled by masonry compression

For $c > c_b$, the steel will remain elastic, that is, $\varepsilon_s < \varepsilon_y$ and $f_s < f_y$, while the masonry reaches its maximum strain of 0.003. The designer needs to assume the neutral axis depth (c) value so that $c > c_b$, and the strain in steel can then be determined from the following proportion (see Figure C-8c)):

$$\frac{\varepsilon_m}{d} = \frac{\varepsilon_s}{d - c}$$

thus

$$\varepsilon_s = \varepsilon_m \left(\frac{d - c}{c} \right)$$

The stress in the steel can be determined from Hooke's Law as follows

$f_s = E_s * \varepsilon_s$ (note that steel stress $f_s < f_y$)

where E_s is the modulus of elasticity for steel. The equations of equilibrium are the same as used in part 2 above, except that

$T_r = \phi_s f_s A_s$

The point corresponding to $c = t/2$ is considered as a special case. At that point, the strain distribution is defined by the following values

$\varepsilon_m = 0.003$ and $\varepsilon_s = 0$

thus
$T_r = 0$

4. Pure compression (zero eccentricity)
In the case of pure axial compression (S304-14 Cl.10.4.1) the axial load resistance for <u>untied sections</u> can be determined as follows:
$P_r = 0.85\phi_m f'_m A_e$ actual axial compression resistance
and
$P_{r\max} = 0.8P_r$ design axial compression resistance
According to S304-14 Cl.10.4.2, when the steel bars are <u>tied</u> as specified in Cl.12.2, then the steel contribution can be considered for the compression resistance. The design equation for tied wall sections is as follows:
$P_r = 0.85\phi_m f'_m (A_e - A_s) + \phi_s f_y A_s$
and
$P_{r\max} = 0.8P_r$

C.2 Wall Intersections and Flanged Shear Walls

Flanged shear wall configurations are encountered when a main shear wall intersects a cross-wall (or transverse wall). Examples of flanged walls in masonry buildings are very common, since the bearing wall systems often consist of walls laid in two orthogonal directions. Also, in medium-rise wood frame apartment buildings, elevator shafts are usually of masonry construction, and the intersecting masonry walls that form the core can be considered as flanged walls.

C.2.1 Effective Flange Width

10.6.2

In flanged shear walls, a portion of the cross wall is considered to act as the flange, while the main shear wall acts at the web. Depending on the cross-wall configuration, flanged shear walls may be of I, T- or L-section. An I-section is characterized by the two end flanges, similar to that in Figure C-11 (left), a T-section is characterized with one flanged end and one rectangular/ non-flanged end, while a L-section is characterized by one flanged end (similar to that shown in Figure C-11 (right), and one rectangular-shaped (non-flanged) end. Design codes prescribe the maximum effective flange width that may be considered in the shear wall design. The CSA S304-14 requirements for overhanging flange widths for these wall sections are summarized in Table C-1 and Figure C-11. For masonry buildings with substantial flanges the height ratio limits will usually govern.

Table C-1. Overhanging Flange Width Restrictions for T- and L- Section Walls per CSA S304-14 Cl.10.6.2

T-sections (b_T)	**L-sections (b_L)**
$b_T \leq$ the smallest of: a) b_{actual} b) $a_w/2$ c) $6 \cdot t$ d) $h_w/12$	$b_L \leq$ the smallest of: a) b_{actual} b) $a_w/2$ c) $6 \cdot t$ d) $h_w/16$

where
b_{actual} - actual overhang/flange width
a_w - clear distance between the adjacent cross walls
t - actual flange thickness
h_w - wall height

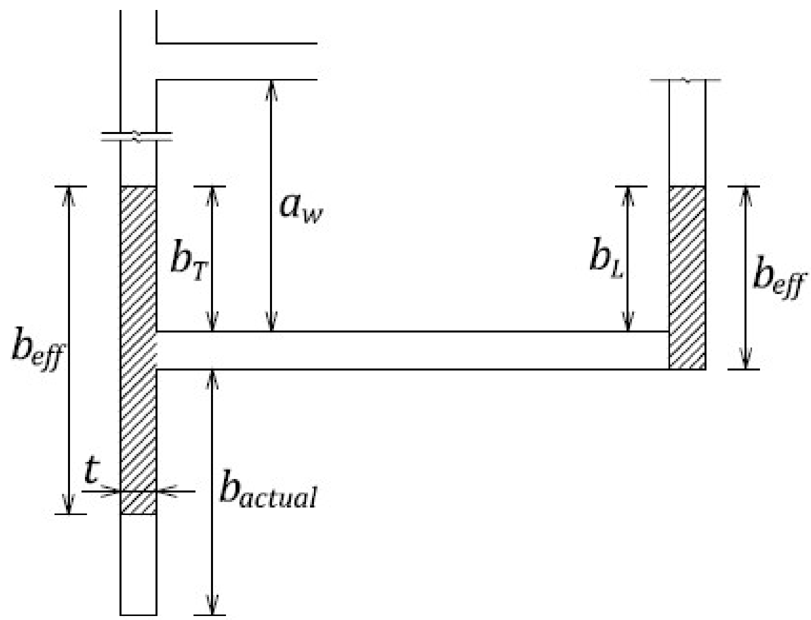

Figure C-11. CSA S304-14 flange width requirements.

C.2.2 Types of Intersections

According to Cl. 7.11, the effective shear transfer across the web-to-flange connection in both unreinforced and reinforced masonry walls can be achieved through bonded or unbonded intersections, as follows (see Figure C-12):

a) Bonded intersections – alternating courses with the units of one wall embedded at least 90 mm into the other wall (Cl.7.11.1),
b) Unbonded intersections (Cl.7.11.2) which can be achieved in the following ways:
    - Mechanical connection with steel connectors (e.g. anchor straps, rods, or bolts) at a maximum vertical spacing of 600 mm, and
    - Connection with a minimum of two 3.65 mm diameter steel wires from joint reinforcement spaced at a maximum of 400 mm vertically, or
    - Fully grouted bond beam intersections with reinforcing bars spaced at 1200 mm or less vertically.
    - Steel connectors, joint reinforcing and reinforcing bars should be detailed to develop the full yield strength on each side of the intersection.

Note that S304-14 Cl.10.11.2 does not permit the use of rigid anchors (approach b)) or joint reinforcement (approach c)) for portions of reinforced masonry shear walls in which the flanges contain tensile steel and are subject to axial tension, but reinforced bond beams (approach d)) may be used.

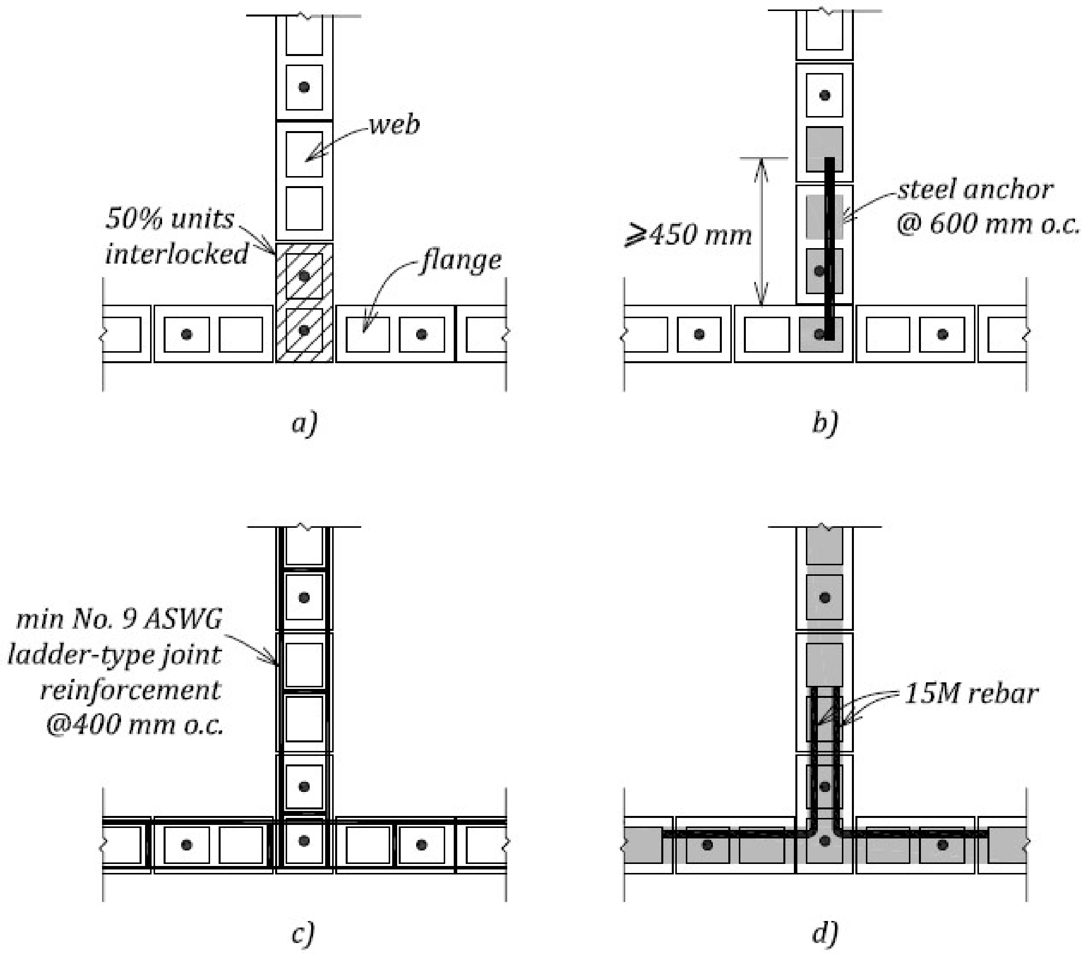

Figure C-12. Masonry wall intersections: a) bonded intersections; b) mechanical connection; c) horizontal joint reinforcement; d) horizontal reinforcing bars (bond beam reinforcement).

Seismic studies in the U.S. under the TCCMAR research program resulted in recommendations related to horizontal reinforcement at the web-to-flange intersections (Wallace, Klingner, and Schuller, 1998). To ensure the effective shear transfer, horizontal reinforcement in bond beams needs to be continued from one wall into other, for a distance of 600 mm (2 feet) or 40 bar diameters, whichever is greater. The grout must be continued across the intersection by removing the face shells of the masonry units in one of the walls, as illustrated in *Figure C-13*. Note that TMS 402/602-16 requires that bond beams in ductile walls be provided at a vertical spacing of 1200 mm (4 feet).

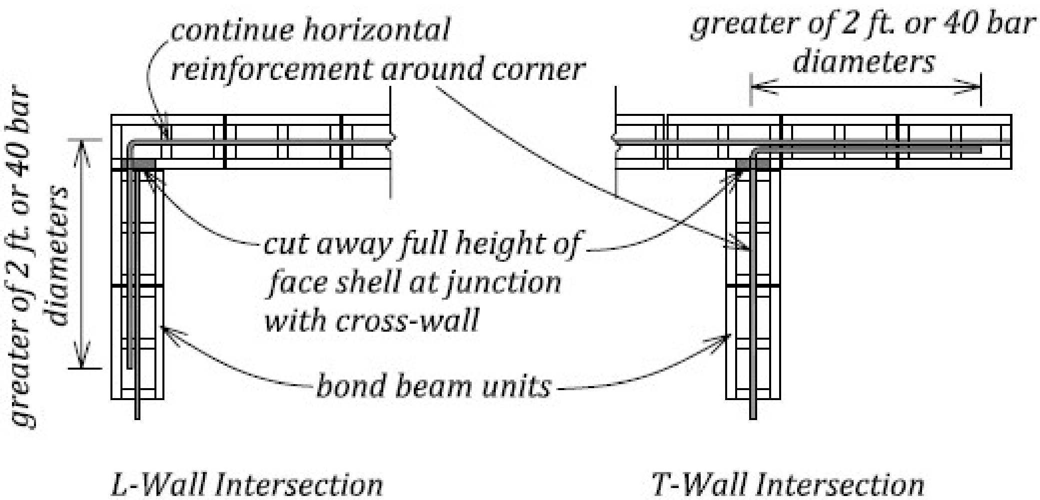

Figure C-13. Horizontal reinforcement at the web-to-flange intersection: TCCMAR recommendations.

C.2.3 Shear Resistance at the Intersections

7.11

Vertical shear resistance of the intersections must be checked by one of the following methods:

- For bonded intersections, vertical shear at the intersection shall not exceed the out-of-plane masonry shear resistance (Cl.7.10.2).
- For flanged sections with the mechanical steel connectors (Figure C-12 approach b), the connectors must be capable of resisting the vertical shear at the intersection. The connector resistance should be determined according to CSA A370-14.
- For flanged sections with the horizontal reinforcement (approaches c and d), the reinforcement must be capable of resisting the vertical shear at the intersection.

Vertical shear resistance for bonded wall intersections

7.11.1

The factored vertical shear resistance at bonded intersections should not exceed the factored shear resistance of the masonry taken as

$$V_r = 0.16\phi_m \sqrt{f'_m} A_e$$

where A_e is effective mortared area of the bed joint for hollow and partially grouted walls. For fully grouted walls A_e is gross cross-sectional area.

Minimum horizontal reinforcement shall be provided across the vertical intersection. This reinforcement shall be equivalent in area to at least two 3.65 mm diameter steel wires spaced 400 mm vertically.

Vertical shear resistance for unbonded wall intersections

7.11.2

Where wall intersections are not bonded in accordance with Cl.7.11.1, or where additional capacity is required, the factored shear resistance of the web-to-flange joint shall be based on the shear friction resistance taken as

$$V_r = \phi_m \mu C_h$$

where

μ = 1.0 coefficient of friction for the web-to-flange joint

C_h = compressive force in the masonry acting normal to the head joint, normally taken as the factored tensile force at yield of the horizontal reinforcement that crosses the vertical section. The reinforcement must be detailed to enable it to develop its yield strength on both sides of the vertical masonry joint, which may be hard to achieve in practice.

Commentary

For flanged walls with horizontal reinforcement, resistance to vertical shear sliding is provided by the frictional forces between the sliding surfaces, that is, the web and the flange of the wall. The shear friction resistance V_r is proportional to the coefficient of friction μ, and the clamping force C_h acting perpendicular to the joint of height h (see Figure C-14a)).

C_h is equal to the sum of the tensile yield forces developed in reinforcement of area A_s spaced at the distance s, that is,

$$C_h = \varphi_s f_y A_s \, h/s$$

In case of a flanged shear wall with openings, shear friction resistance V_r is provided by wall segments between the openings, as shown in Figure C-14b).

Reinforcement providing the shear friction resistance should be distributed uniformly across the joint. The bars should be long enough so that their yield strength can be developed on both sides of the vertical joint, as shown in Figure C-15b).

Cl.7.11.2 lists three approaches (a, b, and c) that can be used to ensure shear transfer at the web-to-flange interface for unbonded masonry. The U.S. masonry design standard TMS 402/602-16 prescribes intersecting bond beams in intersecting walls at maximum spacing of 1200 mm (4 ft) on centre. The bond beam reinforcement area shall not be less than 200 mm^2 per metre of wall height (0.1 in^2/ft), and the reinforcement shall be detailed to develop the full yield stress at the intersection.

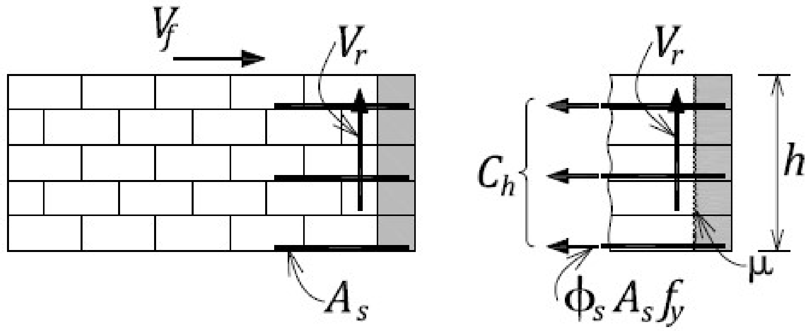

a)

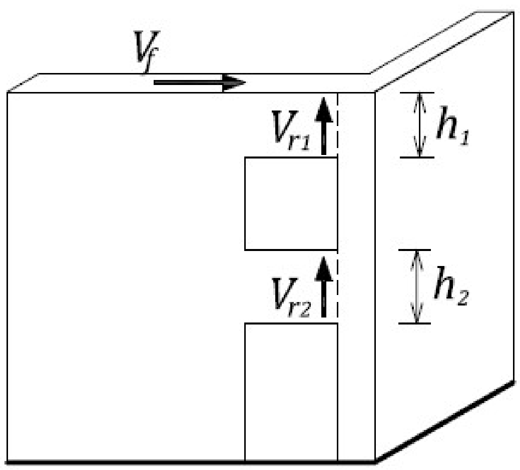

b)

Figure C-14. Shear friction resistance at the web-to-flange intersection: a) resistance provided by the reinforcement; b) flanged shear wall with openings.

When the shear resistance of the web-to-flange interface relies on masonry only (see Figure C-15a)), the horizontal shear stress v_f, due to shear force V_f, can be given by:

$$v_f = \frac{V_f}{t_e l_w}$$

where

t_e - effective web width

l_w - wall length

The designer should also find the vertical shear stress caused by the resultant compression force P_{fb}:

$$v_f = \frac{P_{fb}}{b_w * h_w}$$

The larger of these two values governs. The factored shear stress should be less than the factored masonry shear resistance, v_m, as follows

$v_f \leq v_m$

where

$v_m = 0.16\phi_m\sqrt{f'_m}$

If the above condition is not satisfied, horizontal reinforcement needs to be provided (see Figure C-15b)), and the following shear resistance check should be used

$v_r = v_m + v_s$

and

$v_f \leq v_r$

where v_s is the factored shear resistance provided by the steel reinforcement, which can be determined as follows:

$$v_s = \frac{\phi_s A_s f_y}{s \cdot t_e}$$

where A_s is area of horizontal steel reinforcement crossing the web-to-flange intersection at the spacing s.

Note that the reinforcement that crosses the vertical section has to be detailed to develop yield strength on both sides of the vertical masonry joint (see Figure C-15b)).

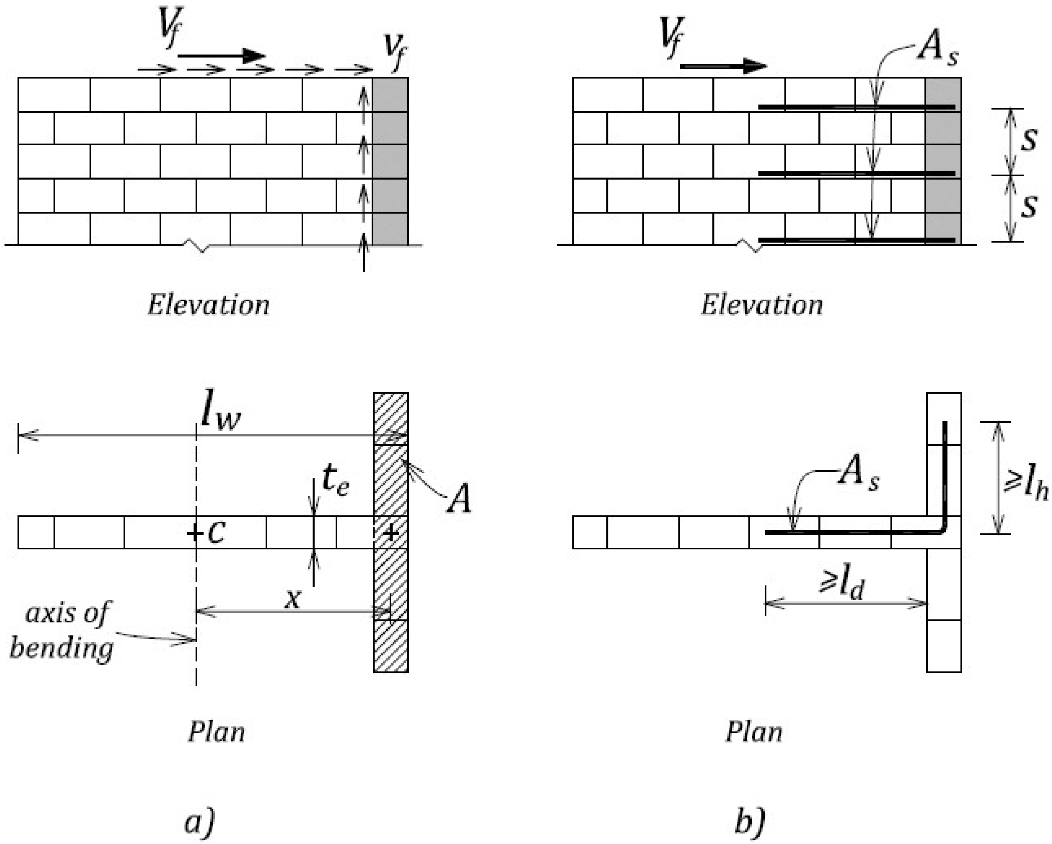

Figure C-15. Shear resistance of the web-to-flange interface: a) bonded masonry intersection; b) horizontal reinforcement at the intersection.

C.3 Wall Stiffness Calculations

The determination of wall stiffness is one of the key topics in the seismic design of masonry walls. Although this topic has been covered in other references (e.g. Drysdale and Hamid, 2006, and Hatzinikolas, Korany and Brzev 2015), a few key concepts are discussed in this section. Section C.3.2 derives expressions for the in-plane lateral stiffness of walls under the assumption that the walls are uncracked. For seismic analysis it is expected that the walls will be pushed into the nonlinear range, and so cracking will occur and the reinforcement will yield. The stiffness to be used in seismic analysis should not be the linear elastic (uncracked) stiffness but some effective stiffness that reflects the effect of cracking up to the yield capacity of the wall. Section C.3.5 gives some suggestions for the effective stiffness of shear walls responding in shear-dominant and flexure-dominant modes.

C.3.1 Lateral Load Distribution

The distribution of lateral seismic loads to individual walls can be performed once the storey shear forces have been determined from the seismic analysis. The flexibility of floor and/or roof diaphragms is one of the key factors influencing the load distribution (for more details, see Example 3 in Chapter 3). In the case of a flexible diaphragm, the lateral storey forces are usually distributed to the individual walls based on the tributary area. In the case of a rigid diaphragm, these forces are distributed in proportion to the stiffness of each wall. In calculating the wall forces, torsional effects must be considered, as discussed in Section 1.11. The distribution of lateral loads (without torsional effects) in a single-storey building with a rigid diaphragm is shown in Figure C-16.

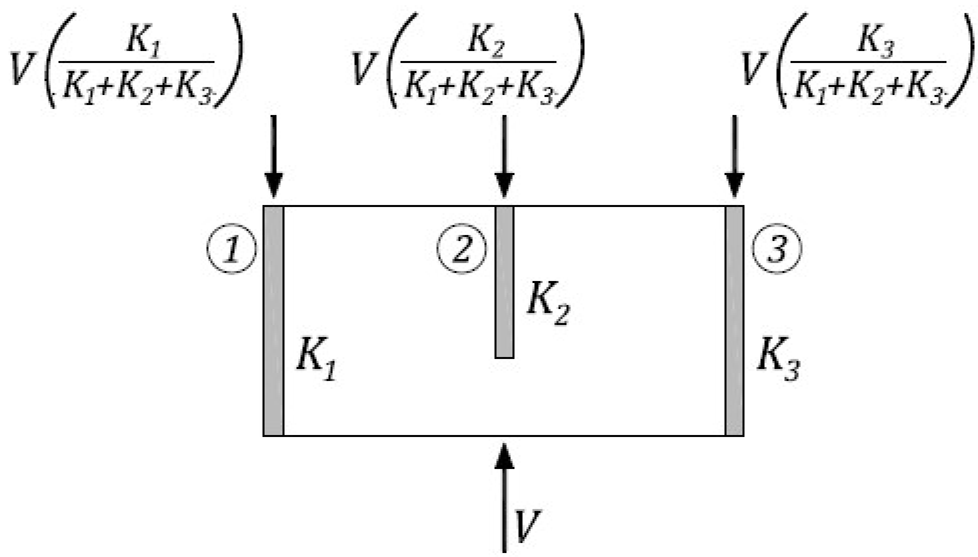

Figure C-16. Distribution of lateral loads to individual walls.

Wall stiffness is usually determined from the elastic analysis, and depends on wall height/length aspect ratio, thickness, mechanical properties, extent of cracking, size and location of openings, etc.

C.3.2 Wall Stiffness: Cantilever and Fixed-End Model

Wall stiffness depends on the end support conditions, that is, whether a wall or pier is fixed or free to move and/or rotate at its ends. Two models for wall stiffness include the cantilever model and the fixed-end model, as shown in Figure C-17. In the cantilever model, the wall is free to rotate and move at the top in the horizontal direction – this is usually an appropriate model for the walls in a single-storey masonry building.

The stiffness can be defined as the lateral force required to produce a unit displacement, but it is determined by taking the inverse of the combined flexural and shear displacements produced by a unit load. It should be noted that flexural displacements will govern for walls with an aspect ratio of 2 or higher. For example, the contribution of shear deformation in a wall with a height/length aspect ratio of 2.0, is 16% for the cantilever model and 43% for the fixed-end model. The stiffness equations presented in this section take into account both shear and flexural deformations.

The stiffness of a cantilever wall or a pier can be determined from the following equation (see Figure C-17 a)):

$$\frac{K}{E_m * t} = \frac{1}{\left(\frac{h}{l_w}\right)\left[4\left(\frac{h}{l_w}\right)^2 + 3\right]} \qquad (13)$$

The stiffness of a wall or a pier with the fixed ends can be determined from the following equation (see Figure C-17 b)):

$$\frac{K}{E_m * t} = \frac{1}{\left(\frac{h}{l_w}\right)\left[\left(\frac{h}{l_w}\right)^2 + 3\right]} \qquad (14)$$

where

h - wall height (cantilever model) or clear pier height (fixed-end model)

l_w - wall or pier length

$E_m = 850 f'_m$ modulus of elasticity for masonry

The following assumptions have been taken in deriving the above equations:

$G_m = 0.4 E_m$ modulus of rigidity for masonry (shear modulus)

$I = \frac{t_e * l_w^{\ 3}}{12}$ uncracked wall moment of inertia

$A_v = \frac{5 * t_e * l_w}{6}$ shear area (applies to rectangular wall sections only)

where t_e = effective wall thickness.

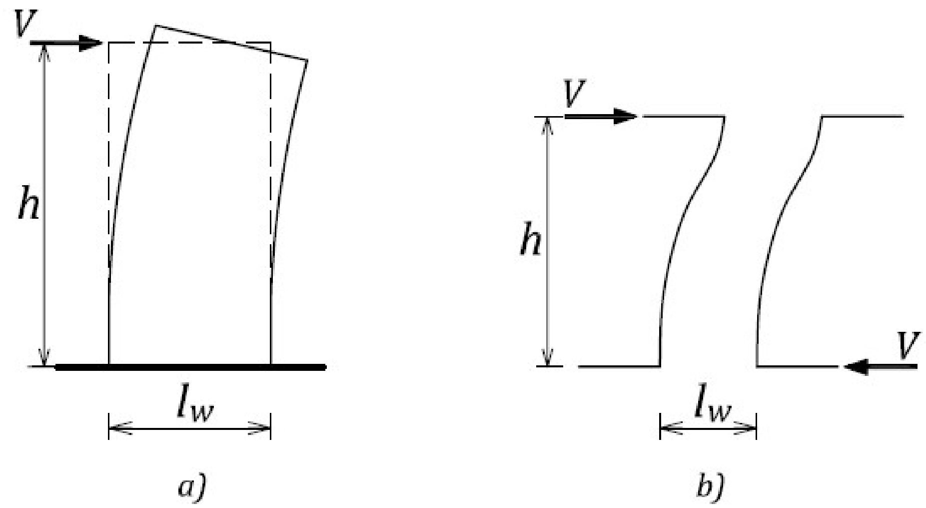

Figure C-17. Wall stiffness models: a) cantilever model, and b) fixed-end model.

The wall stiffnesses for both models for a range of height/length aspect ratios are presented in Table D-3. Note that the derivation of stiffness equations has been omitted since it can be found in other references (see Hatzinikolas, Korany and Brzev 2015).

C.3.3 Approximate Method for Force Distribution in Masonry Shear Walls

In most real-life design applications, walls are perforated with openings (doors and windows). The seismic shear force in a perforated wall can be distributed to the piers in proportion to their stiffnesses. This approach is feasible when the openings are very large and the stiffness of lintel beams is small relative to the pier stiffnesses, or if the lintel beam is very stiff so that connected piers act as fixed-ended walls. Figure C-18 illustrates the distribution of the wall shear force V to individual piers in direct proportion to their stiffness. Note that, according to this model, the wall shear force is equal to the sum of shear forces in the piers, that is,

$$V = \sum V_i$$

where

$V_i = K_i * \Delta_i$ force in the pier i

Thus

$$V = \sum (K_i * \Delta_i)$$

If the floor diaphragm is considered to be rigid, it can be assumed that the lateral displacement in all piers is equal to Δ, that is,

$$\Delta_A = \Delta_B = \Delta_C = \Delta$$

and so

$$V = (\sum K_i) * \Delta$$

Thus

$$\Delta = \frac{V}{\sum K_i}$$

where

$$K = \sum K_i$$

denotes the overall wall stiffness for the system.

Therefore, the force in each pier is proportional to its stiffness relative to the sum of all pier stiffnesses within the wall, as follows

$$V_i = K_i * \Delta_i = K_i * \frac{V}{\sum K_i} = V * \frac{K_i}{\sum K_i}$$

This means that stiffer piers are going to attract a larger portion of the overall shear force. This can be explained by the fact that a larger fraction of the total lateral force is required to produce the same deflection in a stiffer wall as in a more flexible one.

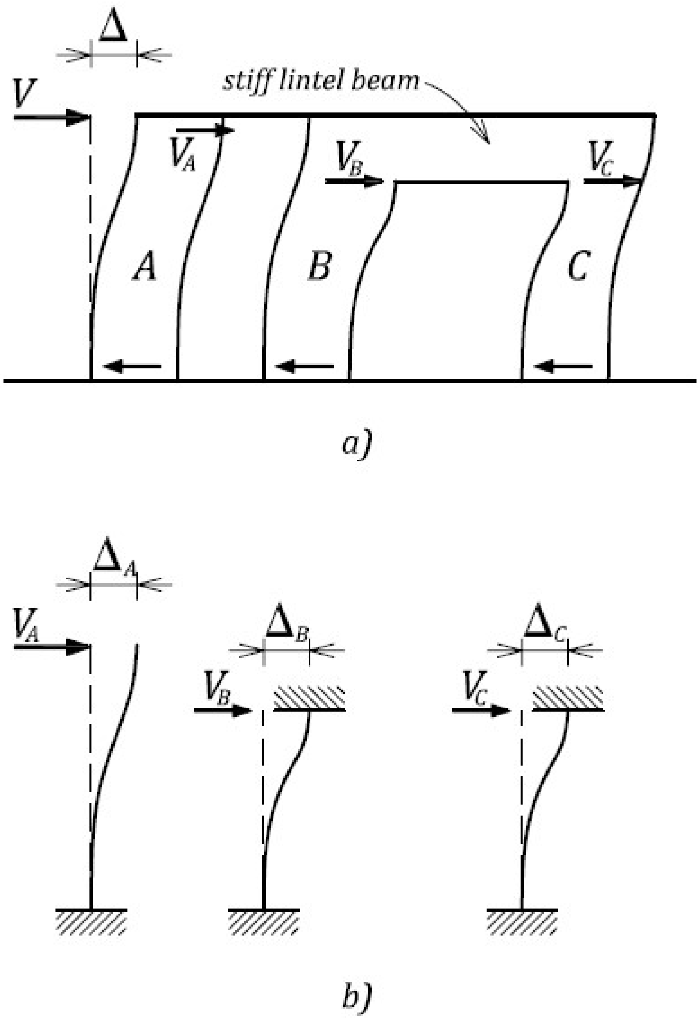

Figure C-18. Shear force distribution in a wall with a rigid diaphragm: a) wall in the deformed shape: b) pier forces.

An approximate approach for determining the stiffness of a solid shear wall in a multi-storey building is to consider the structure as an equivalent single-storey structure, as shown in Figure C-19. The entire shear force is applied at the effective height, h_e, defined as the height at which the shear force V_f must be applied to produce the base moment M_f, that is,

$$h_e = \frac{M_f}{V_f}$$

The wall stiffness is found to be equal to the reciprocal of the deflection at the effective height Δ_e, as follows

$$K = \frac{1}{\Delta_e}$$

This model, although not strictly correct, can be used to determine the elastic distribution of the torsional forces as well as the displacements, as illustrated in Example 2 in Chapter 4.

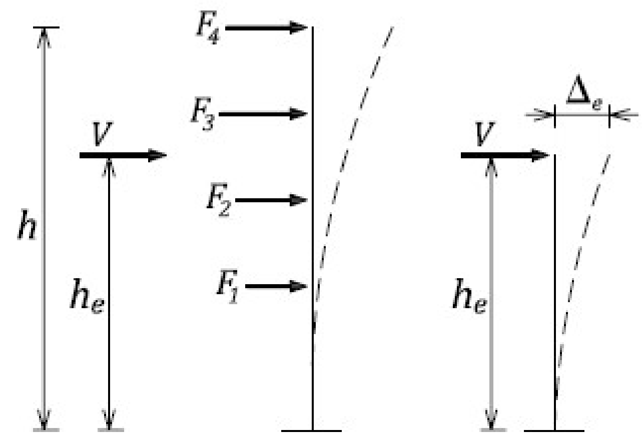

Figure C-19. Vertical combination of wall segments with different stiffness properties.

Several different elastic analysis approaches can be used to determine the stiffness of a wall with openings. A simplified approach suitable for the stiffness calculation of a perforated wall in a single-storey building can be explained with the help of an example of the wall X_1 shown in Figure C-20 (see also Example 3 in Chapter 3). For a unit load applied at the top, the wall stiffness calculation involves the following steps:

- First, calculate the deflection at the top for a cantilever wall, considering the wall to be solid (Δ_{solid}).
- Next, calculate the deflection for the strip containing openings (Δ_{strip}), considering the full wall length (i.e. ignore openings).
- Finally, calculate the deflection for the piers A, B, C, and D (Δ_{ABCD}) assuming that all piers have the same deflection.

Note that the deflections for individual components are calculated as the inverse of their stiffness values, and that the pier stiffnesses are determined assuming either the cantilever or fixed-end models. In most cases, the use of the cantilever model is more appropriate.

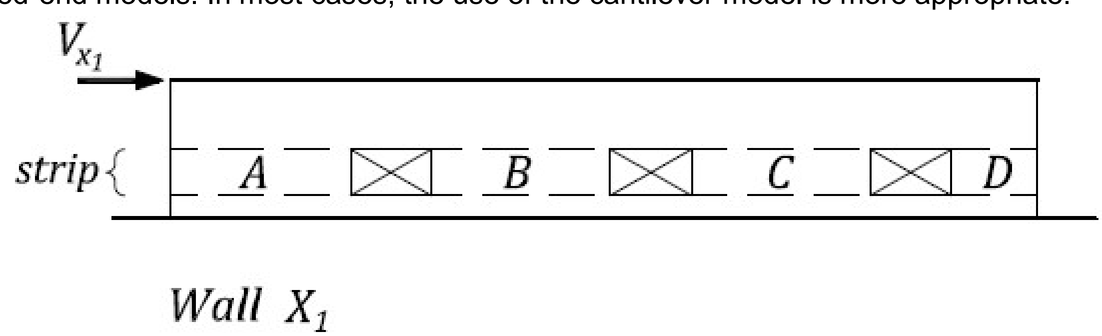

Figure C-20. An example of a perforated wall.

The overall wall deflection can be determined by combining the deflections for these components, as follows:

$$\Delta = \Delta_{solid} - \Delta_{strip} + \Delta_{ABCD}$$

Note that the strip deflection is subtracted from the solid wall deflections - this removes the entire portion of the wall containing all the openings, which is then replaced by the four segments.

Finally, the wall stiffness is equal to the reciprocal of the deflection, as follows

$$K = \frac{1}{\Delta}$$

C.3.4 Advanced Design Approaches for Reinforced Masonry Shear Walls with Openings

The approximate approach based on elastic analysis presented in Section C.3.3 is appropriate for determining the lateral force distribution in masonry walls. However, that method is not adequate for predicting the strengths in perforated reinforced masonry shear walls (walls with openings). Openings in a masonry shear wall alter its behaviour and add complexity to its analysis and design. When the openings are relatively small, their effect can be ignored, however in most walls the openings need to be considered. The following two design approaches can be used to design walls with openings:

1) Plastic analysis method, and
2) Strut-and-tie method.

These two approaches have been evaluated by experimental studies and have shown very good agreement with the experimental results (Voon, 2007; Elshafie et al., 2002; Leiva and Klingner, 1994). The key concepts will be outlined in this section.

C.3.4.1 Plastic analysis method

The plastic analysis method, also known as limit analysis, can be used to determine the ultimate load-resisting capacity for statically indeterminate structures. A masonry wall with an opening as shown in Figure C-21a) can be modeled as a frame (see Figure C-21b)). The model is subjected to an increasing load until the flexural capacity of a specific section is reached and a *plastic hinge* is formed at that location. (The plastic hinge is a region in the member that is assumed to be able to undergo an infinite amount of deformation, and can therefore be treated as a hinge for further analysis.) With further load increases, plastic hinges will be formed at other sections as their flexural capacity is reached. This process continues until the system becomes statically determinate, at which point the formation of one more plastic hinge will result in a collapse under any additional load. This is called a collapse mechanism, and an example is shown in Figure C-21c). There is usually more than one possible collapse mechanism for a statically indeterminate structure, and the mechanism that gives the lowest capacity is closest to the ultimate capacity, as this is an upper bound method.

For specific application to perforated masonry walls, the wall is idealized as an equivalent frame, where piers are modeled as fixed at the base, and either pinned or fixed at the top, while lintels are modeled as fixed at the ends. A failure state is reached when plastic hinges form at the member ends, and the collapse mechanism forms. The sequence of plastic hinge formation depends on the relative strength and stiffness of the elements. In this approach, structural members must be designed to behave mainly in a flexural mode, while a shear failure is avoided by applying the capacity design approach.

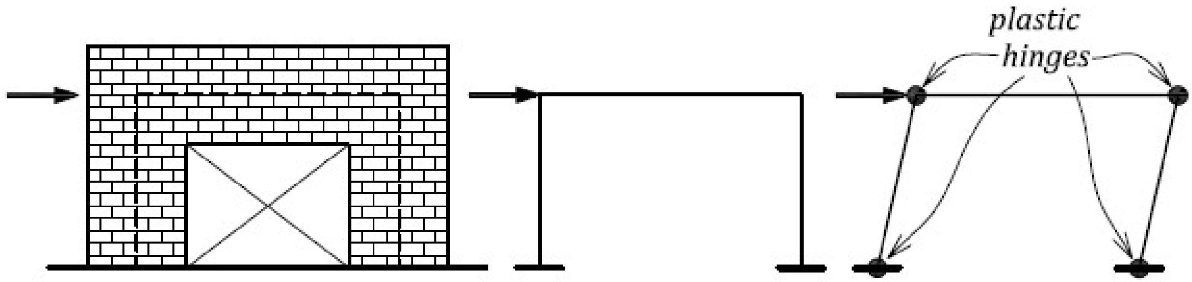

a) b) c)

Figure C-21. An example of a plastic collapse mechanism for a frame system: a) perforated masonry wall; b) frame model; c) plastic collapse mechanism.

The following two mechanisms are considered appropriate for the plastic analysis of reinforced masonry walls with openings, as shown in Figure C-22 (Leiva and Klingner, 1994; Leiva et al. 1990):

b) pier mechanism, and

c) coupled wall mechanism.

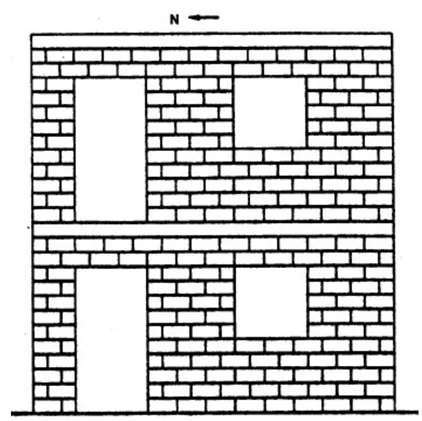

a)

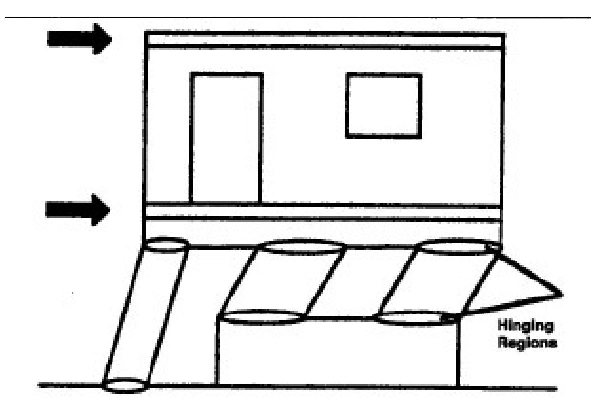

b)

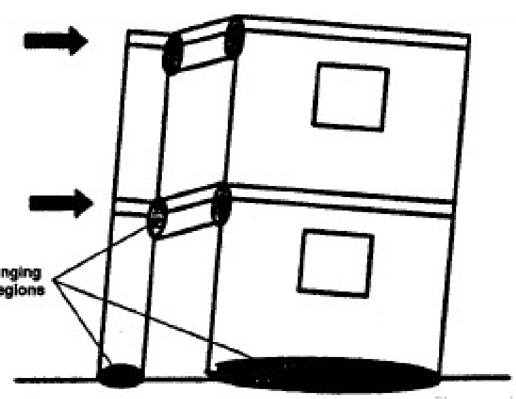

c)

Figure C-22. Plastic analysis models for perforated walls: a) actual wall; b) pier model; c) coupled wall model (Leiva and Klingner, 1994, reproduced by permission of The Masonry Society).

A pier mechanism is a collapse mechanism with flexural hinges at the tops and bottoms of the piers. A pier-based design philosophy visualizes a perforated wall as a ductile frame. Horizontal reinforcement above and below the openings is needed to transfer the pier shears into the rest of the wall. A drawback of the pier mechanism is that the formation of plastic hinges at the top and bottom of all piers at a story level can lead to significant damage to the piers, which are the main vertical load-carrying elements.

A coupled wall mechanism is a collapse mechanism in which flexural hinges are formed at the base of the wall and at the ends of the coupling lintels. A perforated wall is modeled as a series of ductile coupled walls; this concept is similar to that used for seismic design of reinforced concrete shear walls. The vertical reinforcement in each pier must be designed so that the flexural capacity of the piers exceeds the flexural capacity of the coupling beams. To achieve this, additional longitudinal reinforcement is placed in the piers, but cut off before it reaches the wall base. The shear reinforcement in the coupling beams is designed based on the flexural and shear capacity of the piers. Since masonry walls are usually long in plan, the formation of plastic hinges at their bases produces large strains in the wall longitudinal reinforcement. Plastic hinges must have adequate rotational capacity to allow the complete mechanism to form; this can be achieved in wall structures with low axial load. To ensure the successful application of the plastic analysis method, the wall reinforcement must be detailed to develop the necessary strength and inelastic deformation capacity.

Figure C-23 shows a simple single-storey wall that is analyzed for the two mechanisms. Ultimate shear forces corresponding to the pier and coupled wall mechanisms can be determined from the equations of equilibrium assuming that the moments at the plastic hinge locations are known. These equations are summarized in Figure C-23 (Elshafaie et al., 2002).

The plastic analysis method has a few advantages: stiffness calculations are not required, and the designer can choose the failure mechanism, which ensures a desirable ductile response. The designer needs to have a general background in plastic analysis, which is covered in several references, e.g. Bruneau, Uang, and Whittaker (1998) and Ferguson, Breen, and Jirsa (1988). This method is also used for the seismic analysis of concrete and steel structures, and is referred to as nonlinear static analysis or pushover analysis.

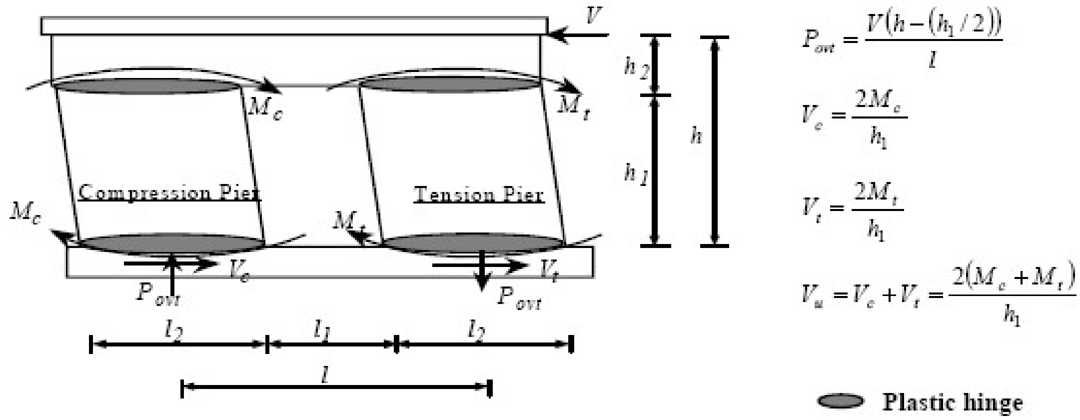

a)

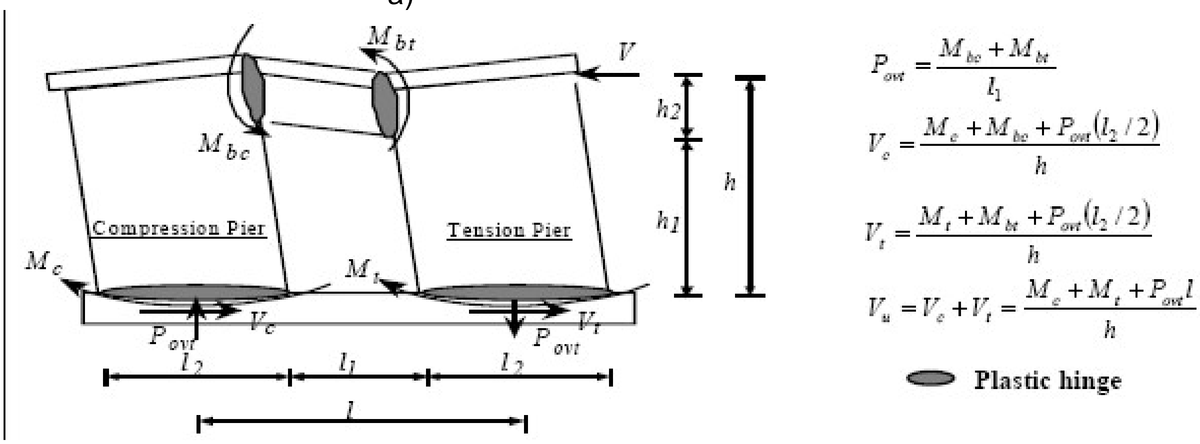

b)

Figure C-23. Ultimate wall forces according to the plastic analysis method: a) pier mechanism; b) coupled wall mechanism (Elshafaie et al., 2002, reproduced by permission of the Masonry Society).

C.3.4.2 Strut-and-Tie Method

The strut-and-tie method essentially follows the truss analogy approach used for shear design of concrete and masonry structures. Pin-connected trusses consist of steel tension members (ties), and masonry compression members (struts). The masonry compression struts develop between parallel inclined cracks in the regions of high shear. The essential feature of this approach is that the designer needs to find a system of internal forces that is in equilibrium with the externally applied loads and support conditions. A further essential feature is that the designer must ensure that the steel and masonry tie members provided adequately resist the forces obtained from the truss analysis.

The design of tension ties is particularly important. If a ductile response is to be assured, the designer should choose particular tension chords in which yielding can best be accommodated. Other ties can be designed so that no yielding will occur by using the capacity design approach. The magnitudes of the forces in critical tension ties can be determined from statics, corresponding to the overturning moment capacity of the wall using the nominal material properties (rather than the factored ones). The remaining forces are then determined from the equilibrium of nodes (conventional truss analysis). Compression forces developed in masonry struts are usually small due to the small compression strains and do not govern the design.

Careful detailing of the wall reinforcement is necessary to ensure that the actual structural response will correspond to that predicted by the analytical model.

The designer needs to use judgement to simplify the force paths that are chosen to represent the real structure – these differ considerably depending on individual judgement.

An example of a strut-and-tie model for a two-storey perforated masonry wall subjected to seismic lateral load is shown in Figure C-24 (note that gravity load also needs to be considered in the analysis, however it is omitted from the figure). It can be seen that two different models are required to account for the alternate direction of seismic load. The examples show the seismic load being applied as a compressive load to the building; however, these loads should be applied to the floor levels, depending on the diaphragm-to-wall connection. The designated tie members in one model will become struts in the other model (when the seismic load changes direction). An advantage of the reversible nature of seismic forces is that a significant fraction of the inelastic tensile strains imposed on the end strut members is recoverable due to force reversal, thereby providing hysteretic energy dissipation. A detailed solution for this example is presented in the User's Guide by NZCMA (2004).

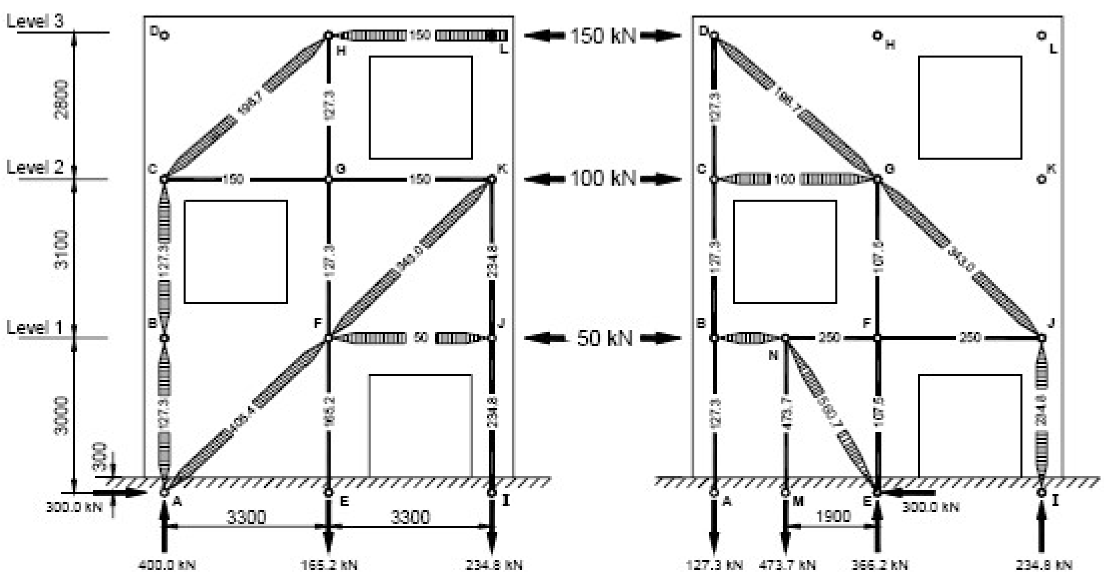

Figure C-24. Strut-and-tie models for a masonry wall corresponding to different directions of seismic loading (NZCMA, 2004, reproduced by the permission of the New Zealand Concrete Masonry Association Inc.).

Strut-and-tie models are used for the design of masonry walls in New Zealand, and this approach is explained in more detail by Paulay and Priestley (1992). The New Zealand Masonry Standard NZS 4230:2004 (SANZ, 2004) recommends the use of strut-and-tie models for the design of perforated reinforced masonry shear walls. In Canada, strut-and-tie models are used to design discontinuous regions of reinforced concrete structures according to the Standard CSA A23.3-04 Design of Concrete Structures. The design concepts and applications of strut-and-tie models for concrete structures in Canada are covered by McGregor and Bartlett (2000).

C.3.5 The Effect of Cracking on Wall Stiffness

The behaviour of masonry walls under seismic load conditions is rather complex and depends on the failure mechanism (shear-dominant or flexure-dominant), as discussed in Section 2.3.1. Figure C-25 shows the hysteretic response of shear-dominant and flexure-dominant walls. The effective stiffness discussed in this section reflects the secant stiffness up to first crack in brittle shear-dominant walls, and the stiffness for an elastic-perfectly-plastic model that would approximate the strength envelope of the hysteretic plot in ductile flexure-dominant walls.

For the *shear-dominant mechanism*, the response is initially elastic until cracking takes place, at which point there is a substantial drop in stiffness. This is particularly pronounced after the development of diagonal shear cracks. After a few major cracks develop, the load resistance is taken over by the diagonal strut mechanism, and the shear stiffness can be estimated by an appropriate strut model. However, the stiffness drops significantly shortly after the strut mechanism is formed and can be considered to be zero for most practical purposes (see Figure C-25b)). It is expected that an increase in the quantity of vertical and horizontal steel and/or the magnitude of axial compressive stress causes a reduced crack size and an increase in the shear stiffness (Shing et al., 1990).

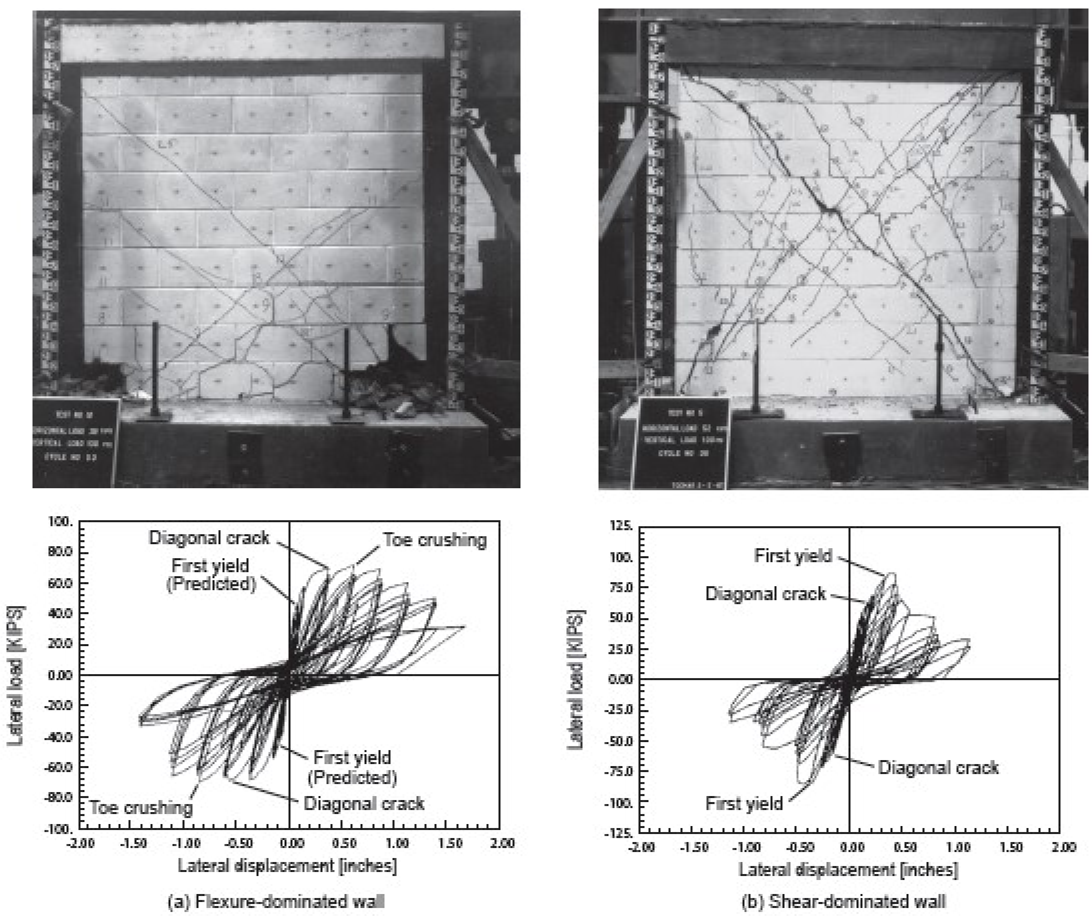

Figure C-25. Cracking pattern and load-displacement curves for damaged masonry wall specimens tested by Shing et al. (1990, 1991): a) flexure-dominant response, and b) shear-dominant response (Kingsley, Shing, and Gangel, 2014).

For the *flexure-dominant mechanism*, a drop in the stiffness immediately after the onset of cracking is not very significant. As can be seen from Figure C-25a), the stiffness drops after the yielding of vertical reinforcement takes place, and continues to drop with increasing inelastic lateral deformations (this depends on the ductility capacity of the wall under consideration). The specimen for which the results are shown in Figure C-25a) showed yielding of vertical reinforcement and compressive crushing of masonry at the wall toes (Shing et al., 1989).

Note that the height of wall test specimens shown in Figure C-23 was 1.8 m (6 feet), thus a 2.5% drift ratio permitted by the NBC 2015 for regular buildings corresponds to 45 mm (1.8 inch) displacement. It can be seen that the displacements and drifts in these specimens are very low, particularly so for the shear-dominant specimen shown in Figure C-25b).

Evidence from studies that focus on quantifying the changes in in-plane wall stiffness under increasing lateral loading are limited, so CSA S304-14 and other masonry codes do not provide guidance related to this issue. Shing et al. (1990) tested a series of 22 cantilever block masonry wall specimens that were laterally loaded at the top, with a height/length aspect ratio of 1.0. Based on the experimental test data, they have recommended the following empirical equation for the lateral stiffness of a wall with a shear-dominant response

$$K_e = (0.2 + 0.1073 f_c) K_{shear} \le K_{el} \qquad (15)$$

where

$K_{shear} = \dfrac{E_m * t_e}{3 * \left(\dfrac{h}{l_w}\right)}$ is the shear stiffness of a wall/pier

h = wall height

l_w = wall length

t_e = effective wall thickness

f_c = axial compressive stress (MPa)

The above equation is based on the force/displacement measurements taken just after the first diagonal crack developed, in specimens with a height/length ratio of 1.0. For seismic applications where the walls are expected to yield in flexure before failing in shear, and the lateral stiffness is used to estimate the fundamental period of the structure and to determine the seismic displacements, it is more appropriate to determine the effective stiffness from a cracked section analysis at first yield of the tension reinforcement.

A study by Priestley and Hart (1989), based on the cracked transformed section stiffness at first yield of the tension reinforcement, recommends that the effective moment of inertia, I_e, of a wall can be approximated by:

$$I_e = \left(\frac{100}{f_y} + \frac{P_f}{f'_m A_e}\right) I_g \qquad (16)$$

where

f_y = steel yield strength (MPa)

P_f = factored axial load

A_e = effective cross-sectional area for the wall

f'_m = masonry compressive strength, and

$I_g = \dfrac{t_e * l_w^3}{12}$ is the gross moment of inertia of the wall.

Note that the first term in the bracket, $100/f_y$, is equal to 0.25 for $f_y = 400$ MPa (Grade 400 steel). The second term is a ratio of axial compressive stress in the wall, equal to P_f / A_e , and the masonry compressive strength, f'_m .

The above relation is based solely on consideration of flexural stiffness, and is a best fit relationship for several different values of height/length ratio (h/l_w), steel strength, vertical reinforcement ratio and axial load. Other considerations are whether the vertical reinforcement is uniformly distributed across the wall length or concentrated at the ends, and the effect of tension stiffening. The vertical reinforcement ratio is not included in the above expression, and as a result, the wall stiffness is overestimated for lightly reinforced walls and underestimated for heavily reinforced walls.

If it is assumed that wall cracking causes the same proportional decrease in the effective shear area as it does for the moment of inertia, then the stiffnesses can be combined to give the following equation for the reduced wall stiffness, K_{ce} ,

$$K_{ce} = \left(\frac{100}{f_y} + \frac{P_f}{f'_m A_e}\right) K_c \qquad (17)$$

where

$$K_c = \frac{E_m * t_e}{\left(\dfrac{h}{l_w}\right)\left[4\left(\dfrac{h}{l_w}\right)^2 + 3\right]}$$

is the combined stiffness of an uncracked <u>cantilever</u> wall or pier, considering both the flexural and shear deformation components (refer to Section C.3.2 for the wall stiffness equations).

The terms in the large right-hand bracket of the K_c equation give the comparative value of flexural deformation to shear deformation. At a h/l_w ratio of 1.0, flexure contributes 4/7 of the total deformation and shear 3/7, while at a h/l_w ratio of 0.5, shear contributes ¾ of the total defection.

The Priestley and Hart equation was obtained using experimental data related to cantilever wall specimens, however it may also be used for fixed-end walls. The stiffness equation for these walls, K_{fe} , is the same as for the cantilever walls, that is,

$$K_{fe} = \left(\frac{100}{f_y} + \frac{P_f}{f'_m A_e}\right) K_f \qquad (18)$$

where

$K_f = \dfrac{E_m * t_e}{\left(\dfrac{h}{l_w}\right)\left[\left(\dfrac{h}{l_w}\right)^2 + 3\right]}$ is the stiffness of an uncracked <u>fixed-end</u> wall or a pier

A comparison of the proposed equations for a masonry block wall under axial compressive stress is presented in Figure C-26. The following values were used in the calculations: $f_y = 400$ MPa, P_f / A_e = 1 MPa, and f'_m = 10 MPa.

Note that the Shing equation is only shown for h/l_w up to 1.5 as it is based entirely on shear deformation. Since the Shing equation represents stiffness at first diagonal cracking, it is expected to give higher stiffness values than the Priestley-Hart equation. Use of the Priestley-Hart stiffness equation is recommended since it is valid for all h/l_w ratios.

The elastic uncracked stiffness could be used to distribute lateral seismic load to individual walls and piers, but the reduced cracked stiffness should be used for period estimation and deflection calculations.

The wall design deflections can be found from the following equation:

$$\Delta_{design} = \Delta_{el} * \frac{R_d * R_o}{I_E}$$

where

Δ_{el} = elastic deflections calculated using the reduced wall stiffness (K_{ce} or K_{fe}) and the factored design forces, and

$\frac{R_d * R_o}{I_E}$ = deflection multiplier to account for the effects of ductility, overstrength, and the building importance factor (see Section 1.13)

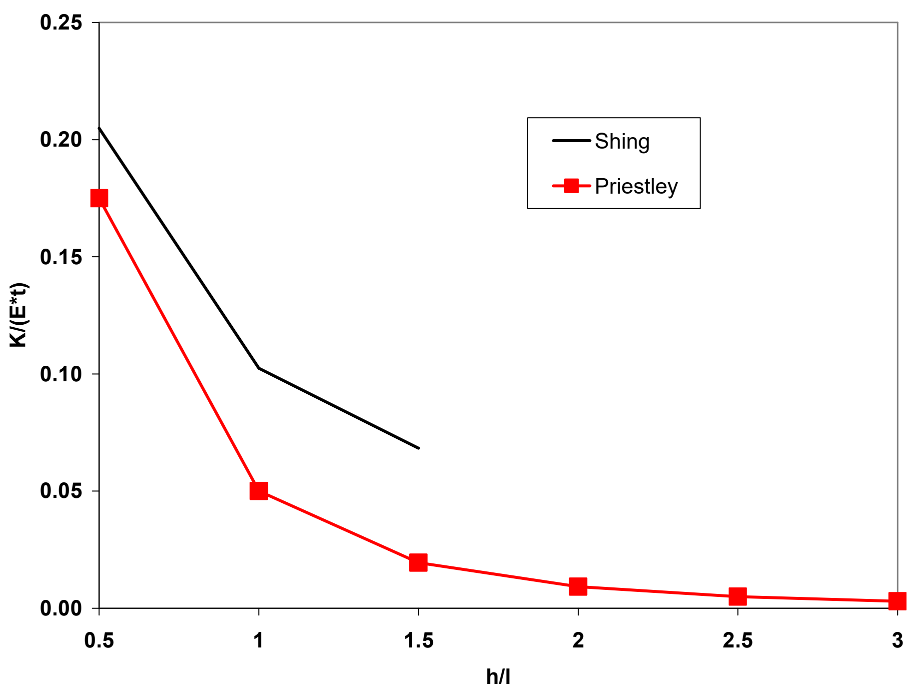

Figure C-26. A comparison of the stiffness values obtained using the Shing and Priestley-Hart equations.

TABLE OF CONTENTS – APPENDIX D

D DESIGN AIDS **D-2**

Table D-1. Properties of Concrete Masonry Walls (per metre or foot length) D-2
Table D-2. c/l_w ratio, f_y = 400 MPa D-3
Figure D-1. c/l_w ratio, f_y = 400 MPa D-4
Table D-3. Wall Stiffness Values $K/(E_m * t)$ D-5

D Design Aids

Table D-1. Properties of Concrete Masonry Walls (per metre or foot length)[1]

Grouted Cells / metre		0.00	0.83	1.00	1.25	1.67	2.50	5.00
Cell/dowel Spacing (mm)		*none*	1200	1000	800	600	400	200
Nominal Size		***150***	mm		*6*	inch		
A_e	$(mm^2 \times 10^3)$	52.0	66.7	69.6	74.0	81.3	96.0	140.0
	(in^2)	24.6	31.5	32.9	35.0	38.4	45.4	66.2
I_x	$(mm^4 \times 10^6)$	172	181	183	186	191	201	229
	(in^4)	126	133	134	136	140	147	168
S_x	$(mm^3 \times 10^6)$	2.46	2.59	2.62	2.66	2.73	2.87	3.27
	(in^3)	45.8	48.2	48.7	49.5	50.7	53.3	60.8
Weight	(kN/m^2)	1.90	2.09	2.13	2.19	2.29	2.49	3.08
	(psf)	39.6	43.7	44.6	45.8	47.9	52.0	64.3
Nominal Size		***200***	mm		*8*	inch		
A_e	$(mm^2 \times 10^3)$	75.4	94.5	98.3	104.0	113.6	132.7	190.0
	(in^2)	35.6	44.6	46.5	49.2	53.7	62.7	89.8
I_x	$(mm^4 \times 10^6)$	442	464	468	475	485	507	572
	(in^4)	324	340	343	347	355	371	419
S_x	$(mm^3 \times 10^6)$	4.66	4.88	4.93	5.00	5.11	5.34	6.02
	(in^3)	86.7	90.9	91.7	93.0	95.0	99.3	112.0
Weight	(kN/m^2)	2.46	2.75	2.81	2.89	3.03	3.32	4.18
	(psf)	51.4	57.4	58.6	60.4	63.4	69.4	87.3
Nominal Size		***250***	mm		*10*	inch		
A_e	$(mm^2 \times 10^3)$	81.7	108.1	113.4	121.3	134.5	160.9	240.0
	(in^2)	38.6	51.1	53.6	57.3	63.5	76.0	113.4
I_x	$(mm^4 \times 10^6)$	816	872	883	900	928	984	1152
	(in^4)	598	638	647	659	679	721	844
S_x	$(mm^3 \times 10^6)$	6.80	7.27	7.36	7.50	7.73	8.20	9.60
	(in^3)	126.5	135.2	136.9	139.5	143.8	152.5	178.6
Weight	(kN/m^2)	2.97	3.35	3.43	3.55	3.74	4.12	5.28
	(psf)	62.0	70.0	71.7	74.1	78.1	86.1	110.3
Nominal Size		***300***	mm		*12*	inch		
A_e	$(mm^2 \times 10^3)$	88.3	121.9	128.6	138.7	155.5	189.2	290.0
	(in^2)	41.7	57.6	60.8	65.5	73.5	89.4	137.0
I_x	$(mm^4 \times 10^6)$	1341	1456	1479	1514	1571	1687	2032
	(in^4)	982	1066	1083	1108	1150	1235	1488
S_x	$(mm^3 \times 10^6)$	9.25	10.04	10.20	10.44	10.83	11.63	14.01
	(in^3)	172.1	186.8	189.7	194.1	201.5	216.3	260.6
Weight	(kN/m^2)	3.53	4.00	4.10	4.24	4.48	4.95	6.38
	(psf)	73.7	83.6	85.6	88.6	93.6	103.5	133.3
Note:	Assume Bond Beams at 2.4 m (8 ft) O.C.							
	Table based on Metric blocks and modules (190 mm high units)							
	Assumed Weight	22	kN/m3	140.4	pcf			

[1] Source: Masonry Technical Manual (MIBC, 2017, reproduced by permission of the Masonry Institute of BC)

Table D-2. c/l_w *ratio,* f_y *= 400 MPa*

ω	α										
	0.000	0.025	0.050	0.075	0.100	0.150	0.200	0.250	0.300	0.350	0.400
0	0.000	0.037	0.074	0.110	0.147	0.221	0.294	0.368	0.441	0.515	0.588
0.01	0.014	0.050	0.086	0.121	0.157	0.229	0.300	0.371	0.443	0.514	0.586
0.02	0.028	0.063	0.097	0.132	0.167	0.236	0.306	0.375	0.444	0.514	0.583
0.03	0.041	0.074	0.108	0.142	0.176	0.243	0.311	0.378	0.446	0.514	0.581
0.04	0.053	0.086	0.118	0.151	0.184	0.250	0.316	0.382	0.447	0.513	0.579
0.05	0.064	0.096	0.128	0.160	0.192	0.256	0.321	0.385	0.449	0.513	0.577
0.06	0.075	0.106	0.138	0.169	0.200	0.263	0.325	0.388	0.450	0.513	0.575
0.07	0.085	0.116	0.146	0.177	0.207	0.268	0.329	0.390	0.451	0.512	0.573
0.08	0.095	0.125	0.155	0.185	0.214	0.274	0.333	0.393	0.452	0.512	0.571
0.09	0.105	0.134	0.163	0.192	0.221	0.279	0.337	0.395	0.453	0.512	0.570
0.1	0.114	0.142	0.170	0.199	0.227	0.284	0.341	0.398	0.455	0.511	0.568
0.11	0.122	0.150	0.178	0.206	0.233	0.289	0.344	0.400	0.456	0.511	0.567
0.12	0.130	0.158	0.185	0.212	0.239	0.293	0.348	0.402	0.457	0.511	0.565
0.13	0.138	0.165	0.191	0.218	0.245	0.298	0.351	0.404	0.457	0.511	0.564
0.14	0.146	0.172	0.198	0.224	0.250	0.302	0.354	0.406	0.458	0.510	0.563
0.15	0.153	0.179	0.204	0.230	0.255	0.306	0.357	0.408	0.459	0.510	0.561
0.16	0.160	0.185	0.210	0.235	0.260	0.310	0.360	0.410	0.460	0.510	0.560
0.17	0.167	0.191	0.216	0.240	0.265	0.314	0.363	0.412	0.461	0.510	0.559
0.18	0.173	0.197	0.221	0.245	0.269	0.317	0.365	0.413	0.462	0.510	0.558
0.19	0.179	0.203	0.226	0.250	0.274	0.321	0.368	0.415	0.462	0.509	0.557
0.2	0.185	0.208	0.231	0.255	0.278	0.324	0.370	0.417	0.463	0.509	0.556

Input parameters:

$$\rho_{vflex} = \frac{A_{vt}}{t * l_w}$$

$$\omega = \frac{566.7 * \rho_{vflex}}{f'_m}$$

$$\alpha = \frac{1667 * P_f}{f'_m \, l_w t}$$

Units:

P_f (kN)

l_w, t (mm)

A_{vt} (mm^2)

f'_m (MPa)

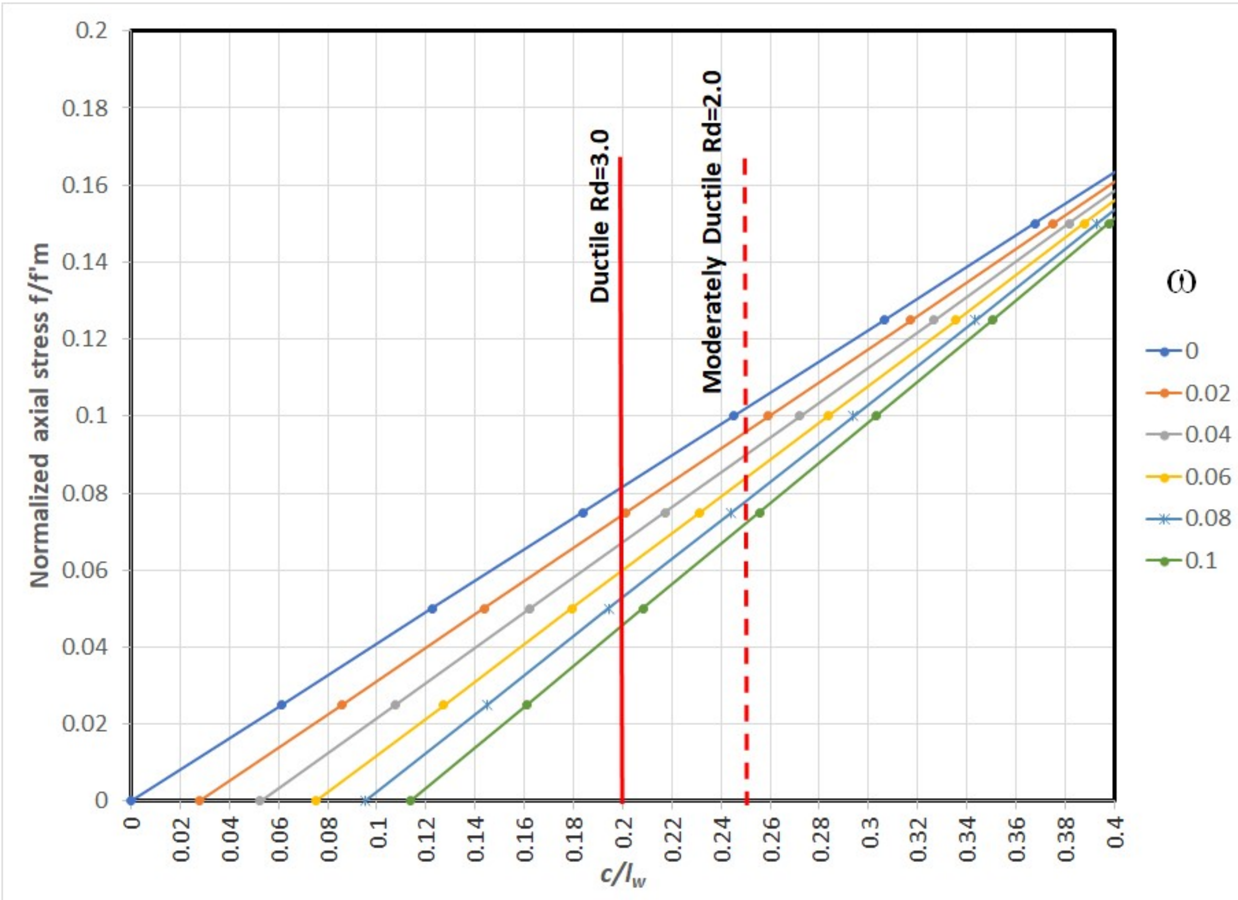

Figure D-1: c/l_w *ratio,* f_y *= 400 MPa*

Table D-3. Wall Stiffness Values $K/(E_m * t)$

h/l	Cantilever	Fixed
0.05	6.645	6.661
0.1	3.289	3.322
0.15	2.157	2.206
0.2	1.582	1.645
0.25	1.231	1.306
0.3	0.992	1.079
0.35	0.819	0.915
0.4	0.687	0.791
0.45	0.583	0.694
0.5	0.500	0.615
0.55	0.432	0.551
0.6	0.375	0.496
0.65	0.328	0.450
0.7	0.288	0.409
0.75	0.254	0.374
0.8	0.225	0.343
0.85	0.200	0.316
0.9	0.178	0.292
0.95	0.159	0.270
1	0.143	0.250
1.05	0.129	0.232
1.1	0.116	0.216
1.15	0.105	0.201
1.2	0.095	0.188
1.25	0.086	0.175
1.3	0.079	0.164
1.35	0.072	0.154
1.4	0.066	0.144
1.45	0.060	0.135
1.5	0.056	0.127
1.55	0.051	0.119
1.6	0.047	0.112
1.65	0.044	0.106
1.7	0.040	0.100
1.75	0.037	0.094
1.8	0.035	0.089
1.85	0.032	0.084
1.9	0.030	0.080
1.95	0.028	0.075
2	0.026	0.071

Cantilever model:

$$\frac{K}{E_m * t} = \frac{1}{\left(\frac{h}{l_w}\right)\left[4\left(\frac{h}{l_w}\right)^2 + 3\right]}$$

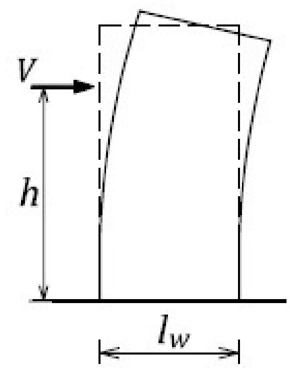

Fixed both ends:

$$\frac{K}{E_m * t} = \frac{1}{\left(\frac{h}{l_w}\right)\left[\left(\frac{h}{l_w}\right)^2 + 3\right]}$$

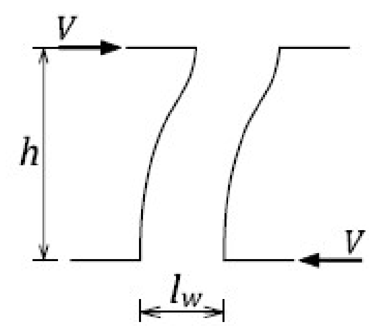

$E_m = 850 f'_m$ Modulus of elasticity

$G = 0.4 E_m$ Modulus of rigidity (shear modulus)

$A_v = 5A/6$ Shear area

E Notation

$a_{\max}$ = maximum acceleration

a = depth of the compression zone (equivalent rectangular stress block)

a_w = clear distance between the adjacent cross walls

A_b = area of reinforcement bar

A_c = area of concentrated reinforcement at each end of the wall

A_{ch} = cross-sectional area of core of the boundary element

A_d = area of distributed reinforcement along the wall length

A_e = effective cross-sectional area of masonry

A_g = gross cross-sectional area of masonry

A_L = area of the compression zone (flanged wall section)

A_r = response amplification factor to account for the type of attachment of equipment or veneer ties

A_s = area of steel reinforcement

A_{sh} = total area of rectangular hoop reinforcement (buckling prevention ties) in each horizontal direction of the boundary element

A_{uc} = uncracked area of the cross-section

A_v = area of horizontal wall reinforcement

A_{vt} = total area of the distributed vertical reinforcement

A_v = shear area of the wall section

A_x = amplification factor at level x to account for variation of response with the height of the building (veneer tie design)

b = effective width of the compression zone

b_{actual} = actual flange width

b_c = critical wall thickness

b_T = overhanging flange width

b_w = overall web width (shear design)

B = torsional sensitivity factor

c = neutral axis depth (distance from the extreme compression fibre to the neutral axis)

C = compressive force in the masonry acting normal to the sliding plane

C_m = the resultant compression force in masonry

C_h = compressive force in the masonry acting normal to the head joint

C_p = seismic coefficient for a nonstructural component (veneer tie design)

d = effective depth (distance from the extreme compression fibre to centroid of tension reinforcement)

d_v = effective wall depth for shear calculations

d' = distance from the extreme compression fibre to the centroid of the concentrated compression reinforcement

D_{nx} = plan dimension of the building at level x perpendicular to the direction of seismic loading being considered

e = load eccentricity

e_a = accidental torsional eccentricity

e_x = torsional eccentricity (distance measured perpendicular to the direction of earthquake loading between the centre of mass and the centre of rigidity at the level being considered)

E_f = modulus of elasticity of the frame material (infill walls)

E_m = modulus of elasticity of masonry

f_t = flexural tensile strength of masonry (see Table 5 of CSA S304-14)

f'_m = compressive strength of masonry normal to bed joints at 28 days (see Table 4 of CSA S304-14)

f_y = yield strength of reinforcement

f_{yh} = specified yield strength of hoop reinforcement in a boundary element

F = force

$F(T)$ = site coefficient (NBC 2015 Cl.4.1.8.4)

F_t = a portion of the base shear V applied at the top of the building

F_{el} = elastic force

F_s = factored tensile force at yield of horizontal reinforcement

F_a = acceleration-based site coefficient

F_v = velocity-based site coefficient

F_x = seismic force applied to level x

F_y = yield force

G = modulus of rigidity for masonry (shear modulus)

h = unsupported wall height/height of the infill wall

h_c = dimension of core of rectangular section measured perpendicular to the direction of the hoop bars (boundary elements)

h_n = building height

h_p = extent of the plastic hinge region above the critical section of the shear wall (previously l_p)

h_s = storey height

h_w = total wall height

h_x = height from the base of the structure up to the level x

I_b = moment of inertia of the beam

I_c = moment of inertia of the column

I_E = earthquake importance factor of the structure

J = numerical reduction coefficient for base overturning moment

k = effective length factor for compression member

k_n = factor accounting for the effectiveness of transverse reinforcement in a boundary element

k_{p1} = factor accounting for the compressive strain level in a boundary element

K = stiffness

l = length of the infill wall

l_d = length of the diagonal (infill wall)

l_s = design length of the diagonal strut (infill wall)

l_w = wall length

L_n = clear vertical distance between lines of effective horizontal support or clear horizontal distance between lines of effective vertical support

M = mass

M_f = factored bending moment

M_r = factored moment resistance

M_n = nominal moment resistance

M_p = probable moment resistance

M_v = factor to account for higher mode effect on base shear

n_l = total number of longitudinal bars in the boundary element cross-section that are laterally supported by the corner of hoops or by hooks of seismic cross-ties

N = axial load arising from bending in coupling beams or piers

p_f = distributed axial stress

PGA_{ref} = reference Peak Ground Acceleration (PGA) for determining $F(T)$

P_d = axial compressive load on the section under consideration

P_{cr} = critical axial compressive load

P_{DL} = dead load

P_{fb} = the resultant compression force (flanged walls)

P_r = factored axial load resistance

P_1 = compressive force in the unreinforced masonry acting normal to the sliding plane

P_h = horizontal component of the diagonal strut compression resistance (infill walls)

P_v = the vertical component of the diagonal strut compression resistance (infill walls)

P_{ult} = ultimate tie strength

R_d = ductility-related force modification factor

R_o = overstrength-related force modification factor

R_p = element or component response modification factor (veneer tie design)

s = reinforcement spacing

$S(T)$ = design spectral acceleration

$S_a(T)$ = 5% damped spectral response acceleration

S_e = section modulus of effective wall cross-sectional area

S_p = horizontal force factor for part or portion of a building and its anchorage (veneer tie design)

t = overall wall thickness

t_e = effective wall thickness

t_f = face shell thickness

T = fundamental period of vibration of the building

T_x = torsional moment at level x

T_r = the resultant force in steel reinforcement

T_y = factored tensile force at yield of the vertical reinforcement

v_f = distributed shear stress

v_m = masonry shear strength

$v_{\max}$ = maximum velocity

V = lateral earthquake design force at the base of the structure

V_e = lateral earthquake elastic force at the base of the structure

V_f = factored shear force

V_{fr} = shear flow resistance

V_{nb} = the resultant shear force corresponding to the development of nominal moment resistance M_n at the base of the wall

V_m = masonry shear resistance

V_r = factored shear resistance

$\overline{V}_s$ = average shear wave velocity in the top 30 m of soil or rock

V_s = factored shear resistance of steel reinforcement

w = diagonal strut width (infill walls)

w_e = effective diagonal strut width (infill walls)

W = seismic weight, equal to the dead weight plus some portion of live load that would move laterally with the structure

W_p = weight of a part or a portion of a structure (veneer tie design)

W_x = a portion of seismic weight W that is assigned to level x

α_h = vertical contact length between the frame and the diagonal strut (infill walls)

α_L = horizontal contact length between the frame and the diagonal strut (infill walls)

β = damping ratio

β_d = ratio of the factored dead load moment to the total factored moment

β_1 = ratio of depth of rectangular compression block to depth of the neutral axis

γ_g = factor to account for partially grouted or ungrouted walls that are constructed of hollow or semi-solid units

$\delta_{\max}$ = the maximum storey displacement at level x at one of the extreme corners in the direction of earthquake

δ_{ave} = the average storey displacement determined by averaging the maximum and minimum displacements of the storey at level x

Δ = lateral displacement

Δ_p = plastic displacement

Δ_y = displacement at the onset of yielding

Δ_{el} = elastic displacement

$\Delta_{\max}$ = maximum displacement

Δ_u = inelastic (plastic) displacement

ε_m = the maximum compressive strain in masonry

ε_s = strain in steel reinforcement

ε_y = yield strain in steel reinforcement

χ = factor used to account for direction of compressive stress in a masonry member relative to the direction used for determination of f'_m

φ = curvature

φ_u = ultimate curvature

φ_y = yield curvature corresponds to the onset of yielding

ϕ_{er} = resistance factor for member stiffness

ϕ_m = resistance factor for masonry

ϕ_s = resistance factor for steel reinforcement

ϕ = resistance factor

ρ_h = horizontal reinforcement ratio

ρ_s = volumetric ratio of circular hoop reinforcement for buckling prevention ties

ρ_v = vertical reinforcement ratio

μ = coefficient of friction

μ_Δ = displacement ductility ratio

μ_φ = curvature ductility ratio

μ_Δ = displacement ductility ratio

θ = angle of diagonal strut measured from the horizontal

θ_e = elastic rotation

θ_{ic} = inelastic rotational capacity

θ_{id} = inelastic rotational demand

θ_p = plastic rotation

ω = natural frequency